iScience

CellPress

Article

Multifunctional Protein Conjugates with Built-in Adjuvant (Adjuvant-Protein-Antigen) as Cancer Vaccines Boost Potent Immune Responses

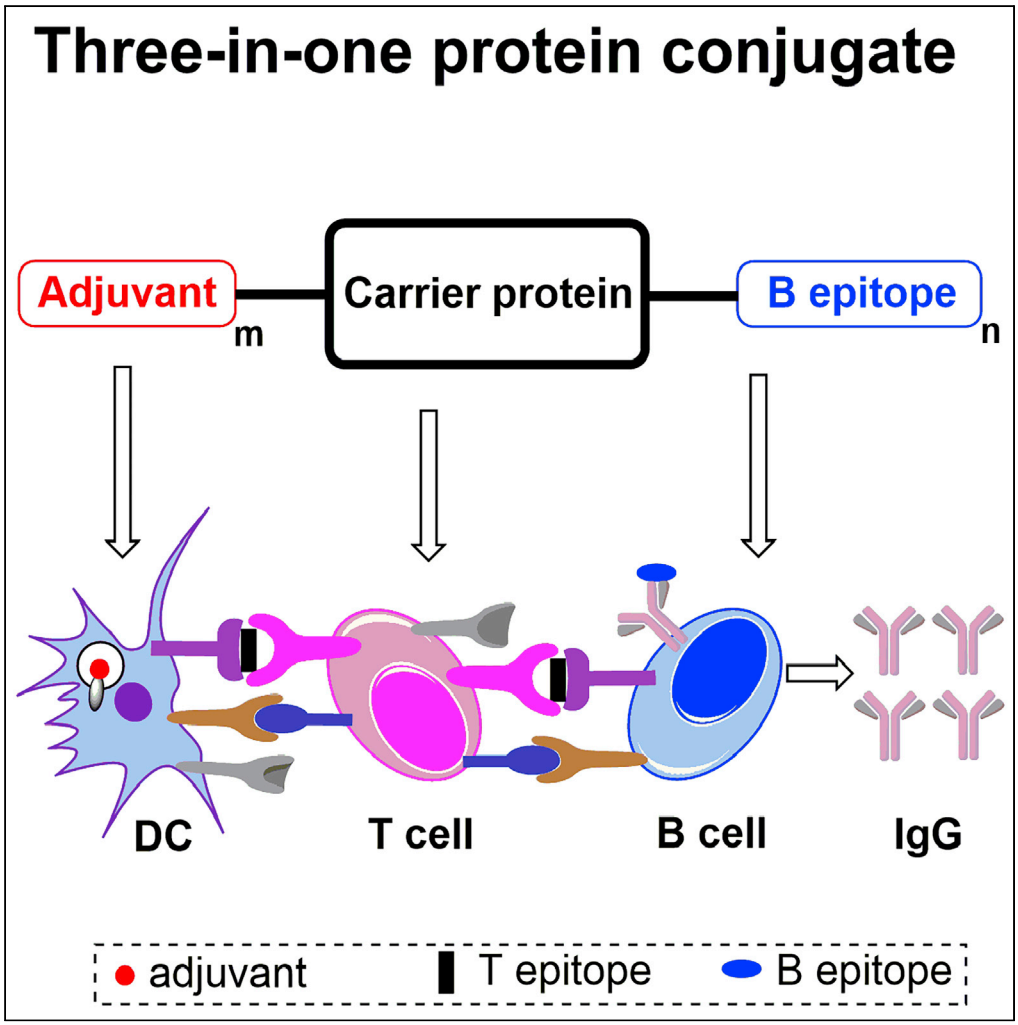

Jing-Jing Du, Chang-Wei Wang, Wen-Bo Xu, ..., Xiao-Fei Gao, Guang-Fu Yang, Jun Guo

gfyang@mail.ccnu.edu.cn (G.-F.Y.)
jguo@mail.ccnu.edu.cn (J.G.)

HIGHLIGHTS

Adjuvant-protein-antigen protein conjugates act as new cancer vaccine strategy

Built-in adjuvant of TLR7 agonist can reduce toxicities and enhance immune stimulations

Three-in-one protein conjugates boost potent immune responses against cancer cells

Du et al., iScience 23, 100935 March 27, 2020
https://doi.org/10.1016/j.isci.2020.100935

iScience

CellPress

Article

Multifunctional Protein Conjugates with Built-in Adjuvant (Adjuvant-Protein-Antigen) as Cancer Vaccines Boost Potent Immune Responses

Jing-Jing Du,[1,3] Chang-Wei Wang,[1,3] Wen-Bo Xu,[1] Lian Zhang,[1] Yuan-Kai Tang,[1] Shi-Hao Zhou,[1] Xiao-Fei Gao,[2] Guang-Fu Yang,[1,*] and Jun Guo[1,4,*]

SUMMARY

Many cancer vaccines are not successful in clinical trials, mainly due to the challenges associated with breaking immune tolerance. Herein, we report a new strategy using an adjuvant-protein-antigen (three-in-one protein conjugates with built-in adjuvant) as an anticancer vaccine, in which both the adjuvant (small-molecule TLR7 agonist) and tumor-associated antigen (mucin 1, MUC1) are covalently conjugated to the same carrier protein (BSA). It is shown that the protein conjugates with built-in adjuvant can increase adjuvant's stimulation, prevent adjuvant's systemic toxicities, facilitate the codelivery of adjuvants and antigens, and enhance humoral and cellular immune responses. The IgG antibody titers elicited by the self-adjuvanting three-in-one protein conjugates were significantly higher than those elicited by the vaccine mixed with TLR7 agonist (more than 15-fold) or other traditional adjuvants. Importantly, the potent immune responses against cancer cells suggest that this new vaccine construct is an effective strategy for the personalized antitumor immunotherapy.

INTRODUCTION

Aberrantly glycosylated mucin 1 (MUC1) is an important tumor-associated antigen of epithelial cells, mainly due to its overexpression on the tumor cell surface together with the formation of truncated glycans and exposed peptide epitopes (Lloyd et al., 1996). Therefore, the MUC1 glycoprotein constitutes a promising target (Acres and Limacher, 2005;Barratt-Boyes, 1996;Bhatia et al., 2019; Cheever et al., 2009; Singh and Bandyopadhyay, 2007) for tumor immunotherapies using a vaccination or chimeric antigen receptor T cell (CAR T) strategy. However, because most tumor-associated antigens act as autoantigens, which are tolerated by the immune system and unable to elicit potent immune responses, many antitumor vaccines have encountered difficulties in clinical trials (Tang et al., 2008, 2018). Therefore, it is highly necessary to develop a new strategy for antitumor vaccines to promote potent immunity to overcome the poor antigenicity of tumor-associated antigens and kill tumor cells (Gaidzik et al., 2013; Hossain and Wall, 2016;Martínez-Sáez et al., 2017; Rivalland et al., 2015).

In cancer vaccine research, tremendous efforts have been made to improve the immunogenicity of tumor-associated antigens. In fully synthetic anticancer vaccines, such as two-component anticancer vaccines (Scheme 1A) (Cai et al., 2014; Hossain et al., 2018; Kaiser et al., 2010; Liu et al., 2016; Toyokuni et al., 1994; Wang et al., 2012, 2019; Wilkinson et al., 2010; Yin et al., 2017), three-component anticancer vaccines with Th epitopes (Scheme 1B) (Abdel-Aal et al., 2014; Cai et al., 2017; Ingale et al., 2007; Wilkinson et al., 2011; Wu et al., 2018a), and multicomponent anticancer vaccines with CD4+ T helper cell (Th) and CD8+ T cytotoxic/killer cell (Tc) epitopes (Scheme 1C) (Renaudet et al., 2008, 2010), built-in adjuvants have been proven to efficiently stimulate the immune system to recognize tumor-associated antigens and induce increased levels of antibodies against B epitopes. The generally utilized built-in adjuvants include Pam_3CSK_4 (TLR1/2 lipopeptide ligand) (Abdel-Aal et al., 2014; Cai et al., 2014, 2017; Hossain et al., 2018; Ingale et al., 2007; Kaiser et al., 2010; Toyokuni et al., 1994; Wilkinson et al., 2010, 2011), monophosphoryl lipid A (MPLA; TLR4 agonist) (Wang et al., 2012), CpG-ODN 1826(TLR9 agonist) (Abdel-Aal et al., 2014), αGalCer (NKT cell agonist) (Yin et al., 2017), etc. Results have indicated that immune responses against tumor-associated antigens might increase gradually as the number of vaccine components increases, but the difficulty of synthesis is also raised. Previously, we reported that fully synthetic vaccines with a built-in or mixed NKT cell agonist acted as a potent adjuvant simplified vaccine construction and achieved

[1]Key Laboratory of Pesticide and Chemical Biology, Ministry of Education, Hubei International Scientific and Technological Cooperation Base of Pesticide and Green Synthesis, International Joint Research Center for Intelligent Bio-sensing Technology and Health, College of Chemistry, Central China Normal University, Wuhan, Hubei 430079, China

[2]Jiangxi Key Laboratory for Mass Spectrometry and Instrumentation, East China University of Technology, Nanchang, Jiangxi 330013, China

[3]These authors contributed equally

[4]Lead Contact

*Correspondence: gfyang@mail.ccnu.edu.cn (G.-F.Y.), jguo@mail.ccnu.edu.cn (J.G.)

https://doi.org/10.1016/j.isci.2020.100935

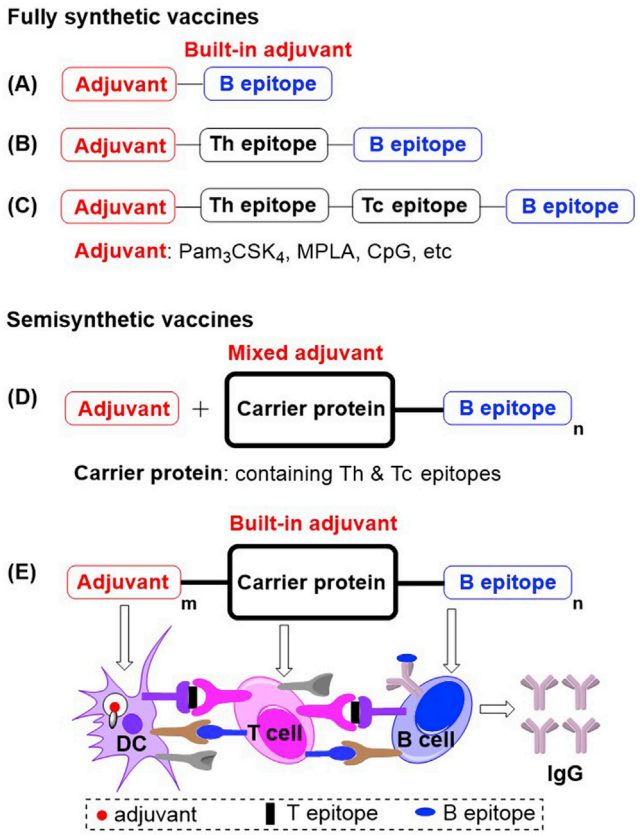

Scheme 1. The Cancer Vaccines Comprising Built-in or Mixed Adjuvants.

(A) Two-component vaccines; (B) three-component vaccines with Th epitopes; (C) multicomponent vaccines with Th and Tc epitopes; (D and E) traditional semisynthetic vaccines with mixed adjuvants.

antibody class switching from IgM to IgG (Chen et al., 2019; Du et al., 2019; Liu and Guo, 2017;Yin et al., 2017). Alternatively, in semisynthetic anticancer vaccines (Scheme 1D), tumor-associated antigens are usually conjugated to different carriers, including BSA (Cai et al., 2012; Dziadek et al., 2005; Hoffmann-Röder and Johannes, 2011), diphtheria toxoid cross-reactive material (CRM) 197 (DT) (Lee et al., 2014), tetanus toxoid (TTox) (Hoffmann-Röder et al., 2010; Oberbillig et al., 2012; Straβburger et al., 2018), keyhole limpet hemocyanin (KLH) (Xiao et al., 2016; Zhu et al., 2009), and virus-like particles (VLPs) (Wu et al., 2018b; Yin et al., 2018), then these conjugates are mixed with adjuvants. Because the multiple Th and Tc epitopes of carrier proteins can synergistically activate immunity, semisynthetic anticancer vaccines generally produce improved immune responses. However, it is still a major challenge to develop potent anticancer immunotherapies.

To address the challenge of antitumor vaccines, we present a novel strategy using three-in-one protein conjugates (Scheme 1E) with built-in adjuvants on carrier proteins that exploit the advantages of both fully synthetic vaccines and semisynthetic vaccines. In this strategy, the multiple built-in adjuvants have enhanced activity due to their cluster effect, prevent adjuvant's systemic toxicity, and the adjuvant's codelivery with antigens to the lymph nodes for immune stimulation is guaranteed. Additionally, the carrier proteins also contain various Tc and Th epitopes to elicit synergistic immune help for T-cell-dependent B epitopes.

Toll-like receptors (TLRs) are highly conserved cellular receptors that recognize unique molecular cell wall and nucleic acid components of invading pathogens and have the potential to regulate the activation of antigen-presenting cells, subsequently strengthening the signaling of costimulatory molecules and the secretion of many cytokines (Dowling, 2018). In particular, TLR7 mediate recognition of purine-rich ssRNA in the endosome to elicit immune responses to the recognized pathogens; numerous studies have demonstrated that conjugation of small molecular TLR7 agonists (TLR7a) to various polymers (Chan et al., 2009; Francica et al., 2016; Kim et al., 2016; Lynn et al., 2015, 2019; Shinchi et al., 2015; Van Herck et al., 2018;

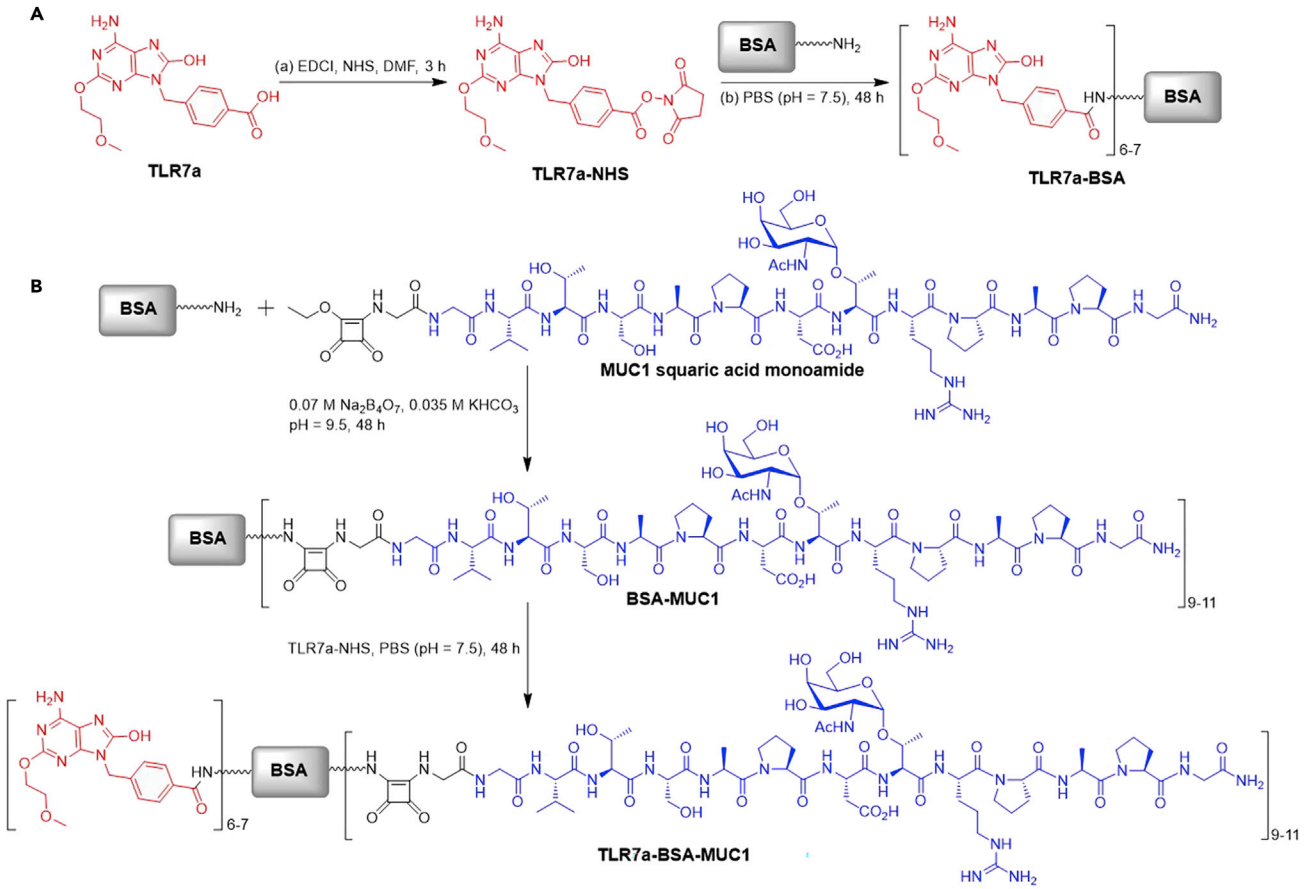

Scheme 2. Synthesis of Vaccine Components

(A) Synthesis of TLR7a-BSA; (B) synthesis of TLR7a-BSA-MUC1 from MUC1 glycopeptide squaric acid monoamide and Fmoc-SPPS.

Yoo et al., 2018) or proteins (Donadei et al., 2016; Feng et al., 2013; Gao et al., 2014, 2015, 2016; Oh and Kedl, 2010; Wu et al., 2007) can facilitate trafficking to the lymph nodes, enhance immunostimulatory activities, and decrease sideeffects due to the clustered arrangement of TLR7a adjuvants conjugated on carriers.

Therefore, we employed the strategy of a self-adjuvanting three-in-one protein conjugate for an antitumor vaccine for the first time and synthesized the vaccine conjugate TLR7a-BSA-MUC1 (adjuvant-protein-antigen), in which several small-molecule TLR7a (Donadei et al., 2016; Gao et al., 2014, 2015) were conjugated to the carrier protein BSA, the tumor-associated MUC1 antigens (Bermejo et al., 2018; Compañón et al., 2019) served as B epitopes, and their PDTRP motifs contained Tn antigens (Burchell et al., 1989; Du et al., 2019; Karsten et al., 1998). The immunological results revealed that the TLR7a-BSA-MUC1 vaccine triggered a robust response with production of antibodies targeting MUC1 antigens and exhibiting strong binding to MCF-7 cancer cells and B16-MUC1 cells expressing MUC1 antigens.

RESULTS AND DISCUSSION

Preparation of Vaccine Components

The synthesis of TLR7a-BSA conjugate and three-in-one protein conjugate TLR7a-BSA-MUC1 is shown in Scheme 2. The small-molecule TLR7a was converted to active ester TLR7a-NHS (Gao et al., 2016), which reacted with the protein to form conjugates. The MUC1 antigen (sequence, GVTSAPDTRPAPG) containing a Tn antigen in the PDTRP motif was synthesized and conjugated to BSA through the squaric acid diethyl ester method (Cai et al., 2012; Du et al., 2019; Dziadek et al., 2005). Next, a TLR7a was covalently attached to the carrier protein of the MUC1-BSA conjugate. MALDI-TOF MS indicated that there was an average of 6–7 TLR7a and 9–11 MUC1 glycopeptides covalently linked to BSA.

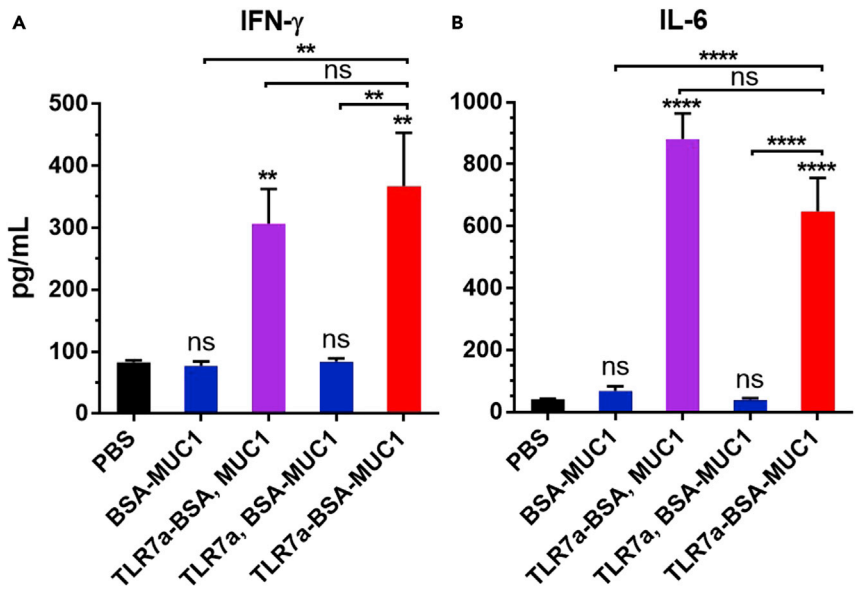

Figure 1. Cytokine Quantification of Mouse IFN-γ and IL-6

The secretion of the cytokines IFN-γ (A) and IL-6 (B) was measured in serum samples from vaccinated mice at 2 h after the first immunization. Differences were determined by ANOVA using Tukey's HSD test. Asterisks represent statistically significant differences (****$p < 0.0001$, **$p < 0.01$), and ns indicates no significant difference compared with the PBS group. Data are shown as the mean ± SEM of five mice and are representative of three separate experiments.

To evaluate immune responses induced by the TLR7a-BSA-MUC1 vaccine *in vivo*, a group of mice (n = 5) was intraperitoneally injected with TLR7a-BSA-MUC1 (dose of 21 μg of MUC1 peptide) on days 1, 15, and 29 (Scheme S8) (Chen et al., 2019; Du et al., 2019). To decipher the essentiality of the various components of the vaccine, control groups of mice were injected with BSA-MUC1, TLR7a-BSA and MUC1, TLR7a and BSA-MUC1, MPLA and BSA-MUC1, Pam_3CSK_4 and BSA-MUC1, alum (an adjuvant approved for human applications) and BSA-MUC1, with the same dose of MUC1 and optimized doses of the adjuvants (Table S1).

Evaluation of Cytokine Levels

To investigate whether the covalent attachment of three components affected immune activation, the differences in the production of the Th1-type cytokine interferon-γ (IFN-γ) and Th2- and Th17-type pro-inflammatory cytokine interleukin 6 (IL-6) were evaluated (Figures 1 and S1) (Chen et al., 2019; Du et al., 2019). Mice immunized with the protein conjugates with built-in adjuvant (TLR7a-BSA and MUC1 or TLR7a-BSA-MUC1) showed significantly increased release of IFN-γ and IL-6, exhibiting four- to ten-fold higher cytokine levels than mice treated with a vaccine with mixed TLR7a adjuvants (TLR7a and BSA-MUC1) or without adjuvant.

The ability to generate high levels of cytokines was mainly contributed by covalent conjugation of several copies of TLR7a on one carrier protein to achieve cluster effect, and facilitated draining of the adjuvant TLR7a together with the carrier protein to the lymph nodes, uptake and processing by the same one antigen-presenting cell (APC) (Gao et al., 2014, 2015, 2016; Wu et al., 2007). In addition, protein conjugates can prevent the small molecular TLR7a to rapidly enter the blood to cause systemic toxicity of waste inflammation (Dowling, 2018).

Evaluation of Antigen-Specific Antibodies

The anti-MUC1 antibody titers induced by vaccine candidates were measured by enzyme-linked immunosorbent assay (ELISA) (Du et al., 2019), in which a low concentration (0.125 μg/mL) of biotinylated MUC1 (Figures S39–S43) (Miermont et al., 2008) formed a complex with avidin to act as the coating antigen. As shown in Figure 2, the three-in-one protein conjugate vaccine (TLR7a-BSA-MUC1) elicited the highest IgG antibody titers against the MUC1 antigen: the titers were 500-fold higher than those of BSA-MUC1 without adjuvant, 100-fold higher than those of TLR7a-BSA and MUC1, and 15-fold higher than those of

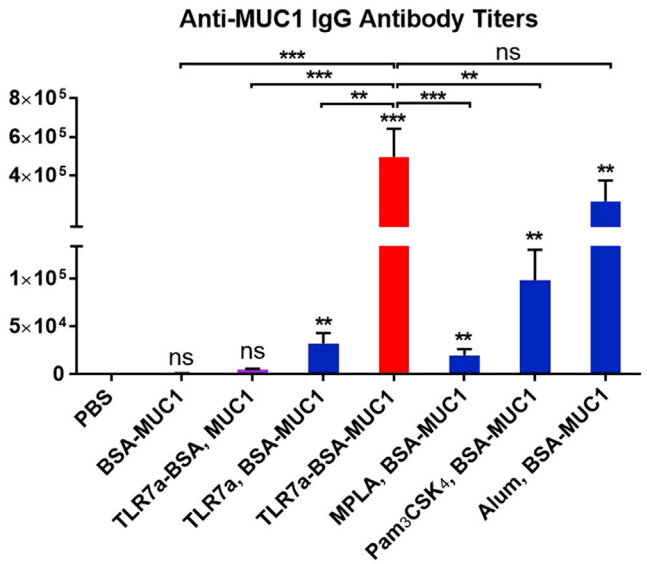

Figure 2. Quantification of Antigen-specific Antibodies Production via ELISA

Anti-MUC1 IgG antibody titers were detected in serum samples from vaccinated mice collected on day 42. Differences were determined by ANOVA and Tukey's HSD test. Asterisks represent statistically significant differences (***$p < 0.001$, **$p < 0.01$), and ns indicates no significant difference compared with the PBS group. Data are shown as the mean ± SEM of five mice and are representative of three separate experiments.

TLR7a and BSA-MUC1. Moreover, the anti-MUC1 IgG antibody titers of the three-in-one protein conjugate are also significantly higher than those of the mixed-adjuvant vaccines with the classic TLR4 agonist MPLA or TLR1/2 agonist Pam_3CSK_4 and slightly higher than those of the vaccine absorbed on the traditional alum adjuvant. This finding indicated that it is essential to covalently conjugate both the adjuvant TLR7a and the antigenic MUC1 glycopeptide to the carrier protein to produce the most potent vaccine, and this approach may provide the advantages of the cluster effect of the adjuvant and codelivery of the adjuvant and antigen on the carrier protein for immune cell uptake, processing, and immunomodulation (Donadei et al., 2016; Feng et al., 2013; Gao et al., 2014, 2015, 2016; Oh and Kedl, 2010; Wu et al., 2007).

The titers of the anti-MUC1 IgG antibodies elicited by the three-in-one protein conjugate increased gradually following immunizations (Figures 3A and S2–S4), whereas the IgM titers did not increase between days 28 and 42 (Figures 3B and S5–S7). Therefore, the three-in-one protein conjugates enhanced B cell stimulation and promoted differentiation into memory B cells and plasma cells for the induction of high-affinity IgG antibodies.

Evaluation of Antibody Subtypes

To evaluate the immunological properties of these vaccines, an analysis of IgG subtypes was performed. As depicted in Figures 4 and S8–S15, the IgG1 subclasses of the MUC1-specific antibodies were dominant for most vaccines, such as BSA-MUC1 alone, BSA-TLR7a and MUC1, or TLR7a and BSA-MUC1. In contrast, when the three-in-one protein conjugate with covalently ligated TLR7a adjuvants was used, it induced Th1-skewed immune responses and produced approximately similar titers of IgG1, IgG2a, IgG2b, and IgG3 antibodies, and the titers of the Th1-type IgG2a antibodies were the highest. In addition, the vaccines containing the mixed adjuvants (MPLA, Pam_3CSK_4, or alum) and BSA-MUC1 displayed skewed Th2-type responses with high levels of IgG1 antibodies and much lower levels of IgG2a antibodies than those induced by the TLR7a-BSA-MUC1 vaccine (Figure S9).

Previous studies indicate that this small molecule TLR7a is an effective adjuvant to induce cytokines optimal for Th1 cell immunity and antibody production (Dowling, 2018). Herein, the results demonstrated that the built-in adjuvant with several TLR7a molecules in the TLR7a-BSA-MUC1 conjugates greatly enhanced the efficacy of TLR7a, preferentially promoted Th1-type adaptive immunity, and implemented antibody subclass and isotype switching, which is preferred in antitumor immunotherapy.

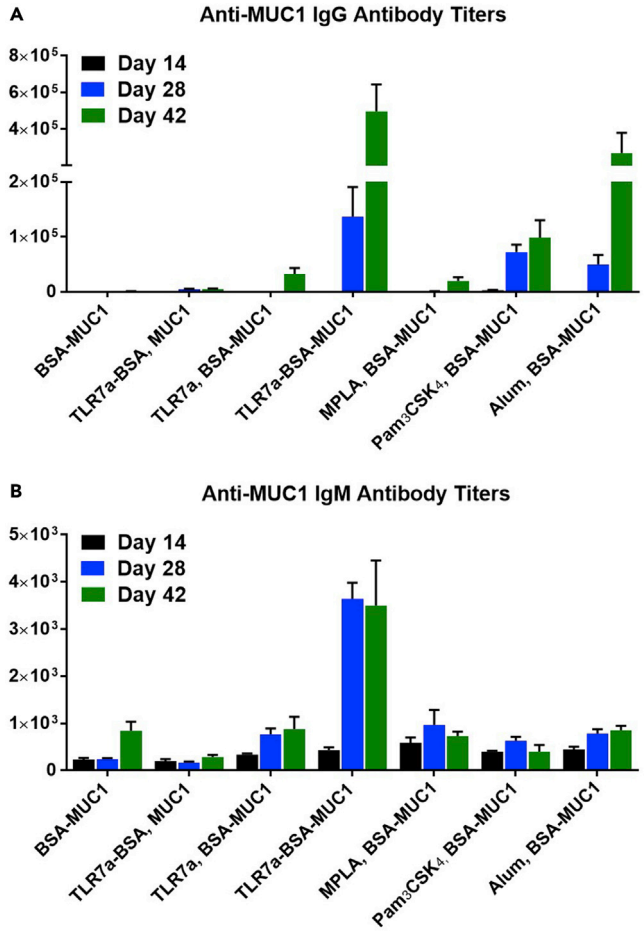

Figure 3. Quantification of Antigen-Specific Antibodies Production via ELISA

Anti-MUC1 IgG (A) and IgM (B) antibody titers in serum samples from vaccinated mice were measured on days 14, 28, and 42. Data are shown as the mean ± SEM of five mice and are representative of three separate experiments.

Evaluation of Carrier-Protein-Specific Antibodies

On the one hand, the vaccine needs the Th and Tc epitopes from the carrier protein to promote the immune responses against the tumor-associated antigens; on the other hand, eliciting high antibody titers against the carrier protein will increase the burden of immune system. The titers of the IgG antibodies against the carrier protein BSA were also analyzed (Figures 5 and S16). For the anti-BSA IgG antibody titers, the three-in-one protein conjugate vaccine (TLR7a-BSA-MUC1) were higher than BSA-MUC1, TLR7a and BSA-MUC1, or MPLA and BSA-MUC1, but lower than TLR7a-BSA and MUC1, Pam_3CSK_4 and BSA-MUC1, or alum and BSA-MUC1.

Compared with TLR7a-BSA and MUC1, the reduced carrier-specific antibody titers induced by the three-in-one protein conjugates were presumably attributed to the shielding effect of conjugating MUC1 and TLR7a adjuvant to the carrier BSA (Clough et al., 1985; Miermont et al., 2008).

Immunological Studies with Cancer Cells

To determine whether the serum antibodies could bind to MCF-7 cells and B16-MUC1 cells (Wang et al., 2013), fluorescence-activated cell sorting (FACS) analysis (Figures 6A, S17, and S19), confocal fluorescence microscopy (Figures 6B, S20, and S21), and fluorescence microscopy (Figures S23 and S24) were conducted (Du et al., 2019). The results showed that the antibodies induced by the TLR7a-BSA-MUC1 vaccine displayed the highest binding affinity for MCF-7 cells and B16-MUC1 cells, as shown by measuring the mean fluorescence intensity of the cancer cells, whereas relatively lower binding affinity was observed with the antibodies elicited by the BSA-MUC1, BSA-TLR7a and MUC1, or TLR7a and BSA-MUC1 vaccine. Additionally, the antibodies induced by the vaccines

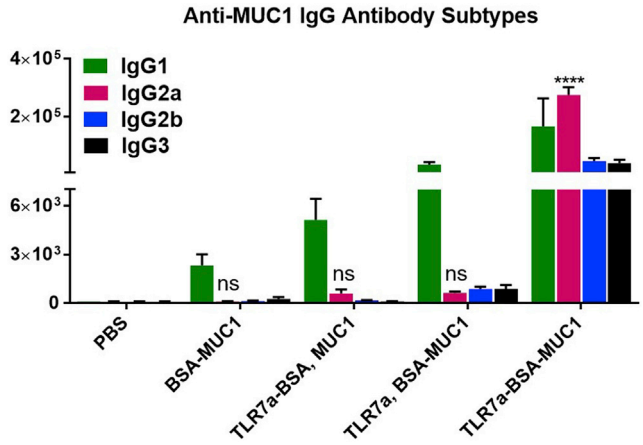

Figure 4. Quantification ofAntibody Subtypes Production via ELISA

Anti-MUC1 IgG antibody subtypes were measured in serum samples from vaccinated mice collected on day 42. Differences were determined by ANOVA and Tukey's HSD test. Asterisks represent statistically significant differences (****$p < 0.0001$), and ns indicates no significant difference compared with the PBS group. Data are shown as the mean ± SEM of five mice and are representative of three separate experiments.

composed of a mixed adjuvant, such as MPLA, Pam_3CSK_4, or alum, with the BSA-MUC1 conjugate exhibited lower binding affinity than those elicited by the TLR7a-BSA-MUC1 vaccine. To further investigate the antibody's binding ability to cell lines that do not express tumor-associated MUC1 antigens on the surface, B16-F10 cells (Hirabayashi et al., 1985) were used as a negative control in both FACS analysis and confocal fluorescence microscopy assays (Figures S18 and S22). We found that all serum antibodies induced by these vaccines (BSA-MUC1, TLR7a-BSA and MUC1, TLR7a and BSA-MUC1, TLR7a-BSA-MUC1) displayed very weak binding affinity for B16-F10 cells, overall there was no difference compared with the PBS group.

The elicited antibodies were able to bind to MCF-7 cancer cells and may initiate lysis of the recognized cancer cells via activation of the complement-dependent cytotoxicity (CDC) of rabbit sera (RC) (Cai et al., 2014; Du et al.,

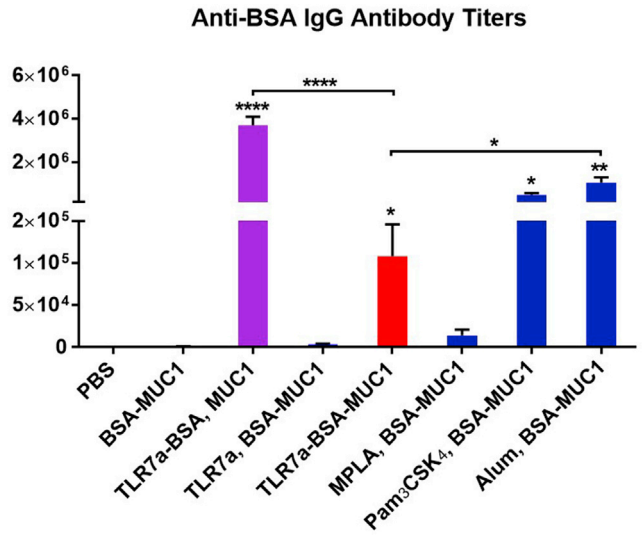

Figure 5. Anti-BSA IgG Antibody Titers Were Detected in Serum Samples from Vaccinated Mice Collected on Day 42

Differences were determined by ANOVA using Tukey's HSD test. Asterisks represent statistically significant differences (****$p < 0.0001$, **$p < 0.01$, *$p < 0.05$), and ns indicates no significant difference compared with the PBS group. Data are shown as the mean ± SEM of five mice and are representative of three separate experiments.

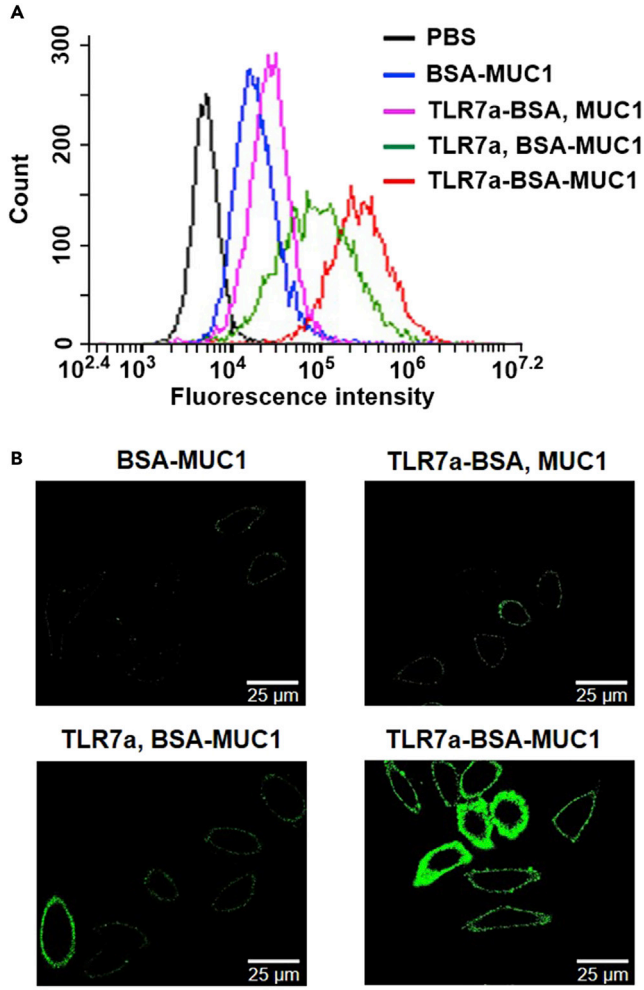

Figure 6. Binding of the Mouse Serum to MCF-7 Cells was Determined by FACS and Confocal Microscopy Analysis

(A) FACS analysis of the binding of vaccinated mouse serum samples to MCF-7 cancer cells. Incubation with PBS group samples (black) served as a control.

(B) Confocal fluorescence microscopy images of MCF-7 cells incubated with serum samples from vaccinated mice (magnification: 63×). The images are representative of five independent experiments. Scale bar = 25 μm.

2019). Sera or complement was diluted 50-fold to determine the cell viability of MCF-7 cells by applying a tetrazolium bromide (MTT) assay. Control groups in these trials included MCF-7 cells incubated with an inactive form of rabbit sera (RC-inactive), rabbit sera, or PBS. As shown in Figure 7A, the MUC1-specific antibodies elicited by the TLR7a-BSA-MUC1 vaccine led to lower than 40% cell viability, and these antibodies were predicted to kill the MCF-7 cells by mediating CDC activation distinctly stronger than that induced by the antibodies elicited by the vaccines composed of the noncovalently linked adjuvants or antigens.

Evaluation of the Mouse T-Cell-Mediated Response to Vaccination

We further studied whether the vaccine candidates could evoke a cytotoxic T lymphocyte (CTL) response. Splenocytes were obtained from immunized mice and incubated with MCF-7 cancer cells (Figure 7B) (Song et al., 2017). The splenocytes isolated from mice immunized with TLR7a and BSA-MUC1 or TLR7a-BSA-MUC1 exhibited significantly higher cytotoxicity to MCF-7 cells than those isolated from BSA-MUC1-vaccinated mice. CTLs activated by TLR7a-BSA-MUC1 displayed more efficient cytotoxicity than those activated by TLR7a and BSA-MUC1, which further suggested that the TLR7a-BSA-MUC1 conjugate could provoke stronger T-cell-mediated immunity than TLR7a and BSA-MUC1. Thus, the three-in-one protein conjugate is an applicable vaccine strategy to trigger a strong CTL immune response and simultaneously enhance immunogenicity.

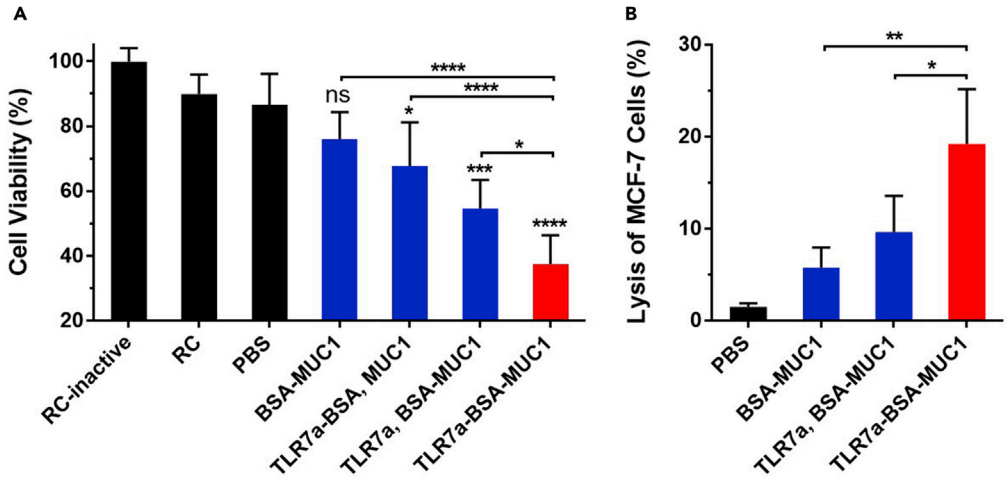

Figure 7. Cell viability and Cytotoxicity Assay

(A) Complement-dependent cytotoxicity of antisera from each group: the cell viability of MCF-7 cells was determined by the MTT assay.

(B) Assay of cytotoxic T-lymphocyte-mediated immune responses: *in vitro* cytotoxicity of splenocytes collected from each group on day 42 to MCF-7 cells. Differences were determined by one-way ANOVA and Tukey's HSD test.

Asterisks indicate statistically significant differences (****$p < 0.0001$, **$p < 0.01$, *$p < 0.05$). Data are the mean ± SD of five mice and are representative of five independent experiments.

Concluding Remarks

We investigated the structure-activity relationships of different constructs of anticancer vaccines with conjugated and mixed adjuvants. In this respect, this study indicated that the most potent antitumor vaccine was the three-in-one protein conjugate construct with a small-molecule TLR7 agonist as the adjuvant and tumor-associated antigen MUC1 as the B epitope covalently attached to a carrier protein containing multiple Tc and Th epitopes; this construct could not only stimulate exceptionally high IgG antibody titers but also affect the distribution of IgG subclasses toward Th1-polarized immune responses. It is essential that the TLR7 agonist be covalently coupled to the MUC1-BSA conjugate, probably due to the agonist providing a multivalent effect and subsequently facilitating codelivery to the lymph nodes to enhance the stimulation of immunity. As a result, the antibodies induced by the three-in-one vaccine bound to MCF-7 cancer cells strongly and killed the bound cancer cells through CDC activation; splenocytes from mice immunized with the three-in-one protein conjugate also lysed MCF-7 cancer cells relatively efficiently.

This three-in-one protein conjugate represents a novel anticancer vaccine strategy with a relatively simple formulation that improves immune responses, thus providing potential applications for personalized anticancer immunotherapy against tumor-associated antigens and tumor-specific neoantigens (Hilf et al., 2019; Keskin et al., 2019; Ott et al., 2017; Sahin et al., 2017).

Limitations of the Study

Three-in-one protein conjugates with built-in adjuvant can facilitate the codelivery of adjuvants and antigens. However, in order to induce potent immune responses, only when the modification with linker does not notably reduce the adjuvant's activity, the adjuvants are applicable for this strategy. Currently we are investigating different kinds of molecular adjuvants to validate this vaccine strategy.

METHODS

All methods can be found in the accompanying Transparent Methods supplemental file.

SUPPLEMENTAL INFORMATION

Supplemental Information can be found online at https://doi.org/10.1016/j.isci.2020.100935.

ACKNOWLEDGMENTS

We thank the National Key Research and Development Program of China (No. 2017YFA0505200), the National Natural Science Foundation of China (No.21772056), the self-determined research funds of CCNU from the colleges' basic research and operation of MOE (No. CCNU18TS011), Program of Introducing Talents of Discipline to Universities of China (111 program, B17019), and the Research Fund of East China University of Technology (No.DHBK2017114).

AUTHOR CONTRIBUTIONS

J.G. and G.-F.Y. conceived the project. J.-J.D. and C.-W.W. designed and carried out the synthesis. X.-F.G. and Y.-K.T. contributed to synthesis. W.-B.X. and L.Z. carried out the immunizations in mice. J.-J.D., C.-W.W., and S.-H.Z. performed the immunological evaluation. J.-J.D. and C.-W.W. wrote the manuscript, and all the authors contributed to the discussion.

DECLARATION OF INTERESTS

J.G., G.-F.Y., J.-J.D., and C.-W.W. have filed a patent application. The authors declare no competing interests.

Received: October 19, 2019
Revised: December 22, 2019
Accepted: February 19, 2020
Published: March 27, 2020

REFERENCES

Abdel-Aal, A.-B.M., Lakshminarayanan, V., Thompson, P., Supekar, N., Bradley, J.M., Wolfert, M.A., Cohen, P.A., Gendler, S.J., and Boons, G.-J. (2014). Immune and anticancer responses elicited by fully synthetic aberrantly glycosylated MUC1 tripartite vaccines modified by a TLR2 or TLR9 agonist. ChemBioChem *15*, 1508–1513.

Acres, B., and Limacher, J.-M. (2005). MUC1 as a target antigen for cancer immunotherapy. Expert Rev. Vaccin. *4*, 493–502.

Barratt-Boyes, S.M. (1996). Making the most of mucin: a novel target for tumor immunotherapy. Cancer Immunol. Immunother. *43*, 142–151.

Bermejo, I.A., Usabiaga, I., Compañón, I., Castro-López, J., Insausti, A., Fernández, J.A., Avenoza, A., Busto, J.H., Jiménez-Barbero, J., Asensio, J.L., et al. (2018). Water sculpts the distinctive shapes and dynamics of the tumor-associated carbohydrate Tn antigens: implications for their molecular recognition. J. Am. Chem. Soc. *140*, 9952–9960.

Bhatia, R., Gautam, S.K., Cannon, A., Thompson, C., Hall, B.R., Aithal, A., Banerjee, K., Jain, M., Solheim, J.C., and Kumar, S. (2019). Cancer-associated mucins: role in immune modulation and metastasis. Cancer Metastasis Rev. *38*, 223–236.

Burchell, J., Taylor-Papadimitriou, J., Boshell, M., Gendler, S., and Duhig, T. (1989). A short sequence, within the amino acid tandem repeat of a cancer-associated mucin, contains immunodominant epitopes. Int. J. Cancer *44*, 691–696.

Cai, H., Huang, Z.-H., Shi, L., Sun, Z.-Y., Zhao, Y.-F., Kunz, H., and Li, Y.-M. (2012). Variation of the glycosylation pattern in MUC1 glycopeptide BSA vaccines and its influence on the immune response. Angew. Chem. Int. Ed. *51*, 1719–1723.

Cai, H., Orwenyo, J., Giddens, J.P., Yang, Q., Zhang, R., LaBranche, C.C., Montefiori, D.C., and Wang, L.-X. (2017). Synthetic three-component HIV-1 V3 glycopeptideimmunogens induce glycan-dependent antibody responses. Cell Chem. Biol. *24*, 1513–1522.e4.

Cai, H., Sun, Z.-Y., Chen, M.-S., Zhao, Y.-F., Kunz, H., and Li, Y.-M. (2014). Synthetic multivalent glycopeptide-lipopeptide antitumor vaccines: impact of the cluster effect on the killing of tumor cells. Angew. Chem. Int. Ed. *53*, 1699–1703.

Chan, M., Hayashi, T., Kuy, C.S., Gray, C.S., Wu, C.C.N., Corr, M., Wrasidlo, W., Cottam, H.B., and Carson, D.A. (2009). Synthesis and immunological characterization of toll-like receptor 7 agonistic conjugates. Bioconjug. Chem. *20*, 1194–1200.

Cheever, M.A., Allison, J.P., Ferris, A.S., Finn, O.J., Hastings, B.M., Hecht, T.T., Mellman, I., Prindiville, S.A., Viner, J.L., and Weiner, L.M. (2009). The prioritization of cancer antigens: a national cancer institute pilot project for the acceleration of translational research. Clin. Cancer Res. *15*, 5323–5337.

Chen, X.-Z., Zhang, R.-Y., Wang, X.-F., Yin, X.-G., Wang, J., Wang, Y.-C., Liu, X., Du, J.-J., Liu, Z., and Guo, J. (2019). Peptide-free synthetic nicotine vaccine candidates with α-galactosylceramide as adjuvant. Mol. Pharm. *16*, 1467–1476.

Clough, E.R., Jolivet, M., Audibert, F., Barrwell, J.W., Schlesinger, D.H., and Chedid, L. (1985). Production of anti-sporozoite antibodies in absence of response to carrier by coupling an MDP derivative to a malaria peptide-tetanus toxoid conjugate. Biochem. Biophys. Res. Commun. *131*, 70–76.

Compañón, I., Guerreiro, A., Mangini, V., Castro-López, J., Escudero-Casao, M., Avenoza, A., Busto, J.H., Castillón, S., Jiménez-Barbero, J., Asensio, J.L., et al. (2019). Structure-Based design of potent tumor-associated antigens: modulation of peptide presentation by single-atom O/S or O/Se substitutions at the glycosidic linkage. J. Am. Chem. Soc. *141*, 4063–4072.

Donadei, A., Balocchi, C., Mancini, F., Proietti, D., Gallorini, S., O'Hagan, D.T., D'Oro, U., Berti, F., Baudner, B.C., and Adamo, R. (2016). The adjuvant effect of TLR7 agonist conjugated to a meningococcal serogroup C glycoconjugate vaccine. Eur. J. Pharm. Biopharm. *107*, 110–119.

Dowling, D.J. (2018). Recent advances in the discovery and delivery of TLR7/8 agonists as vaccine adjuvants. Immunohorizons *2*, 185–197.

Du, J.-J., Zou, S.-Y., Chen, X.-Z., Xu, W.-B., Wang, C.-W., Zhang, L., Tang, Y.-K., Zhou, S.-H., Wang, J., Yin, X.-G., et al. (2019). Liposomal antitumor vaccines targeting mucin 1 elicit a lipid-dependent immunodominant response. Chem. Asian J. *14*, 2116–2121.

Dziadek, S., Kowalczyk, D., and Kunz, H. (2005). Synthetic vaccines consisting of tumor-associated MUC1 glycopeptide antigens and bovine serum albumin. Angew. Chem. Int. Ed. *44*, 7624–7630.

Feng, Y., Forsell, M.N.E., Flynn, B., Adams, W., Loré, K., Seder, R., Wyatt, R.T., and KarlssonHedestam, G.B. (2013). Chemical cross-linking of HIV-1 Env for direct TLR7/8 ligand conjugation compromises recognition of conserved antigenic determinants. Virology *446*, 56–65.

Francica, J.R., Lynn, G.M., Laga, R., Joyce, M.G., Ruckwardt, T.J., Morabito, K.M., Chen, M., Chaudhuri, R., Zhang, B., Sastry, M., et al. (2016). Thermoresponsive polymer nanoparticles Co-

deliver RSV F trimers with a TLR-7/8 adjuvant. Bioconjug. Chem. *27*, 2372–2385.

Gaidzik, N., Westerlind, U., and Kunz, H. (2013). The development of synthetic antitumour vaccines from mucinglycopeptide antigens. Chem. Soc. Rev. *42*, 4421–4442.

Gao, D., Liu, Y., Diao, Y., Gao, N., Wang, Z., Jiang, W., and Jin, G. (2015). Synthesis and evaluation of conjugates of novel TLR7 inert ligands as self-adjuvantingimmunopotentiators. ACS Med. Chem. Lett. *6*, 249–253.

Gao, D., Liu, Y., Li, W., Zhong, F., Zhang, X., Diao, Y., Gao, N., Wang, X., Jiang, W., and Jin, G. (2014). Synthesis and immunoregulatory activities of conjugates of a Toll-like receptor 7 inert ligand. Bioorg. Med. Chem. Lett. *24*, 5792–5795.

Gao, D., Zeng, J., Wang, X., Liu, Y., Li, W., Hu, Y., Gao, N., Diao, Y., Wang, Z., Jiang, W., et al. (2016). Conjugation of weak ligands with weak antigens to activate TLR-7: a step toward better vaccine adjuvants. Eur. J. Med. Chem. *120*, 111–120.

Hilf, N., Kuttruff-Coqui, S., Frenzel, K., Bukur, V., Stevanović, S., Gouttefangeas, C., Platten, M., Tabatabai, G., Dutoit, V., van der Burg, S.H., et al. (2019). Actively personalized vaccination trial for newly diagnosed glioblastoma. Nature *565*, 240–245.

Hirabayashi, Y., Hamaoka, A., Matsumoto, M., Matsubara, T., Tagawa, M., Wakabayashi, S., and Taniguchi, M. (1985). Syngeneic monoclonal antibody against melanoma antigen with interspecies cross-reactivity recognizes GM3, a prominent ganglioside of B16 melanoma. J. Biol. Chem. *260*, 13328–13333.

Hoffmann-Röder, A., and Johannes, M. (2011). Synthesis of a MUC1-glycopeptide–BSA conjugate vaccine bearing the 3′-deoxy-3′-fluoro-Thomsen–Friedenreich antigen. Chem. Commun. (Camb.) *47*, 9903–9905.

Hoffmann-Röder, A., Kaiser, A., Wagner, S., Gaidzik, N., Kowalczyk, D., Westerlind, U., Gerlitzki, B., Schmitt, E., and Kunz, H. (2010). Synthetic antitumor vaccines from tetanus toxoid conjugates of MUC1 glycopeptides with the thomsen–Friedenreich antigen and a fluorine-substituted analogue. Angew. Chem. Int. Ed. *49*, 8498–8503.

Hossain, M.K., and Wall, K.A. (2016). Immunological evaluation of recent MUC1 glycopeptide cancer vaccines. Vaccines *4*, 25.

Hossain, M.K., Vartak, A., Karmakar, P., Sucheck, S.J., and Wall, K.A. (2018). Augmenting vaccine immunogenicity through the use of natural human anti-rhamnose antibodies. ACS Chem. Biol. *13*, 2130–2142.

Ingale, S., Wolfert, M.A., Gaekwad, J., Buskas, T., and Boons, G.-J. (2007). Robust immune responses elicited by a fully synthetic three-component vaccine. Nat. Chem. Biol. *3*, 663–667.

Kaiser, A., Gaidzik, N., Becker, T., Menge, C., Groh, K., Cai, H., Li, Y.-M., Gerlitzki, B., Schmitt, E., and Kunz, H. (2010). Fully synthetic vaccines consisting of tumor-associated MUC1 glycopeptides and a lipopeptide ligand of the toll-like Receptor 2. Angew. Chem. Int. Ed. *49*, 3688–3692.

Karsten, U., Diotel, C., Klich, G., Paulsen, H., Goletz, S., Müller, S., and Hanisch, F.-G. (1998). Enhanced binding of antibodies to the DTR motif of MUC1 tandem repeat peptide is mediated by site-specific glycosylation. Cancer Res. *58*, 2541–2549.

Keskin, D.B., Anandappa, A.J., Sun, J., Tirosh, I., Mathewson, N.D., Li, S., Oliveira, G., Giobbie-Hurder, A., Felt, K., Gjini, E., et al. (2019). Neoantigen vaccine generates intratumoral T cell responses in phase Ibglioblastoma trial. Nature *565*, 234–239.

Kim, W.G., Choi, B., Yang, H.-J., Han, J.-A., Jung, H., Cho, H., Kang, S., and Hong, S.Y. (2016). Covalent conjugation of small-molecule adjuvants to nanoparticles induces robust cytotoxic T cell responses via DC activation. Bioconjug. Chem. *27*, 2007–2013.

Lee, H.-Y., Chen, C.-Y., Tsai, T.-I., Li, S.-T., Lin, K.-H., Cheng, Y.-Y., Ren, C.-T., Cheng, T.-J.R., Wu, C.-Y., and Wong, C.-H. (2014). Immunogenicity study of globo H analogues with modification at the reducing or nonreducingend of the tumor antigen. J. Am. Chem. Soc. *136*, 16844–16853.

Liu, Y., Zhang, W., He, Q., Yu, F., Song, T., Liu, T., Zhang, Z., Zhou, J., Wang, P.G., and Zhao, W. (2016). Fully synthetic self-adjuvanting MUC1-fibroblast stimulating lipopeptide 1 conjugates as potential cancer vaccines. Chem. Commun.(Camb.) *52*, 10886–10889.

Liu, Z., and Guo, J. (2017). NKT-cell glycolipid agonist as adjuvant in synthetic vaccine. Carbohydr. Res. *452*, 78–90.

Lloyd, K.O., Burchell, J., Kudryashov, V., Yin, B.W.T., and Taylor-Papadimitriou, J. (1996). Comparison of O-linked carbohydrate chains in MUC-1 mucin from normal breast epithelial cell lines and breast carcinoma cell lines: DEMONSTRATION OF SIMPLER and FEWERGLYCANCHAINS IN tumor cells. J. Biol. Chem. *271*, 33325–33334.

Lynn, G.M., Chytil, P., Francica, J.R., Lagová, A., Kueberuwa, G., Ishizuka, A.S., Zaidi, N., Ramirez-Valdez, R.A., Blobel, N.J., Baharom, F., et al. (2019). Impact of polymer-TLR-7/8 agonist (adjuvant) morphology on the potency and mechanism of CD8 T cell induction. Biomacromolecules *20*, 854–870.

Lynn, G.M., Laga, R., Darrah, P.A., Ishizuka, A.S., Balaci, A.J., Dulcey, A.E., Pechar, M., Pola, R., Gerner, M.Y., Yamamoto, A., et al. (2015). In vivo characterization of the physicochemical properties of polymer-linked TLR agonists that enhance vaccine immunogenicity. Nat. Biotechnol. *33*, 1201–1210.

Martínez-Sáez, N., Peregrina, J.M., and Corzana, F. (2017). Principles of mucin structure: implications for the rational design of cancer vaccines derived from MUC1-glycopeptides. Chem. Soc. Rev. *46*, 7154–7175.

Miermont, A., Barnhill, H., Strable, E., Lu, X., Wall, K.A., Wang, Q., Finn, M.G., and Huang, X. (2008). Cowpea mosaic virus capsid: a promising carrier for the development of carbohydrate based antitumor. Vaccin. Chem. Eur. J. *14*, 4939–4947.

Oberbillig, T., Mersch, C., Wagner, S., and Hoffmann-Röder, A. (2012). Antibody recognition of fluorinated MUC1 glycopeptide antigens. Chem. Commun.(Camb.) *48*, 1487–1489.

Oh, J.Z., and Kedl, R.M. (2010). The capacity to induce cross-presentation dictates the success of a TLR7 agonist-conjugate vaccine for eliciting cellular immunity. J. Immunol. *185*, 4602–4608.

Ott, P.A., Hu, Z., Keskin, D.B., Shukla, S.A., Sun, J., Bozym, D.J., Zhang, W., Luoma, A., Giobbie-Hurder, A., Peter, L., et al. (2017). An immunogenic personal neoantigen vaccine for patients with melanoma. Nature *547*, 217–221.

Renaudet, O., BenMohamed, L., Dasgupta, G., Bettahi, I., and Dumy, P. (2008). Towards a self-adjuvanting multivalent B and T cell epitope containing synthetic glycolipopeptide cancer vaccine. ChemMedChem *3*, 737–741.

Renaudet, O., Dasgupta, G., Bettahi, I., Shi, A., Nesburn, A.B., Dumy, P., and BenMohamed, L. (2010). Linear and branched glyco-lipopeptide vaccines Follow distinct cross-presentation pathways and generate different magnitudes of antitumor immunity. PLoS One *5*, e11216.

Rivalland, G., Loveland, B., and Mitchell, P. (2015). Update on Mucin-1 immunotherapy in cancer: a clinical perspective. Expert Opin. Biol. Ther. *15*, 1773–1787.

Sahin, U., Derhovanessian, E., Miller, M., Kloke, B.-P., Simon, P., Löwer, M., Bukur, V., Tadmor, A.D., Luxemburger, U., Schrörs, B., et al. (2017). Personalized RNA mutanome vaccines mobilize poly-specific therapeutic immunity against cancer. Nature *547*, 222–226.

Shinchi, H., Crain, B., Yao, S., Chan, M., Zhang, S.S., Ahmadiiveli, A., Suda, Y., Hayashi, T., Cottam, H.B., and Carson, D.A. (2015). Enhancement of the immunostimulatory activity of a TLR7 ligand by conjugation to polysaccharides. Bioconjug. Chem. *26*, 1713–1723.

Singh, R., and Bandyopadhyay, D. (2007). MUC1: a target molecule for cancer therapy. Cancer Biol. Ther. *6*, 481–486.

Song, C., Zheng, X.-J., Liu, C.-C., Zhou, Y., and Ye, X.-S. (2017). A cancer vaccine based on fluorine-modified sialyl-Tn induces robust immune responses in a murine model. Oncotarget *8*, 47330–47343.

Straßburger, D., Glaffig, M., Stergiou, N., Bialas, S., Besenius, P., Schmitt, E., and Kunz, H. (2018). Synthetic MUC1 antitumor vaccine with incorporated 2,3-sialyl-T carbohydrate antigen inducing strong immune responses with isotypespecificity. ChemBioChem *19*, 1142–1146.

Tang, C.-K., Katsara, M., and Apostolopoulos, V. (2008). Strategies used for MUC1 immunotherapy: human clinical studies. Expert Rev. Vaccin. *7*, 963–975.

Tang, J., Pearce, L., O'Donnell-Tormey, J., and Hubbard-Lucey, V.M. (2018). Trends in the global immuno-oncology landscape. Nat. Rev. Drug Discov. *17*, 783.

Toyokuni, T., Hakomori, S.-i., and Singhal, A.K. (1994). Synthetic carbohydrate vaccines: synthesis and immunogenicity of Tn antigen conjugates. Bioorg. Med. Chem. *2*, 1119–1132.

Van Herck, S., Deswarte, K., Nuhn, L., Zhong, Z., Portela Catani, J.P., Li, Y., Sanders, N.N., Lienenklaus, S., De Koker, S., Lambrecht, B.N., et al. (2018). Lymph-node-targeted immune activation by engineered block copolymer amphiphiles–TLR7/8 agonist conjugates. J. Am. Chem. Soc. *140*, 14300–14307.

Wang, F., Li, Q., Ni, W., Fang, F., Sun, X., Xie, F., Wang, J., Wang, F., Gao, S., and Tai, G. (2013). Expression of human full-length MUC1 inhibits the proliferation and migration of a B16 mouse melanoma cell line. Oncol. Rep. *30*, 260–268.

Wang, H., Yang, B., Wang, Y., Liu, F., Fernández-Tejada, A., and Dong, S. (2019). β-Glucan as an immune activator and a carrier in the construction of a synthetic MUC1 vaccine. Chem. Commun.(Camb.) *55*, 253–256.

Wang, Q., Zhou, Z., Tang, S., and Guo, Z. (2012). Carbohydrate-monophosphoryl lipid A conjugates are fully synthetic self-adjuvanting cancer vaccines eliciting robust immune responses in the mouse. ACS Chem. Biol. *7*, 235–240.

Wilkinson, B.L., Day, S., Malins, L.R., Apostolopoulos, V., and Payne, R.J. (2011). Self-adjuvanting multicomponent cancer vaccine candidates combining per-glycosylated MUC1 glycopeptides and the toll-like receptor 2 agonist Pam3CysSer. Angew. Chem. Int. Ed. *50*, 1635–1639.

Wilkinson, B.L., Malins, L.R., Chun, C.K.Y., and Payne, R.J. (2010). Synthesis of MUC1–lipopeptide chimeras. Chem. Commun.(Camb.) *46*, 6249–6251.

Wu, C.C.N., Hayashi, T., Takabayashi, K., Sabet, M., Smee, D.F., Guiney, D.D., Cottam, H.B., and Carson, D.A. (2007). Immunotherapeutic activity of a conjugate of a Toll-like receptor 7 ligand. Proc. Natl. Acad. Sci. U S A *104*, 3990–3995.

Wu, J.-J., Li, W.-H., Chen, P.-G., Zhang, B.-D., Hu, H.-G., Li, Q.-Q., Zhao, L., Chen, Y.-X., Zhao, Y.-F., and Li, Y.-M. (2018a). Targeting STING with cyclic di-GMP greatly augmented immune responses of glycopeptide cancer vaccines. Chem. Commun.(Camb.) *54*, 9655–9658.

Wu, X., Yin, Z., McKay, C., Pett, C., Yu, J., Schorlemer, M., Gohl, T., Sungsuwan, S., Ramadan, S., Baniel, C., et al. (2018b). Protective epitope discovery and design of MUC1-based vaccine for effective tumor protections in immunotolerant mice. J. Am. Chem. Soc. *140*, 16596–16609.

Xiao, A., Zheng, X.-J., Song, C., Gui, Y., Huo, C.-X., and Ye, X.-S. (2016). Synthesis and immunological evaluation of MUC1 glycopeptide conjugates bearing N-acetyl modified STn derivatives as anticancer vaccines. Org. Biomol. Chem. *14*, 7226–7237.

Yin, X.-G., Chen, X.-Z., Sun, W.-M., Geng, X.-S., Zhang, X.-K., Wang, J., Ji, P.-P., Zhou, Z.-Y., Baek, D.J., Yang, G.-F., et al. (2017). IgG antibody response elicited by a fully synthetic two-component carbohydrate-based cancer vaccine candidate with α-galactosylceramide as built-in adjuvant. Org. Lett. *19*, 456–459.

Yin, Z., Wu, X., Kaczanowska, K., Sungsuwan, S., ComellasAragones, M., Pett, C., Yu, J., Baniel, C., Westerlind, U., Finn, M.G., et al. (2018). Antitumor humoral and T cell responses by mucin-1 conjugates of bacteriophage Qβ in wild-type mice. ACS Chem. Biol. *13*, 1668–1676.

Yoo, E., Salyer, A.C.D., Brush, M.J.H., Li, Y., Trautman, K.L., Shukla, N.M., De Beuckelaer, A., Lienenklaus, S., Deswarte, K., Lambrecht, B.N., et al. (2018). Hyaluronic acid conjugates of TLR7/8 agonists for targeted delivery to secondary lymphoid tissue. Bioconjug.Chem. *29*, 2741–2754.

Zhu, J., Wan, Q., Lee, D., Yang, G., Spassova, M.K., Ouerfelli, O., Ragupathi, G., Damani, P., Livingston, P.O., and Danishefsky, S.J. (2009). From synthesis to biologics: preclinical data on a chemistry derived anticancer vaccine. J. Am. Chem. Soc. *131*, 9298–9303.

iScience, Volume *23*

Supplemental Information

Multifunctional Protein Conjugates with Built-in Adjuvant (Adjuvant-Protein-Antigen) as Cancer Vaccines Boost Potent Immune Responses

Jing-Jing Du, Chang-Wei Wang, Wen-Bo Xu, Lian Zhang, Yuan-Kai Tang, Shi-Hao Zhou, Xiao-Fei Gao, Guang-Fu Yang, and Jun Guo

Table of contents

Transparent Methods

1. General information

Fmoc L-amino acids and pre-loaded resins were purchased from Nova Biochem. Anhydrous dichloromethane (DCM) was obtained from the drying solvent system (passed through CaH_2) and can be used without further drying. The purchased anhydrous dimethylformamide (DMF) was stored over 4Å molecular sieves. Ethylene glycol monomethyl ether, potassium carbonate, trichloromethane, methanol, sodium hydroxide, piperidine, hydrazine hydrate, potassium bicarbonate, sodium borate, sodium methyl 4-(bromomethyl) benzoate and bromine were purchased from Sinopharm Chemical Reagent (Shanghai, China). Benzotriazol-1-yl-oxytripyrrolidinophosphonium hexafluorophosphate (PyBOP), trifluoroacetic acid (TFA), *O*-(7-azabenzotriazol-1-yl)-*N,N,N′,N′*-tetramethyluronium hexafluorophosphate (HATU), 1-hydroxy-7-azabenzotriazole (HOAt), 1-hydroxybenzotriazole (HOBt), *N*-hydroxysuccinimide (NHS) and 1-ethyl-3-(3-dimethylaminopropyl)carbodiimide (EDCI) were purchased from Bidepharm (Shanghai, China). *N,N*-Diisopropylethylamine (DIPEA), *N*-methylpyrrolidone (NMP), triisopropylsilane (TIPS) and diethyl squarate were purchased from Energy Chemical (Shanghai, China). Bovine serum albumin (BSA) and aluminum hydroxide (alum) were purchased from Thermo Fisher Scientific Inc. Monophosphoryl Lipid A (MPLA) was purchased from Avanti Polar Lipids, Inc. Pam_3CSK_4 was prepared according to the reported procedure (Chen et al., 2019; Du et al., 2019). Peroxidase-conjugated Affinipure goat anti-mouse kappa antibody IgG (RRID: AB_10015289), IgM (RRID: AB_2338502), and Alexa Fluor® 488-conjugated Affinipure goat anti-mouse IgG (H+L) (RRID: AB_2338840) were purchased from Jackson ImmunoResearch Labs. Peroxidase-conjugated Affinipure goat anti-mouse kappa IgG1, IgG2a, IgG2b, IgG3, IgA and IgE antibodies were purchased from SouthernBiotech. All ^{1}H and ^{13}C-NMR spectra were recorded on Bruker 400 MHz or 600 MHz FT-NMR spectrometers, their signals in deuterated solvents are given δ values from tetramethylsilane (TMS) as an internal standard. Semi-preparative HPLC separations were performed on an Agilent 1260 infinity II prime LC system equipped with a C18 column (Agilent, 250 × 9.4 mm, 5 μm) with a binary mixture of solvent A (100% water with 0.1% trifluoroacetic acid) and solvent B (100% acetonitrile HPLC-grade with 0.1% trifluoroacetic acid) as the mobile phase (flow rates of 4.0 mL/min). UV absorption signals were detected with an UV detector at wavelength of 190-400 nm. The high-resolution mass spectrometry (HRMS) were measured on a Shimadzu LCMS-IT-TOF mass spectrometer or DIONEX UltiMate 3000 & Bruker Compact TOF mass spectrometer by ESI. Matrix-assisted laser desorption/ionization time of flight (MALDI-TOF) MS was performed on an AB SCIEX 5800 spectrometer (Shimadzu AXIMA Assurance).

2. Experimental procedures

a.Synthesis of TLR7 agonist

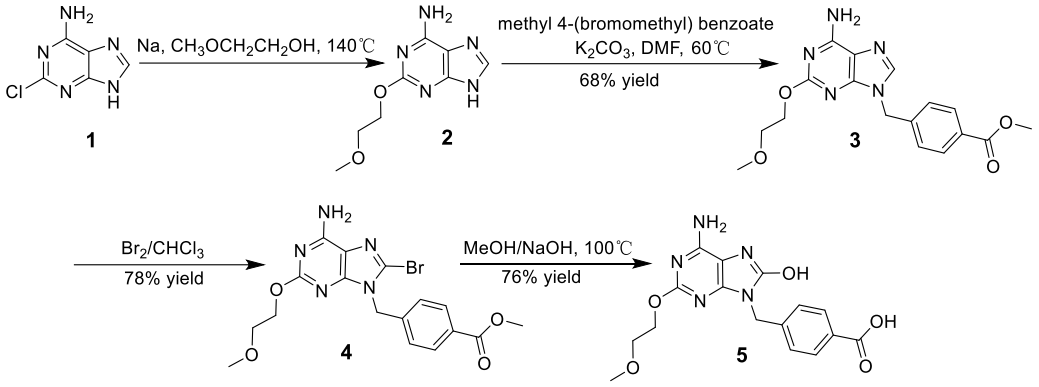

Scheme S1. Synthetic route to TLR7 agonist (Gao et al., 2015). Related to Scheme 2.

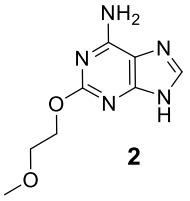

Synthesis of compound 2 (Gao et al., 2015)**.** The sodium salt of ethylene glycol monomethyl ether was prepared by dissolving sodium (4.9 g, 212 mmol) metal in ethylene glycol methyl ether (235 mL, 29.5 mol), and the 2-chloroadenine (**1**) (5.0 g, 29.6 mmol) was added at 140 °C. The reaction mixture was heated for 8 h at this temperature and then cooled to 0 °C, the residue was quenched with 1 M HCl, and concentrated. The crude product was directly applied for next step reaction without purification.

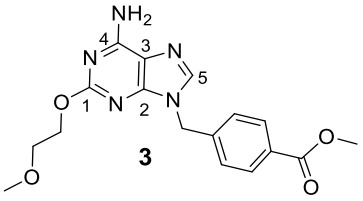

Synthesis of compound 3 (Gao et al., 2015)**.** To a solution of compound **2** (700 mg, 3.34 mmol) in DMF (40 mL) were added methyl 4-(bromomethyl) benzoate (1.5 g, 6.68 mmol) and K_2CO_3 (3.2 g, 23.44 mmol), and stirred for 8 h at 60 °C. The reaction mixture was quenched with 5% citric acid (250 mL), diluted with water (20 mL) and extracted with $CHCl_3$ (3×100 mL), the organic layer was washed with brine, dried ($MgSO_4$), and concentrated. The crude product was purified by silica gel column chromatography (MeOH/DCM = 1:50) to provide compound **3** as a white solid (809 mg, 68%). R_f 0.25 (MeOH/DCM = 1/25). ^{1}H NMR (400 MHz, DMSO-d_6) δ (ppm) 8.10 (s, 1H), 7.95 (d, J =

8.0 Hz, 2H, 2×Ph), 7.42 (d, *J* = 8.1 Hz, 2H, 2×Ph), 7.30 (s, 2H, NH_2), 5.38 (s, 2H, -CH_2-Ph), 4.32 (t, *J* = 4.7 Hz, 2H, CH_2-O), 3.85 (s, 3H, CH_3-O), 3.61 (t, *J* = 4.7 Hz, 2H, CH_2-O), 3.28 (s, 3H, CH_3-O). ^{13}C NMR (100 MHz, DMSO-*d*$_6$) δ (ppm) 166.4 (C=O), 161.8 (C_1), 157.2 (C_4), 151.6 (C_2), 142.9 (C_5), 140.0, 130.0, 129.3, 128.2 (benzene), 115.5 (C_3), 70.7 (O-$\underline{C}H_2$-), 65.8 (-$\underline{C}H_2$-O), 58.5 (-O$\underline{C}H_3$), 52.6 (-O$\underline{C}H_3$), 46.1 (-$\underline{C}H_2$-Ph). HRMS (ESI) calculated for $C_{17}H_{19}N_5O_4$ $[M+H]^+$: 358.1510, found: 358.1513.

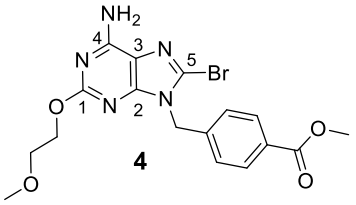

4

Synthesis of compound 4 (Gao et al., 2015)**.** To a solution of compound **3** (800 mg, 2.2 mmol) in $CHCl_3$ (40 mL) was added bromine (227 μL, 4.4 mmol) at room temperature (rt). The mixture was stirred at rt for 8 h. The residue was quenched with saturated $Na_2S_2O_3$ (25 mL), diluted with water (5 mL) and extracted with $CHCl_3$ (3×25 mL). The organic layer was washed with brine, dried (Na_2SO_4), and concentrated. The crude product was purified with silica gel column chromatography (MeOH/DCM = 1/60) to give the product as a white solid (747 mg, 78%). R_f 0.6 (MeOH/DCM = 1/25). ^{1}H NMR (400 MHz, DMSO-*d*$_6$) δ (ppm): 7.96 (d, *J* = 8.1 Hz, 2H, 2×Ph), 7.50 (s, 2H, NH_2), 7.36 (d, *J* = 8.1 Hz, 2H, 2×Ph), 5.36 (s, 2H, -CH_2-Ph), 4.33 (t, *J* = 4.7 Hz, 2H, CH_2-O), 3.85 (s, 3H, CH_3-O), 3.61 (t, *J* = 4.7 Hz, 2H, CH_2-O), 3.29 (s, 3H, CH_3-O). ^{13}C NMR (100 MHz, DMSO-*d*$_6$) δ (ppm): 166.3 (C=O), 161.8 (C_1), 156.2 (C_4), 152.9 (C_2), 141.7, 130.1, 129.5, 127.8 (Ph), 124.2 (C_5), 115.8 (C_3), 70.6 (O-$\underline{C}H_2$-), 66.0 (-$\underline{C}H_2$-O), 58.5 (-O$\underline{C}H_3$), 52.6 (-O$\underline{C}H_3$), 46.5 ($\underline{C}H_2$-Ph). HRMS (ESI) calculated for $C_{17}H_{18}BrN_5O_4$ $[M+H]^+$: 436.0615, found: 436.0619.

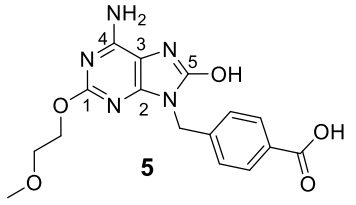

5

Synthesis of compound 5 (Gao et al., 2015)**.** To a solution of compound **4** (500 mg) was added to MeOH/NaOH (6 M NaOH, v/v = 1/4, 200 mL) at 100 °C. The mixture was stirred at rt for 4 h, neutralized with aqueous 1 N HCl aq., and filtrated. The product was purified with silica gel column chromatography (MeOH/DCM = 1/10 with 0.1% HOAc) to give desired product as a white solid (313 mg, 76%). R_f 0.6 (MeOH/DCM = 1/9 with 0.1% HOAc). ^{1}H NMR (400 MHz, DMSO-*d*$_6$) δ (ppm): 10.09 (s, 1H, CO_2H), 7.90 (d, *J* = 7.9 Hz, 2H, 2×Ph), 7.37 (d, *J* = 7.9 Hz, 2H, 2×Ph), 6.53 (s, 2H, NH_2), 4.92 (s, 2H, -CH_2-Ph), 4.24 (t, *J* = 4.7 Hz, 2H, CH_2-O), 3.56 (t, *J* = 4.8 Hz, 2H, CH_2-O), 3.25 (s, 3H, CH_3-O). ^{13}C NMR (100 MHz, DMSO-*d*$_6$) δ (ppm): 167.5 (C=O), 160.3 (C_1), 152.7 (C_4), 149.5 (C_2), 148.2 (C_5), 142.4, 130.4, 130.0, 127.9 (Ph), 98.8 (C_3), 70.6 (O-$\underline{C}H_2$-), 65.7 (-$\underline{C}H_2$-O), 58.5 (-

O<u>C</u>H$_3$), 42.6 (-<u>C</u>H$_2$-Ph). HRMS (ESI) calculated for $C_{16}H_{17}N_5O_5$ $[M+H]^+$: 360.1302, found: 360.1304.

b. General procedure for peptides synthesis

MUC1 glycopeptides were synthesized according to the Fmoc-strategy SPPS starting from Rink amide AM resin (Du et al., 2016; Du et al., 2019). The natural amino acids (3 Eq.) were coupled using PyBOP (78 mg, 0.15 mmol, 3 Eq.) and DIPEA (53 μL, 0.3 mmol, 6 Eq.) in DMF for 1 h. The Fmoc-glycosyl amino acid (Tn antigen) (1.5 Eq.) was coupled using HATU (1.5 Eq.), HOAt (1.5 Eq.) and DIPEA (3 Eq.) in DMF for 4 h, residual free amines were acetylated with capping reagents. The linker of MUC1-glycopeptide with a squaric acid diethyl ester or biotin moiety at the *N*-terminus was achieved by treatment with DIPEA (5 Eq.) or HATU (3 Eq.), HOAt (3 Eq.) and DIPEA (6 Eq.) in DMF for 2 h. After completion of the glycopeptide assembly, the *N*-terminal Fmoc protecting groups or acetyl moieties of glycosyl amino acids were removed using 20% piperidine in DMF or approximately 30% hydrazine in DMF and MeOH. Next, the resin was treated with the cleavage cocktail (trifluoroacetic acid 95%, triisopropylsilane 2.5%, water 2.5%, 10 mL) for 2 h. The resin was filtered, washed three times with trifluoroacetic acid, the residue was concentrated and precipitated with diethyl ether, the crude MUC1 glycopeptides were purified by semi-preparative HPLC and identified with HRMS.

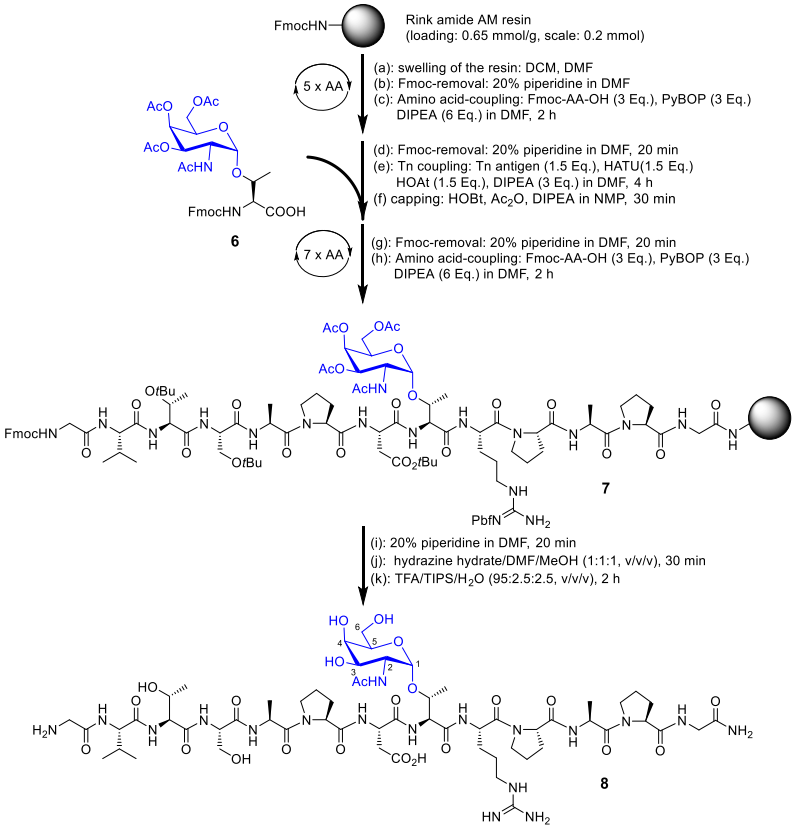

Scheme S2. Synthetic route to MUC1 glycopeptide **8**. Related to Scheme 2.

Synthesis of MUC1 glycopeptide 8. MUC1 glycopeptide **8** was synthesized following the Fmoc-SPPS strategy, which was purified by semipreparative HPLC, and the appropriate fractions were lyophilized to afford pure product. Aanalytical HPLC trace of MUC1 glycopeptide **8** (28 mg, 42% yield) (column: Agilent C18), gradient: water/acetonitrile + 0.1% TFA, 0.0 min (95:5) → 15.0 min (10:90) → 20.0 min (0:100) → 20.1 min (95:5) → 30 min (95:5), R_t = 6.699 min. HRMS spectra of MUC1 glycopeptide **8**. HRMS (ESI) calculated for $C_{59}H_{98}N_{18}O_{23}$ $[M+H+Na]^{2+}$: 725.3509, found: 725.3215. ^{1}H NMR (600 MHz, D_2O) δ (ppm): 4.87 (d, 1H, H_1), 4.64–4.63 (m, 2H, D_α, R_α), 4.59–4.57 (m, 2H, 2×A_α), 4.54–4.43 (m, 6H, 3×P_α, S_α, 2×T_α), 4.29–4.27 (m, 1H, V_α), 4.11–4.09 (m, 4H, 2×T_β), 4.05–4.02 (m, 1H, H_3), 3.99–3.88 (m, 5H, 2×G_α, H_5), 3.86–3.63 (m, 12H, S_β, 3×P_δ, H_2, H_4, H_6), 3.50–3.23 (m, 2H, R_δ), 2.96–2.79 (m, 2H, D_β), 2.34–2.29 (m, 3H, 3×$P_{\beta1}$), 2.16–2.08 (m, 1H, V_β), 2.05–2.01 (m, 6H, 3×$P_{\beta2}$, Ac-NH), 2.00–1.87 (m, 6H, 3×P_γ), 1.73–1.71 (m, 4H, R_β, R_γ), 1.42–1.33 (m, 6H, 2×A_β), 1.27–1.23 (m, 6H, 2×T_γ), 0.99–0.97 (m, 6H, V_γ). ^{13}C NMR (150 MHz, D_2O) δ (ppm): 174.7, 174.0, 173.7, 173.7, 173.4, 173.4, 173.1, 173.0, 172.6, 171.4, 171.0, 170.9, 170.7, 167.2, 163.0 (15×C=O), 156.6, 98.5, 75.3, 71.3, 68.4, 67.9, 67.9, 66.9, 61.2, 60.9, 60.6, 60.2, 59.8, 59.5, 58.8, 57.0, 55.1, 51.1, 50.2, 49.5, 47.8, 47.7, 47.6, 47.5, 41.9, 40.4, 40.2, 36.3, 30.0, 29.3, 29.2, 29.1, 27.2, 24.6, 24.5, 24.5, 24.0, 22.2 (Ac-NH), 18.6, 18.3, 17.3, 15.4, 15.0.

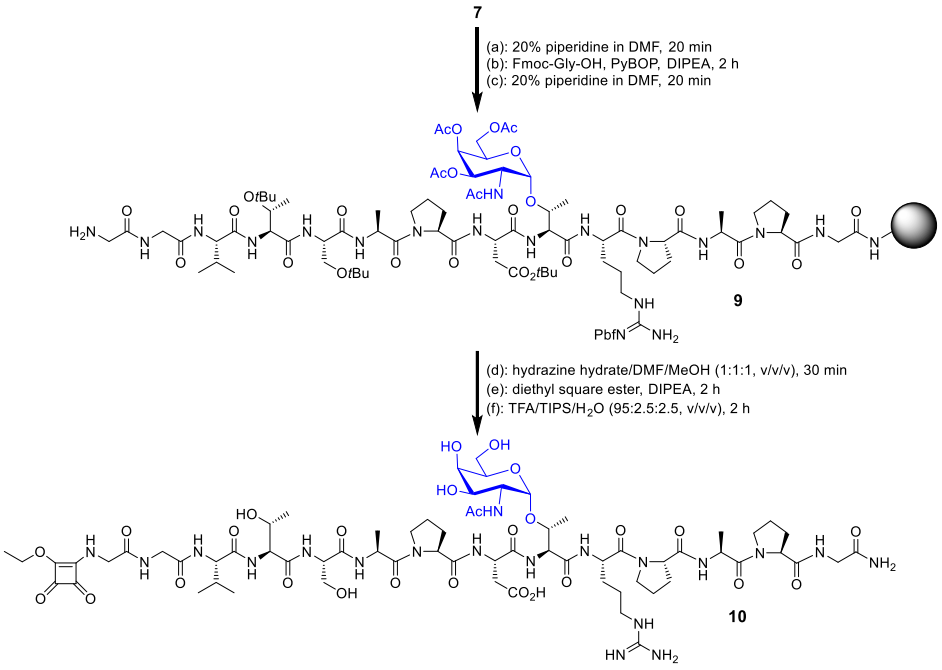

Scheme S3. Synthetic route to MUC1 glycopeptide squaric acid monoamide **10**. Related to Scheme 2.

Synthesis of MUC1 glycopeptide squaric acid monoamide 10. MUC1 glycopeptide squaric acid monoamide **10** was synthesized following the Fmoc-SPPS strategy, which was purified by semipreparative HPLC, and the appropriate fractions were lyophilized to

afford pure product. Analytical HPLC trace of MUC1 glycopeptide squaric acid monoamide **10** (26 mg, 51% yield) (column: Agilent C18, gradient: water/acetonitrile + 0.1% TFA, 0.0 min (95:5) → 15.0 min (10:90) → 20.0 min (0:100) → 20.1 min (95:5) → 30 min (95:5), R_t = 7.152 min. HRMS spectra of MUC1 glycopeptide squaric acid monoamide **10** HRMS (ESI) calculated for $C_{67}H_{105}N_{19}O_{27}$ $[M+H+Na]^{2+}$: 816.3713. found: 816.3729. ^{1}H NMR (600 MHz, CD_3OD) δ (ppm): 4.81 (d, 1H, H_1), 4.77–4.71 (m, 2H, D_α, R_α), 4.63–4.56 (m, 2H, 2×A_α), 4.48–4.45 (m, 2H, -CH_2-), 4.43–4.34 (m, 6H, P_α, S_α, 2×T_α), 4.23–4.21 (m, 2H, V_α), 4.17 (m, 4H, 2×T_β), 4.12–4.08 (m, 1H, H_3), 3.99–3.83 (m, 7H, 3×G_α, H_5), 3.81–3.60 (m, 12H, S_β, 3×P_δ, H_2, H_4, H_6), 3.26–3.17 (m, 2H, R_δ), 2.95–2.83 (m, 3H, D_β), 2.27–2.20 (m, 3H, 3×$P_{\beta1}$), 2.13–2.11 (m, 1H, V_β), 2.07–1.99 (m, 6H, 3×$P_{\beta2}$, Ac-NH), 1.99–1.86 (m, 6H, 3×P_γ), 1.70–1.67 (m, 4H, R_β, R_γ), 1.47–1.43 (m, 3H, CH_3-), 1.42–1.33 (m, 6H, 2×A_β), 1.26–1.18 (m, 6H, 2×T_γ), 1.00–0.98 (m, 6H, V_γ). ^{13}C NMR (150 MHz, CD_3OD) δ (ppm): 188.9, 183.7, 177.4, 174.2, 173.7, 173.5, 173.1, 173.0, 173.0, 172.6, 172.6, 172.2, 172.0, 172.0, 171.9, 170.8, 170.6, 170.6, 170.3, 160.7, 160.4, 157.1, 98.5, 74.2, 71.6, 69.5, 69.5, 68.8, 68.7, 66.6, 61.4, 61.3, 60.7, 59.8, 56.9, 56.3, 56.1, 56.0, 55.9, 55.7, 55.3, 50.5, 50.5, 50.0, 49.8, 48.1, 46.0, 42.0, 41.8, 40.6, 34.7, 30.0, 29.1, 29.0, 28.9, 27.9, 24.7, 24.7, 24.5, 24.4, 22.0 (Ac-NH), 18.3, 18.1, 17.3, 15.7, 15.3.

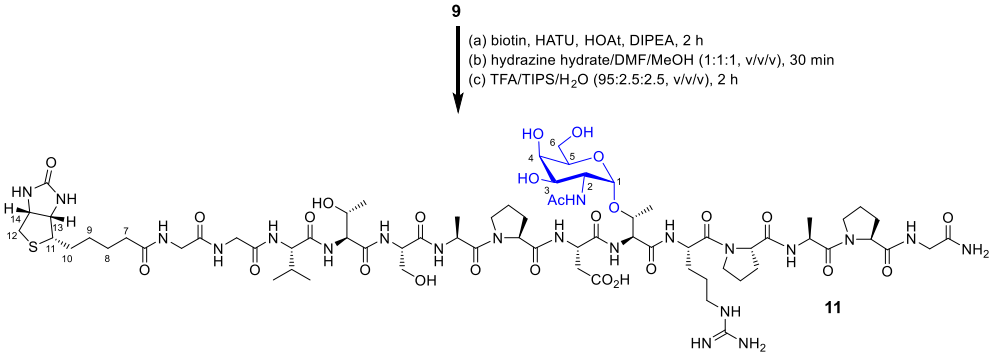

Scheme S4. Synthetic route to biotin-MUC1 glycopeptide **11**. Related to Figures 3 and 4.

Synthesis of biotin-MUC1 glycopeptide 11. Biotin-MUC1 glycopeptide **11** was synthesized following the Fmoc-SPPS strategy, which was purified by semipreparative HPLC, and the appropriate fractions were lyophilized to afford pure product. Analytical HPLC trace of compound **11** (26 mg, 46% yield) (column: Agilent C18, gradient: water/acetonitrile + 0.1% TFA, 0.0 min (95:5) → 15.0 min (40:60) → 15.1 min (95:5), → 20.0 min (95:5), R_t = 8.498 min. HRMS spectra of biotin-MUC1 glycopeptide **11** HRMS (ESI) calculated for $C_{71}H_{115}N_{21}O_{26}S$ $[M+2Na]^{2+}$: 877.8914, found: 877.8908. ^{1}H NMR (600 MHz, CD_3OD) δ (ppm): 4.80 (d, 1H, H_1), 4.77–4.74 (m, 2H, H_{13}, H_{14}), 4.62–4.55 (m, 4H, 2×A_α, D_α, R_α), 4.51–4.41 (m, 6H, 3×P_α, S_α, 2×T_α), 4.37–4.25 (m, 5H, V_α, 2×T_β), 4.21–4.19 (m, 1H, H_3), 4.00–3.87 (m, 7H, 3×G_α, H_5), 3.87–3.65 (m, 12H, S_β, 3×P_δ, H_2, H_4, H_6), 3.65–3.60 (m, 1H, H_{13}), 3.24–3.18 (m, 2H, R_δ), 2.95–2.91 (m, 2H, D_β), 2.87–2.69 (m, 2H, H_{12}), 2.32–2.29 (m, 2H, H_7), 2.26–2.18 (m, 3H, 3×$P_{\beta1}$), 2.12–2.10 (m, V_β), 2.05–1.87 (m, 12H,

3×$P_{\beta 2}$, Ac-NH, 3×P_{γ}), 1.87–1.84 (m, 1H, $H_{10'}$), 1.75–1.73 (m, 2H, H_8), 1.70–1.67 (m, 4H, R_{β}, R_{γ}), 1.48–1.46 (m, 2H, H_9), 1.41–1.34 (m, 6H, 2×A_{β}), 1.33–1.30 (m, 1H, $H_{10'}$), 1.25–1.20 (m, 6H, 3×T_{γ}), 1.01–0.98 (m, 6H, V_{γ}). ^{13}C NMR (150 MHz, CD_3OD) δ (ppm): 176.7, 174.7, 174.3, 174.2, 174.2, 173.9, 173.8, 173.8, 173.4, 173.3, 173.1, 172.4, 172.1, 172.1, 171.9, 171.8, 171.5, 165.9, 158.3, 99.8, 75.4, 72.8, 70.0, 69.9, 67.8, 63.0, 62.5, 61.9, 61.4, 61.1, 61.0, 60.2, 58.1, 57.4, 57.2, 57.1, 56.9, 56.7, 56.5, 54.4, 51.8, 51.2, 51.0, 49.7, 49.3, 43.6, 43.4, 43.0, 41.8, 40.8, 36.2, 35.9, 31.1, 30.3, 30.2, 30.1, 29.4, 29.2, 26.3, 25.9, 25.9, 25.7, 25.6, 23.2 (Ac-NH), 19.8, 19.5, 18.7, 16.5, 16.5.

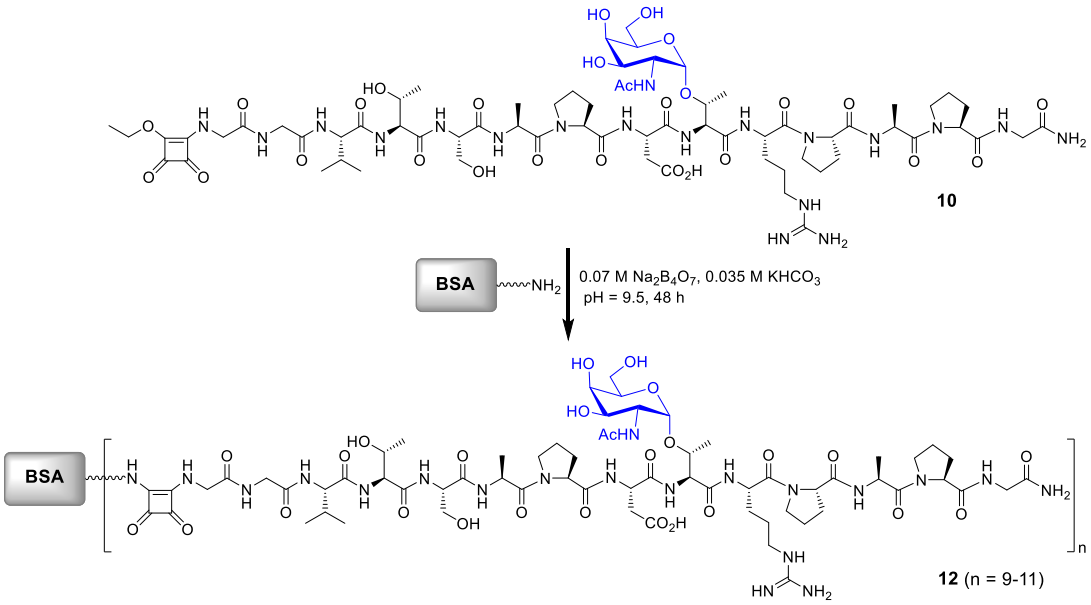

Scheme S5. The synthetic route of BSA-MUC1 conjugate **12**. Related to Scheme 2.

Synthesis of BSA-MUC1 conjugate 12. The glycopeptide squaric acid monoamide **10** (48.4 mg, 0.03 mmol) and BSA (40 mg, 0.6 μmol) were dissolved in 5 mL 0.07 M $Na_2B_4O_7$/0.035 M $KHCO_3$ buffer solution at pH = 9.5. The reaction mixture was stirred at rt for 48 h. The BSA-MUC1 conjugate was purified by size-exclusion gel filtration (Millipore UFC910096 15 M, 10 KD), and lyophilized. The average capacity of MUC1 on BSA was estimated by MALDI-TOF-MS.

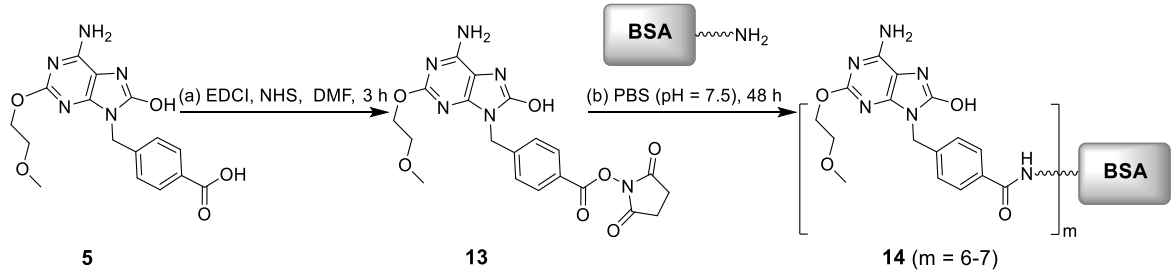

Scheme S6. The synthetic route of TLR7a-BSA conjugate **14**. Related to Scheme 2.

Synthesis of TLR7a-BSA conjugate 14. To a solution of compound **5** (11.2 mg, 0.03 mmol) in DMF (1 mL) were added EDCI (17.2 mg, 0.09 mmol) and NHS (10.3 mg, 0.09 mmol), and the reaction mixture was shaken for 3 h. Then a mixture of BSA (20 mg, 0.3 μmol) in PBS (pH = 7.5) was added and shaken for 48 h. The TLR7a-BSA conjugate was purified by size-exclusion gel filtration (10 KD), and lyophilized. The average capacity of TLR7a on BSA was estimated by MALDI-TOF-MS.

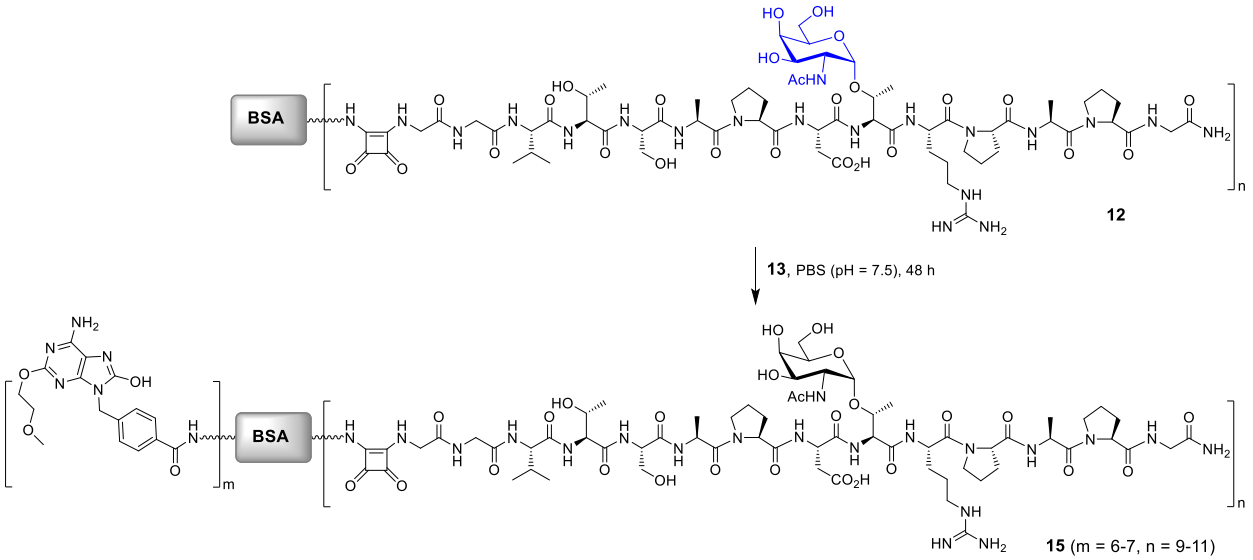

Scheme S7. The synthetic route of TLR7a-BSA-MUC1 **15**. Related to Scheme 2.

Synthesis of TLR7a-BSA-MUC1 protein conjugate 15. To a solution of BSA-MUC1 (**12**) (10 mg, 0.12 μmol) in PBS were added compound **13**, and the reaction mixture was shaken for 48 h. The TLR7a-BSA-MUC1 conjugate was purified by size-exclusion gel filtration (10 KD), and lyophilized. The average capacity of TLR7a on BSA-MUC1 (**12**) was estimated by MALDI-TOF-MS.

3. Vaccine immunizations

a. Immunization of mice

All animal experiments were performed at Laboratory Animal Centre of Huazhong Agriculture University (Number: SYXK (Wuhan) 2015-0084). Animal experiments were conducted in accordance with the animal ethics guidelines and follow the recommendations concerning laboratory animal welfare. For immunological evaluations, seven groups of female BALB/c mice (age of 6-8 weeks, 5 mice per group, Number: SYXK (Wuhan) 2015-0019) were examined with vaccine candidates, i.e. BSA-MUC1 (Figures S37-S41 and S47) (124 μg), TLR7a-BSA (Figure S48) (119 μg) and MUC1 (Figures S32-

S36) (21 μg), TLR7a (Scheme S1, Figures S30 and S31) (3.6 μg) and BSA-MUC1 (124 μg), TLR7a-BSA-MUC1 (Figure S49) (127 μg), MPLA (17.6 μg) and BSA-MUC1 (124 μg), Pam_3CSK_4 (15 μg) and BSA-MUC1 (124 μg), alum (100 μL) and BSA-MUC1 (124 μg), and PBS as a negative control, respectively.

Mice were immunized by intraperitoneal injection on day 1, day 15 and day 29. The mice were bled on day 0 before initial immunization and on 2 h, day 14, day 28, and day 42 after boost immunizations. Sera collected at 2 h after 1st injection were analysed for the secretion of cytokines IL-6 and IFN-γ. Mouse blood samples were clotted to obtain antisera that were stored at -80 °C before use.

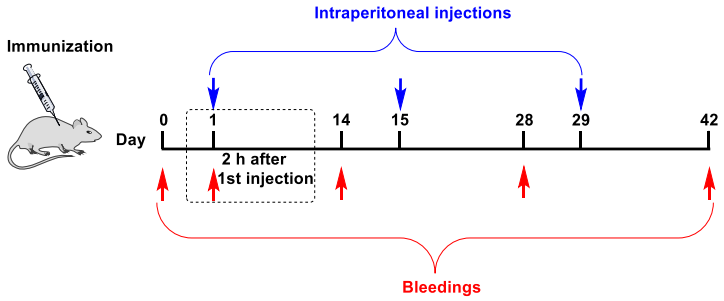

Scheme S8. Immunization strategy. Related to Figures 1-7.

Table S1. The composition of each vaccine candidate, Related to Figures 1-7.[a]

Vaccine candidates	Antigen	Adjuvant
1	BSA-MUC1 (0.0152 μmol, 124 μg)	/
2	MUC1 (0.0152 μmol, 21 μg)	TLR7a-BSA (0.01 μmol, 119 μg)
3	BSA-MUC1 (0.0152 μmol, 124 μg)	TLR7a (0.01 μmol, 3.6μg)
4	TLR7a-BSA-MUC1 (0.0152 μmol, 127 μg)	/
5	BSA-MUC1 (0.0152 μmol, 124 μg)	MPLA (0.01 μmol, 17.6 μg)
6	BSA-MUC1 (0.0152 μmol, 124 μg)	Pam_3CSK_4 (0.01 μmol, 15 μg)
7	BSA-MUC1 (0.0152 μmol, 124 μg)	alum (100 μL)

[a]The amounts of each component in the table are used for one injection per mouse

b. Statistical analyses

Comparison of multiple groups for statistical significance was carried out via one-way ANOVA with Tukey post hoc tests. Statistically significant responses are indicated by asterisks, data were analyzed using GraphPad Prism (GraphPad Software, San Diego, CA).

c. In vivo cytokine assay

Analysis of Cytokine Levels by ELISA. The relative total cytokine levels generated by the vaccine candidates were evaluated using ELISA kits (IFN-γ and IL-6, Biolegend) as per manufacturer's instructions. For this purpose, the high binding 96-well plates (Corning Incorporated, Costar 3590) were coated with capture antibodies (diluted 1:200) dissolved in coating buffer (0.1 M Na_2HCO_3, 0.03 M Na_2CO_3, pH 9.5) at 4 °C overnight. Then, the coated plates were washed four times with PBST (PBS containing 0.05% Tween-20), and blocked by using 1% BSA in PBS (200 μL/well) at 37 ºC for 1 h. After washing four times, the sera samples and standards were diluted with 1% BSA in PBS were added (100 μL/well) and incubated for 2 h at rt. Four additional washing steps were conducted, followed by incubation with the detection antibodies (1:200 dilution) (100 μL/well) for 1 h at rt. After further washing steps, the plates were incubated with Avidin-HRP (1:1000 dilution) (100 μL/well) for 30 min at rt. After final washing steps, the plates were incubated with 3,3',5,5'-tetramethylbenzidine (TMB) substrate solution (100 μL/well) for 20-30 minutes or until the desired color developed. Then, sulfuric acid was added (100 μL/well). Absorbance was measured at 450 nm with a microplate reader (BioTek, Synergy H1).

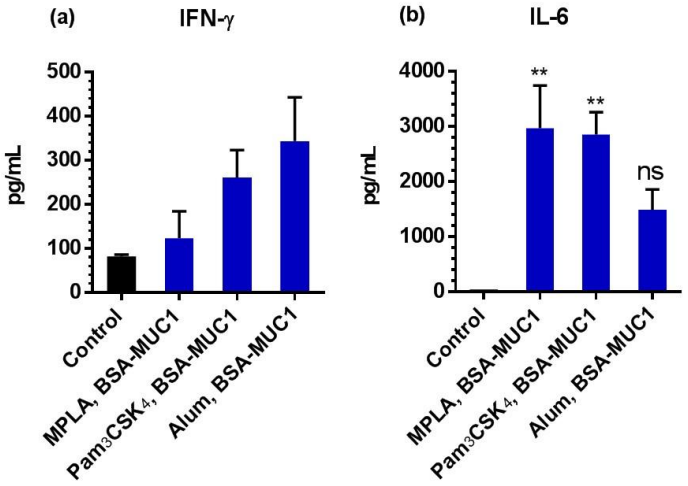

Figure S1. The secretion of cytokines IFN-γ (a) and IL-6 (b) were measured in serum samples from vaccinated mice at 2 h after the first immunization. Data are shown as the mean ± SEM of five mice and are representative of three separate experiments. Related to Figure 1.

d. Analysis of antibody titers and subtypes by ELISA

The antibody titers and antibody isotypes generated by the vaccine candidates were measured by ELISA. The biotinylated MUC1 and avidin (Biosynthesis) were directly dissolved together in the prepared $NaHCO_3/Na_2CO_3$ buffer (50 mM, pH 9.5) with final concentration of 0.125 μg/mL (MUC1) and 1.16 μg/mL (avidin), respectively. Next, 96-well plates were coated with avidin-biotin-MUC1 complex and incubated at 4 °C overnight. Then, the coated plates were washed four times with PBST and blocked with 1% casein in PBS (100 μL/well) at 37 ºC for 1 h. After washing four times, the plates were incubated with the serial diluted sera samples in PBS containing 0.1% casein (100 μL/well) at 37 ºC for 1 h. After another washing steps, the plates were incubated with one of the HRP-linked goat anti-mouse antibody IgG, IgM, IgG1, IgG2a, IgG2b, IgG3, IgA or IgE, 1:5000 dilution in PBST (100 μL/well) at 37 ºC for 1 h. After final washing steps, the plates were washed and TMB (500 μL 0.2 mg/mL) in 9.5 mL 0.05 M phosphate-citrate buffer at pH 5.0 with 32 μL 3% (w/v) urea hydrogen peroxide was added and allowed to react for 5 min. Next, the colorimetric reactions were terminated by 2.0 M sulfuric acid. Absorbance was recorded at 450 nm with a microplate reader. For titer analysis, the OD value was plotted against the sera dilution numbers to obtain a best-fit logarithm line. The dilution number was calculated according to the equation of this line.

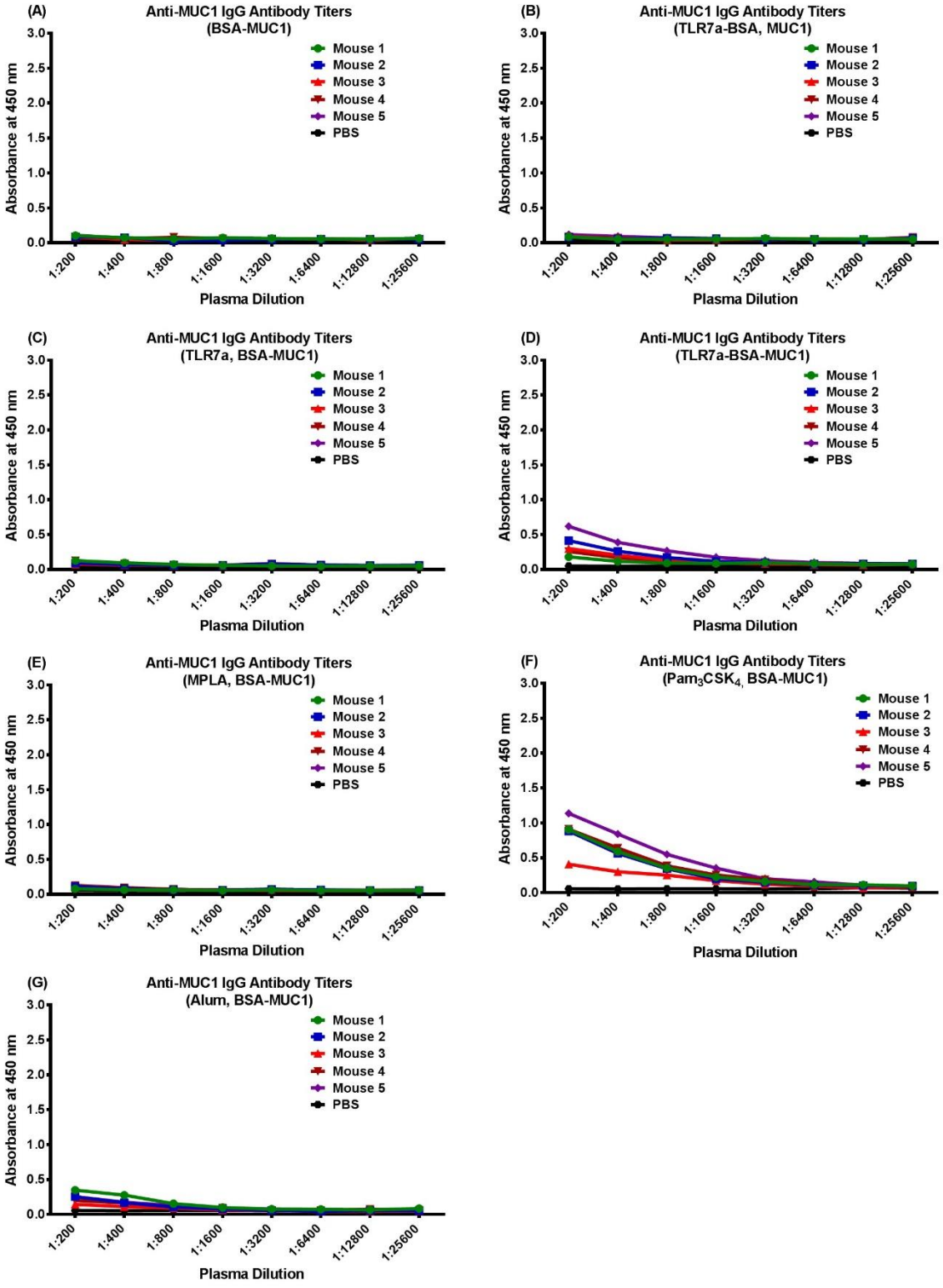

Figure S2. ELISA curves of anti-MUC1 IgG antibody titers in serum samples from vaccinated mice collected on day 14. Related to Figure 3.

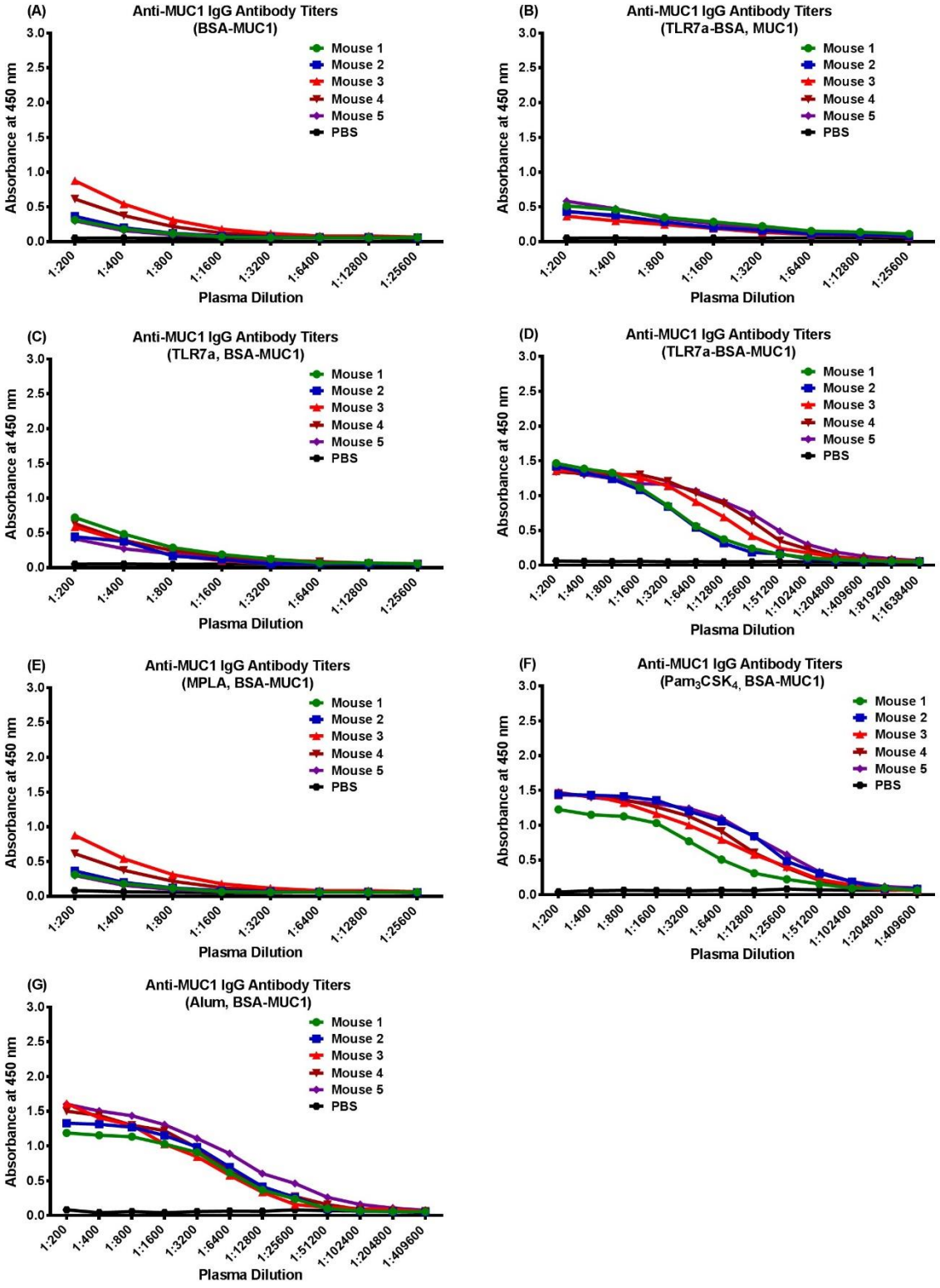

Figure S3. ELISA curves of anti-MUC1 IgG antibody titers in serum samples from vaccinated mice collected on day 28. Related to Figure 3.

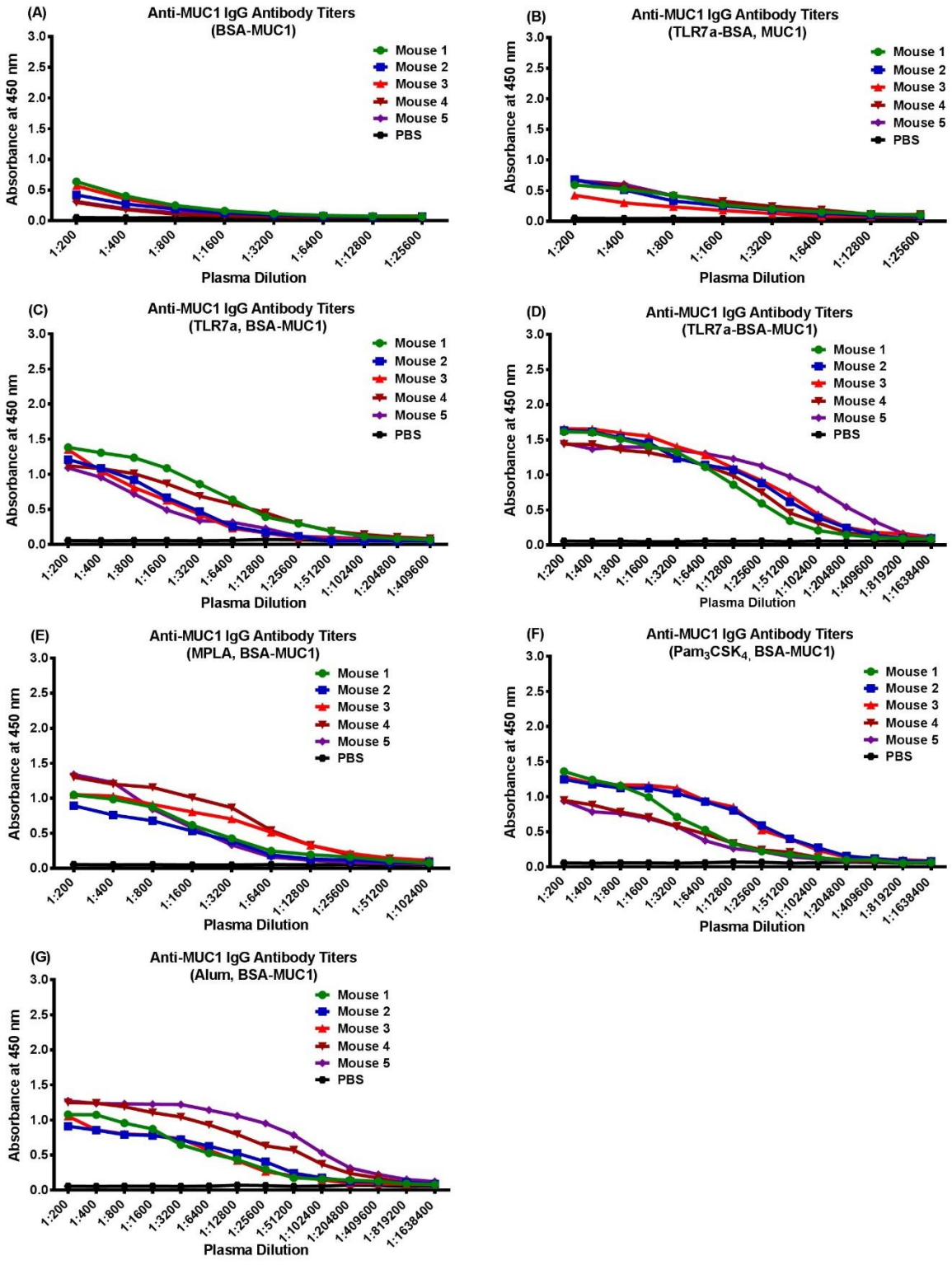

Figure S4. ELISA curves of anti-MUC1 IgG antibody titers in serum samples from vaccinated mice collected on day 42. Related to Figures 2 and 3.

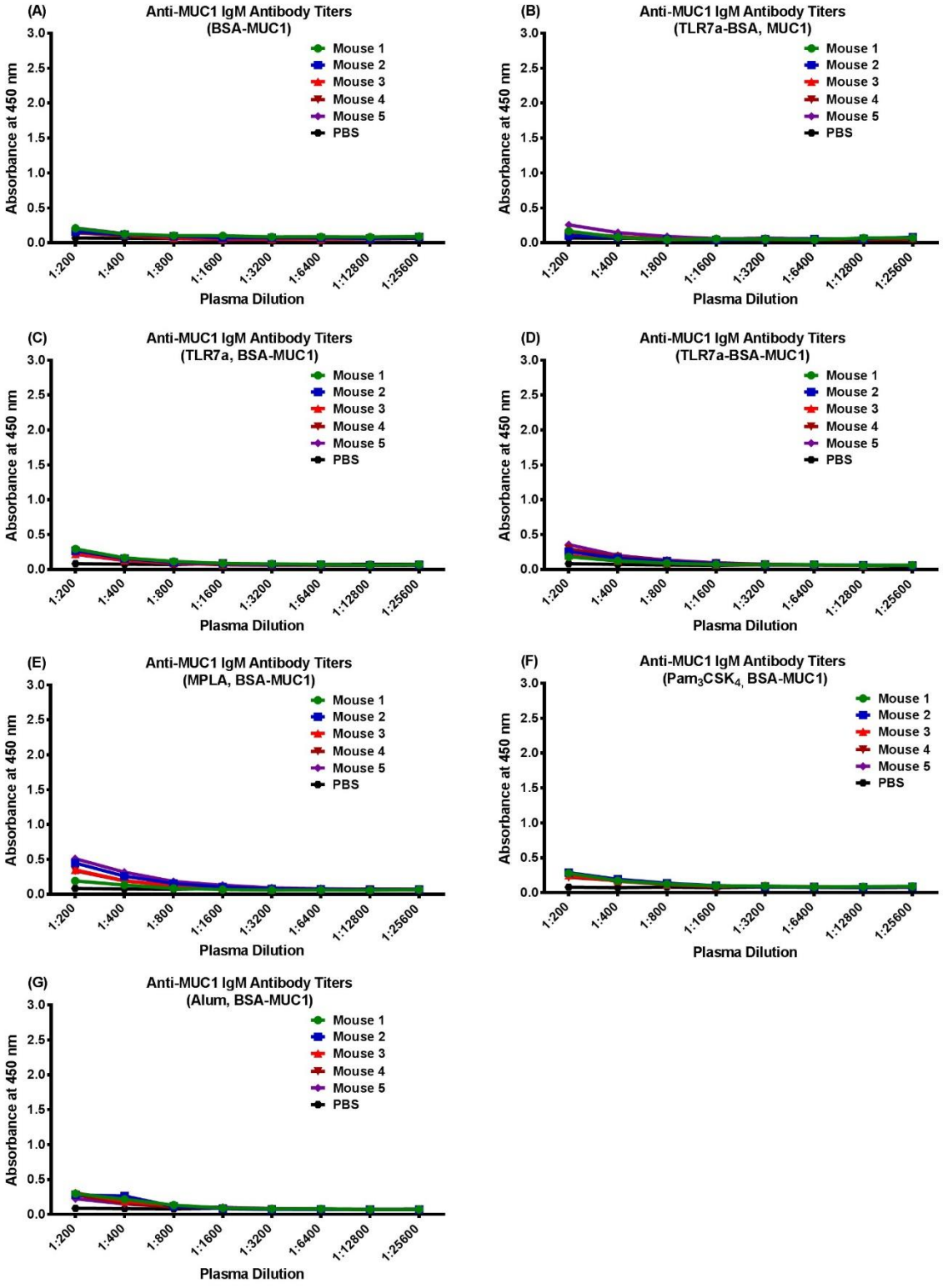

Figure S5. ELISA curves of anti-MUC1 IgM antibody titers in serum samples from vaccinated mice collected on day 14. Related to Figure 3.

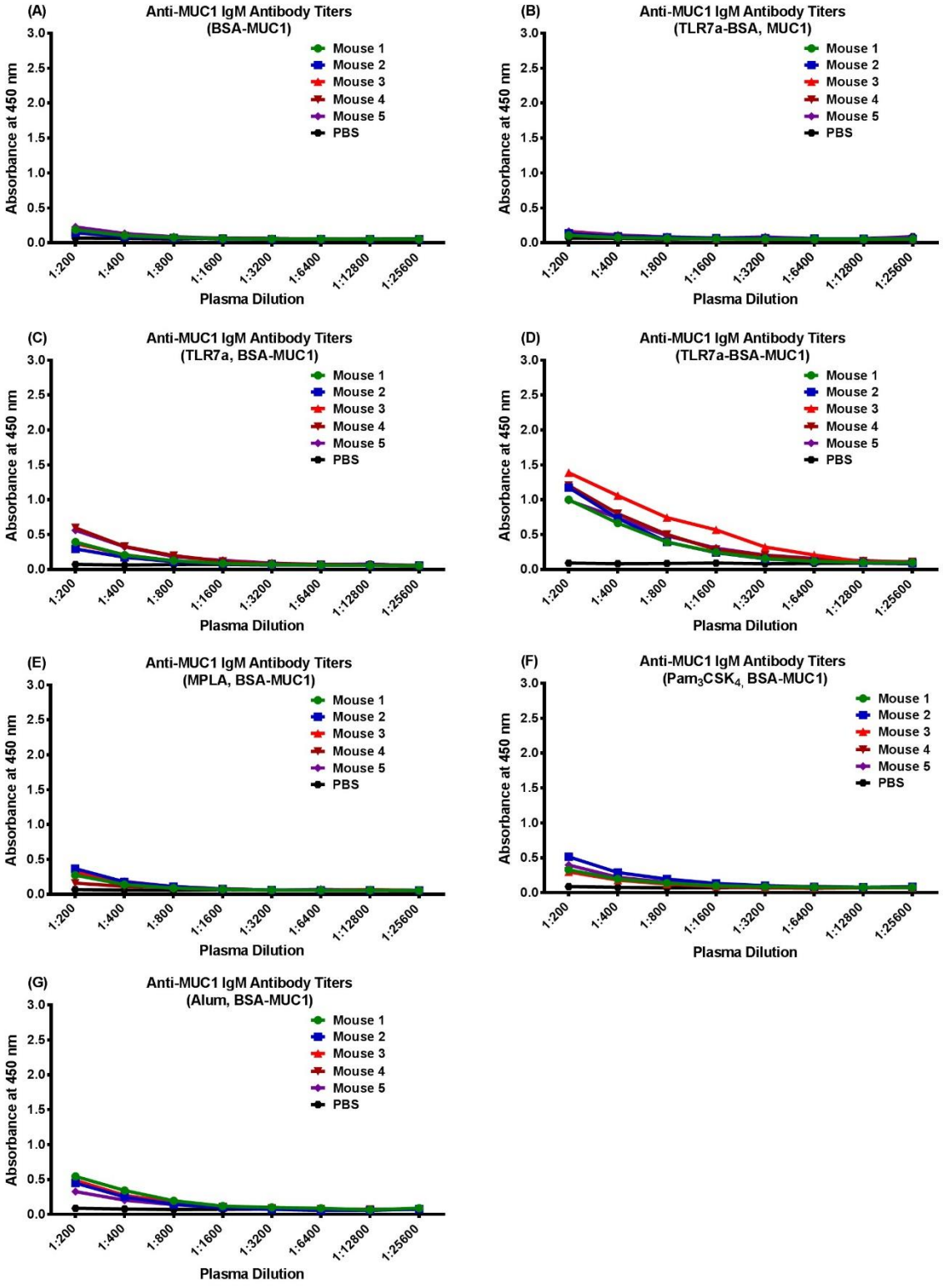

Figure S6. ELISA curves of anti-MUC1 IgM antibody titers in serum samples from vaccinated mice collected on day 28. Related to Figure 3.

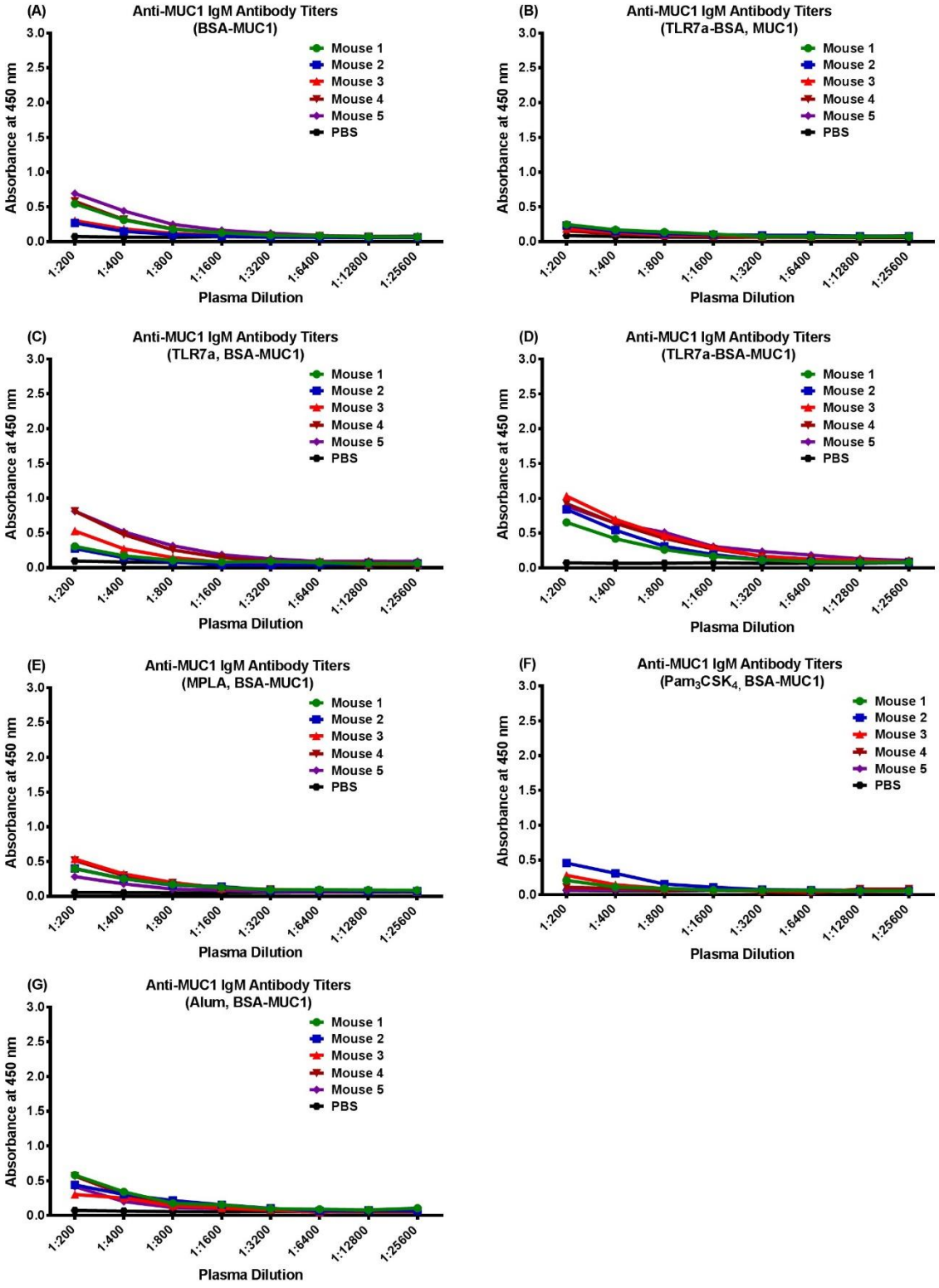

Figure S7. ELISA curves of anti-MUC1 IgM antibody titers in serum samples from vaccinated mice collected on day 42. Related to Figure 3.

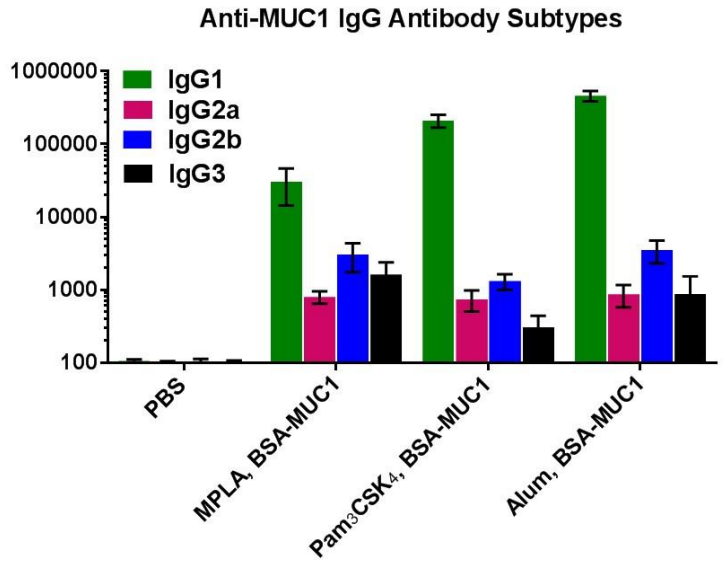

Figure S8. Anti-MUC1 IgG antibody subtype titers were measured in serum samples from vaccinated mice collected on day 42. Data are shown as the mean ± SEM of five mice and are representative of three separate experiments. Related to Figure 4.

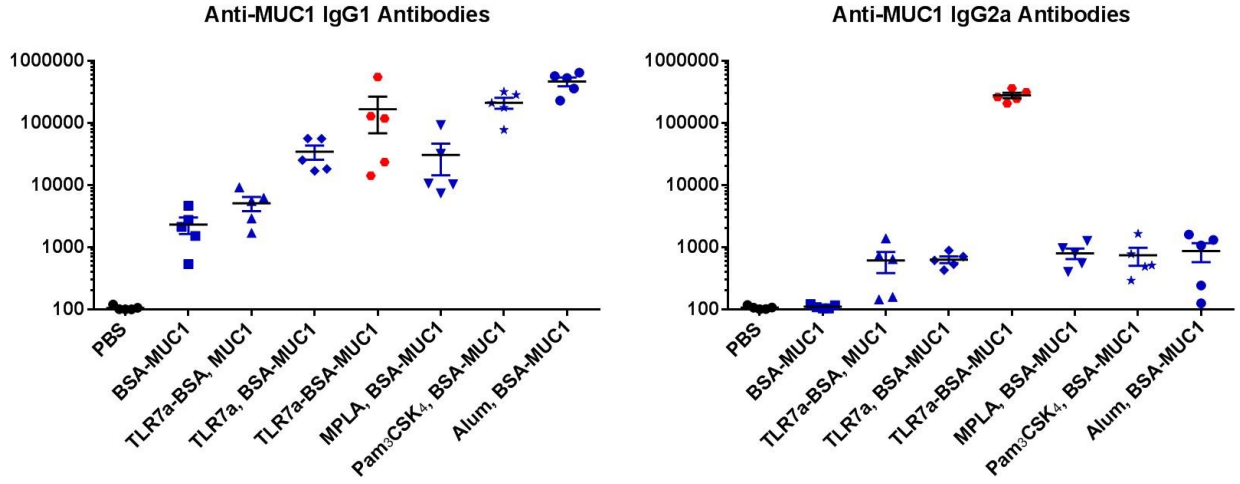

Figure S9. Anti-MUC1 IgG1 and IgG2a antibodies were measured in serum samples from vaccinated mice collected on day 42. Data are shown as the mean ± SEM of five mice and are representative of three separate experiments. Related to Figure 4.

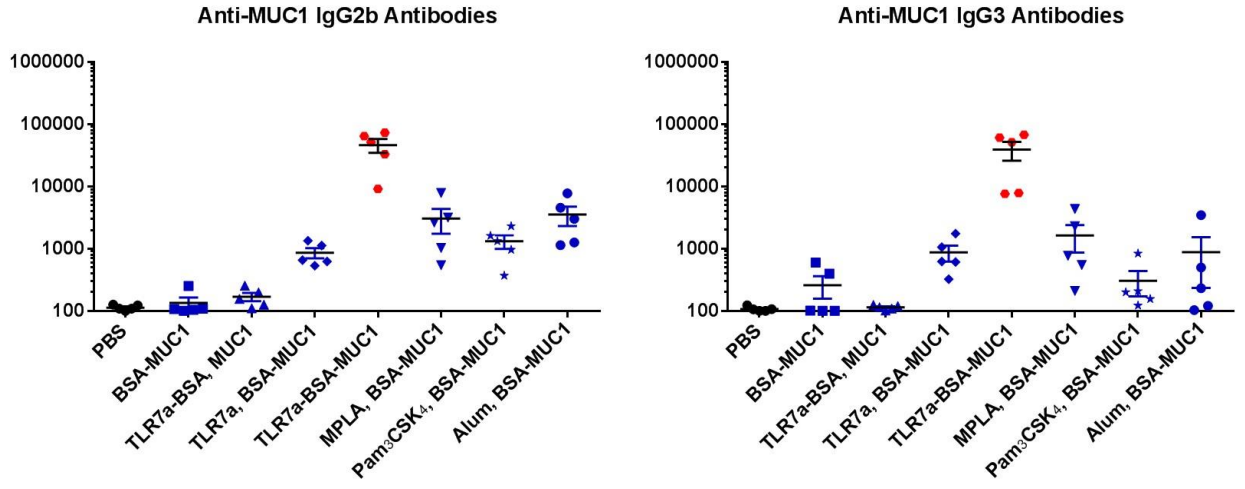

Figure S10. Anti-MUC1 IgG2b and IgG3 antibodies were measured in serum samples from vaccinated mice collected on day 42. Data are shown as the mean ± SEM of five mice and are representative of three separate experiments. Related to Figure 4.

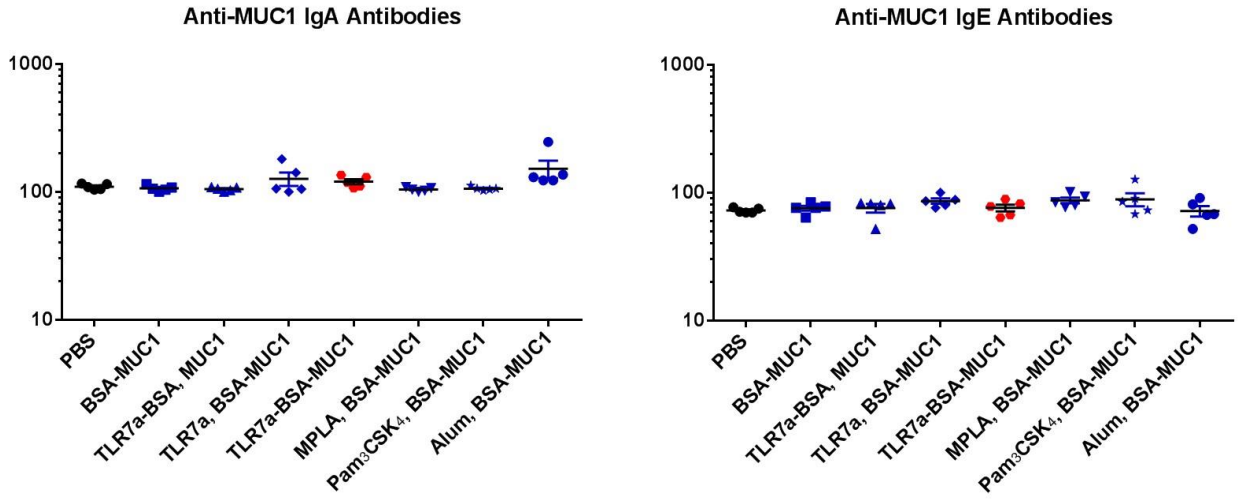

Figure S11. Anti-MUC1 IgA and IgE antibodies were measured in serum samples from vaccinated mice collected on day 42. Data are shown as the mean ± SEM of five mice and are representative of three separate experiments. Related to Figure 4.

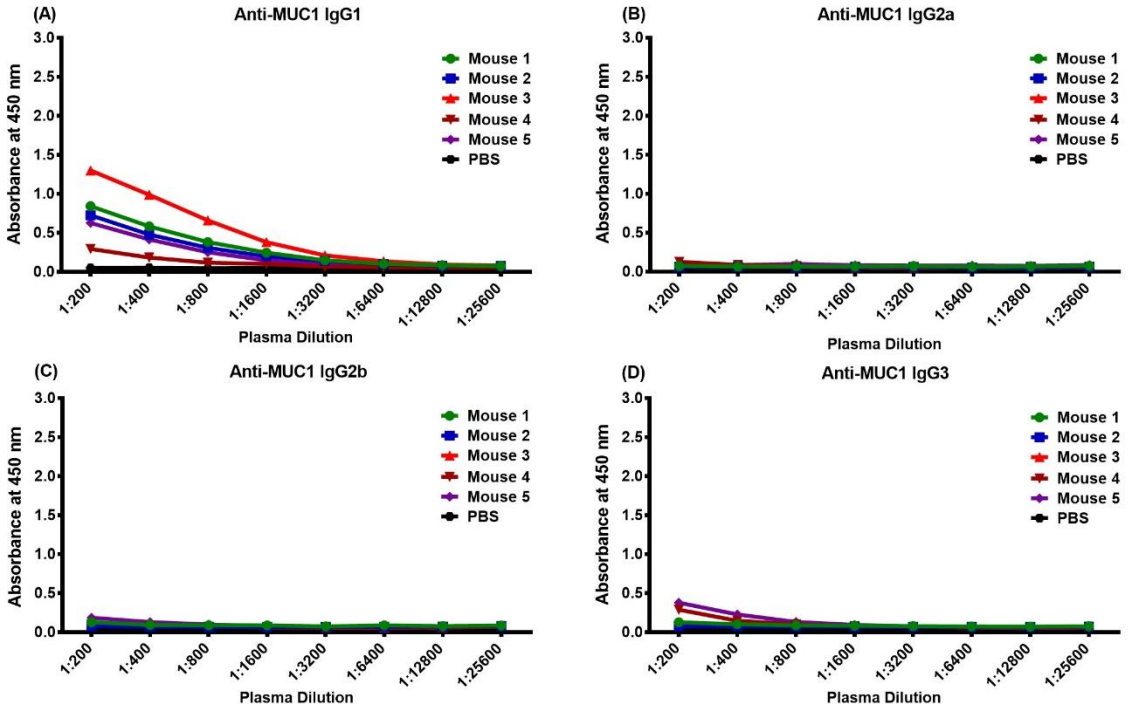

Figure S12. ELISA curves of MUC1-specific (A) IgG1, (B) IgG2a, (C) IgG2b and (D) IgG3 antibodies in plasma 1 (BSA-MUC1) on day 42. Related to Figure 4.

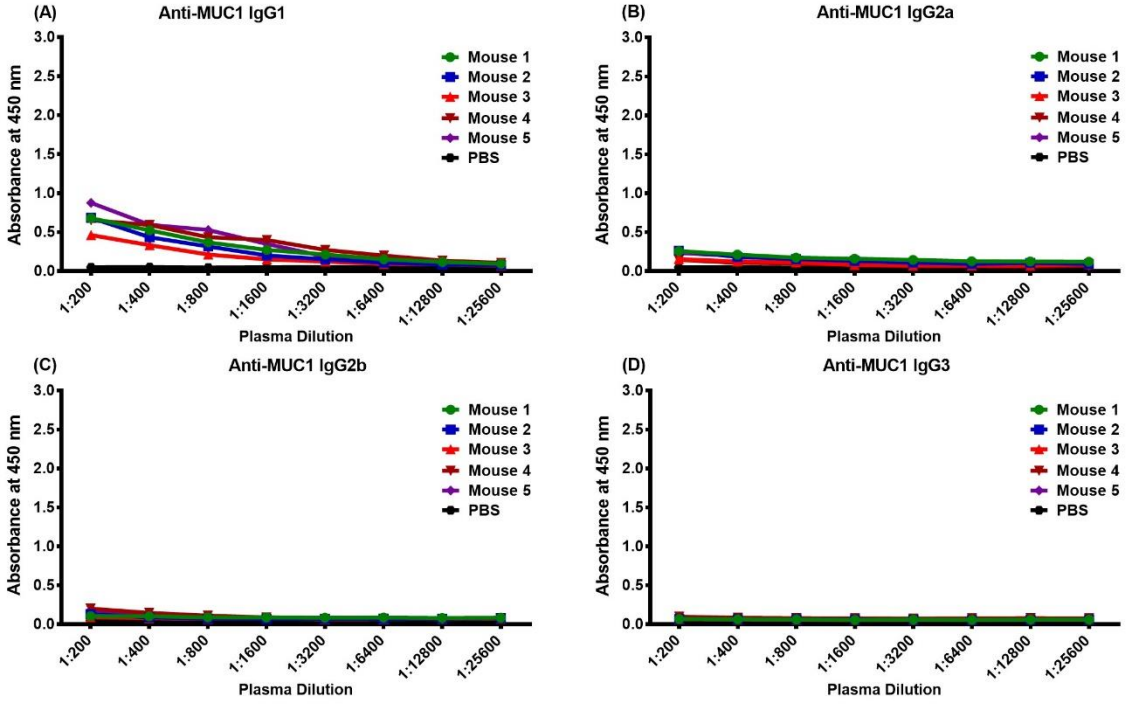

Figure S13. ELISA curves of MUC1-specific (A) IgG1, (B) IgG2a, (C) IgG2b and (D) IgG3 antibodies in plasma 2 (TLR7a-BSA, MUC1) on day 42. Related to Figure 4.

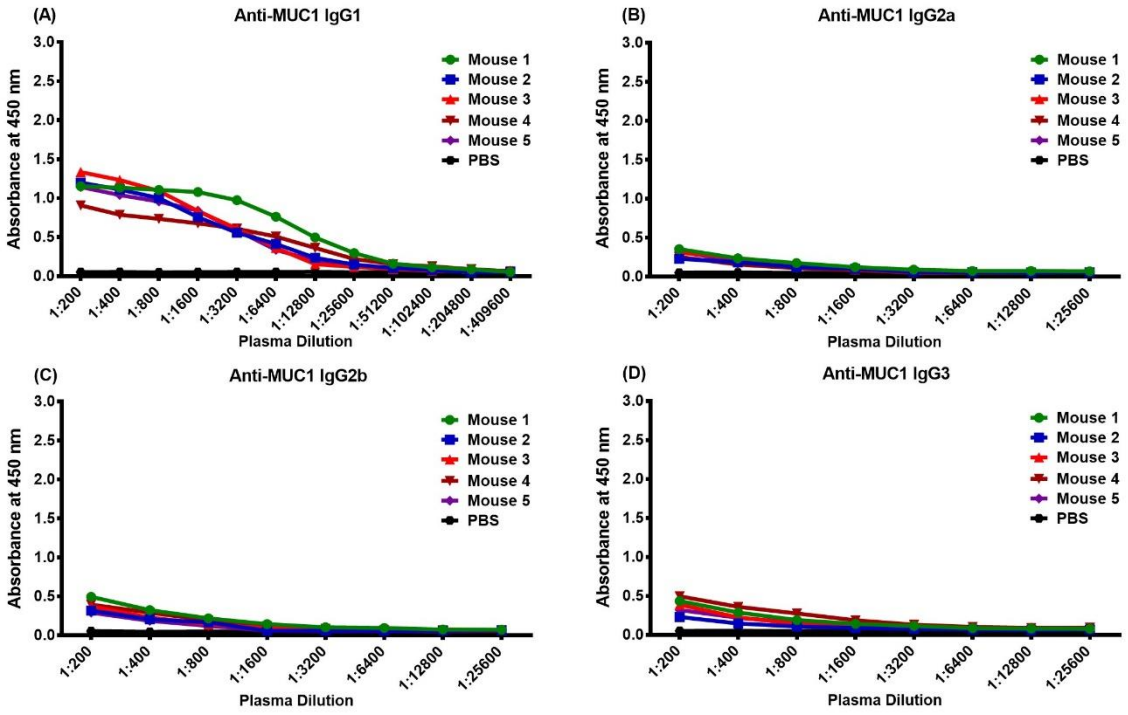

Figure S14. ELISA curves of MUC1-specific (A) IgG1, (B) IgG2a, (C) IgG2b and (D) IgG3 antibodies in plasma 3 (TLR7a, BSA-MUC1) on day 42. Related to Figure 4.

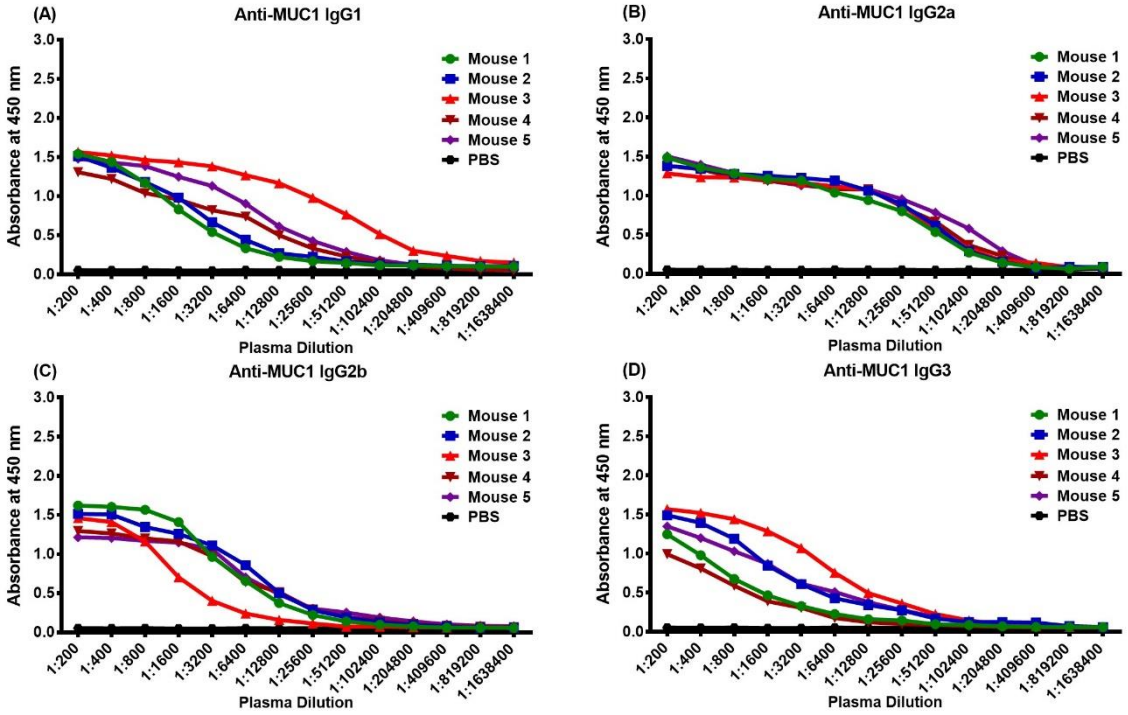

Figure S15. ELISA curves of MUC1-specific (A) IgG1, (B) IgG2a, (C) IgG2b and (D) IgG3 antibodies in plasma 4 (TLR7a-BSA-MUC1) on day 42. Related to Figure 4.

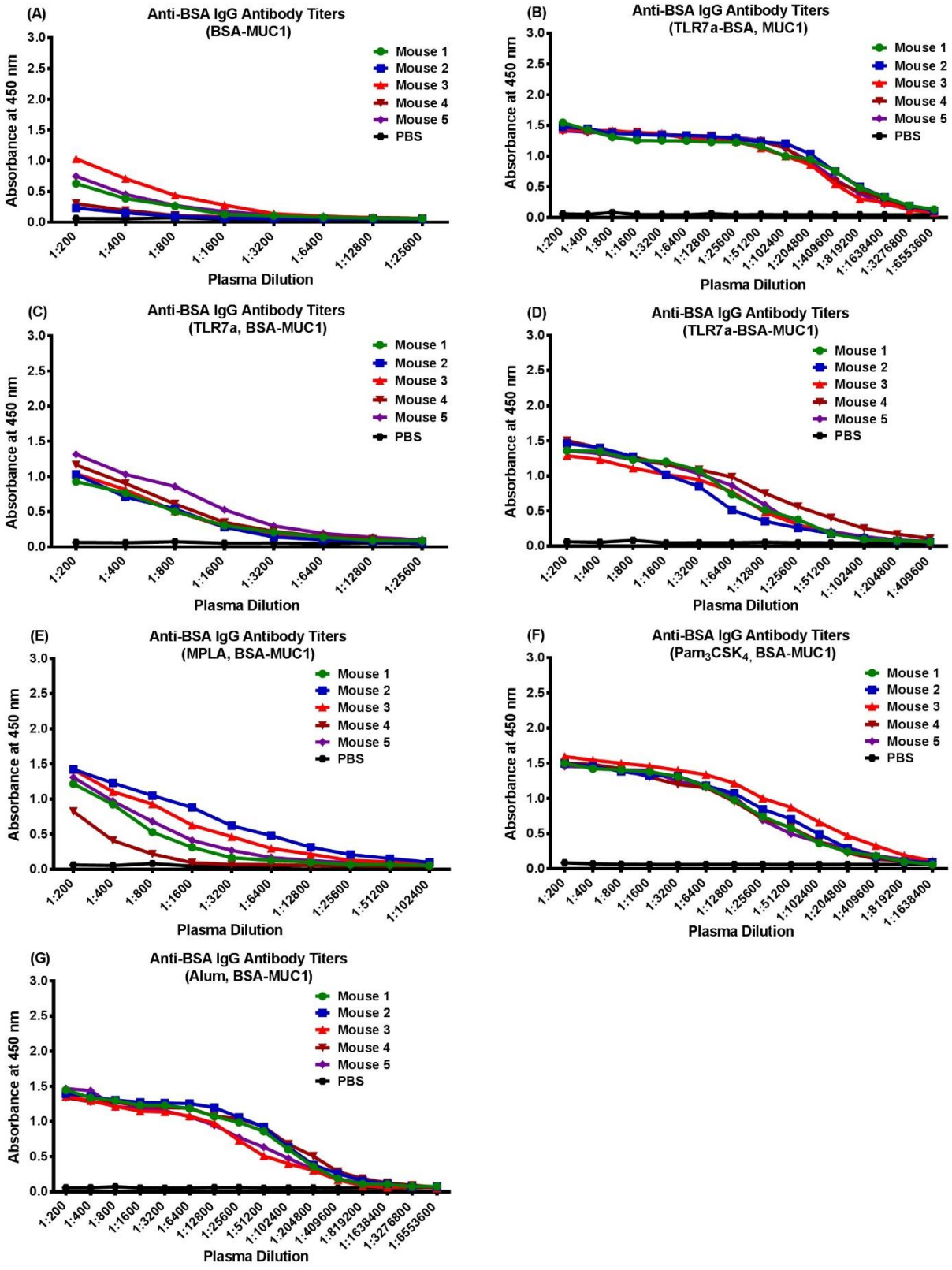

Figure S16. ELISA curves of anti-BSA IgG antibody titers in serum samples from vaccinated mice collected on day 42. Related to Figure 5.

e. Procedures of cellular experiments

Cultures of Cancer Cells. The MCF-7 human breast adenocarcinoma cell lines, the B16-F10 (mouse melanoma tumor cell lines) and B16-MUC1 (human mucin-transfected mouse melanoma tumor cell lines) were obtained from National Infrastructure of Cell Line Resources and used for the in vitro studies. MCF-7 cells maintained in a humidified incubator (Heracell 150i, Thermo Scientific) at 37 ºC with 5% CO_2 and grown using Dulbecco's modified Eagle's medium (DMEM) (Gibco/Thermo Fisher Scientific) supplemented with 10% (v/v) heat-inactivated fetal bovine serum (FBS) (Gibco/Thermo Fisher Scientific), and 1% (v/v) antibiotics (Gibco/Thermo Fisher Scientific). In addition, the B16-F10 and B16-MUC1 cells were grown in 10% (v/v) FBS and 1% (v/v) antibiotics in RPMI-1640 (Gibco/Thermo Fisher Scientific).

Determination of Antibody Binding to Cancer Cells by FACS Analysis. The reactivity of the antibody binding induced by vaccine candidate towards MCF-7, B16-MUC1 and B16-F10 cells was detected staining the cells with mice antisera followed by FACS analysis (Cai et al., 2014). Hence, cancer cells were subjected to a digestion step with 0.25% Trypsin-EDTA (Gibco/Thermo Fisher Scientific) for 1 min, then transferred to different conical centrifuge tubes (1×10^6 cells per tube) and centrifuged at 1,500 rpm for 2 min. After removing the culture medium, cancer cells were incubated with 500 μL of mice antisera (1:50 dilution) (2 μL per mouse, 10 μL per group) in FACS buffer (1% FBS, 0.1% NaN_3 and 1% BSA in PBS) at 0 °C for 1 h. After washing three times with 1% FBS in PBS (centrifugation at 1500 rpm, then the supernatant was removed), cancer cells were incubated with Alexa Fluor® 488-conjugated AffiniPure Goat Anti-Mouse IgG (H+L) secondary antibody in flow cytometry buffer (1:50 dilution) (100 μL per tube) at 0 °C for 1 h. After further washing steps (centrifugation at 1500 rpm, then the supernatant was removed), 300 μL of flow cytometry buffer was added, the cells were detected using a flow cytometry (BD Accuri™).

Determination of Antibody Binding to Cancer Cells by Confocal Microscopy Analysis. Cancer cells were stained with mice antisera to determine their potential in recognizing the MUC1 targets. Initially, cancer cells were subjected to a digestion step with trypsin, transferred to confocal dishes (1×10^6 cells per dish), followed by maintaining in a humidified incubator at 37 ºC for 12 h. After washing five times with 1% BSA in PBS buffer (1 min each wash), cancer cells were incubated with mice antisera (1:50 dilution) at 0 °C for 1 h. Subsequently, the culture medium was removed and cancer cells were washed five times with 1% BSA in PBS buffer, cancer cells were incubated with Alexa Fluor® 488-conjugated AffiniPure Goat Anti-Mouse IgG (H+L) secondary antibody in 1% BSA in PBS buffer (1:50 dilution) at 0 °C for 30 min. After washing, the cancer cells were visualized using confocal microscope (Leica TCS SP8, Wetzlar, Germany) with a 63X oil objective.

Determination of Cell Viability of MCF-7 Cells by MTT Protocol. The purpose of this experiment is to investigate whether the antibodies are able to mediate complement lysis via activation of CDC. MCF-7 cells were incubated in DMEM containing 2% FBS and planted on a 96-well cell culture plate (8000 cells per well). After washing three times with PBS solution, MCF-7 cells were incubated with the mice antisera in PBS containing 1% BSA (1:50 dilution) (50 μL/well) at 37 ºC for 2 h. After another washing steps, the prepared rabbit sera (1:5 dilution) (Cedarlane Labs) in 1% BSA/PBS exited as complement supplier (RC: rabbit complement; RC-inactive: inactivated rabbit complement after treatment at high temperature) were added (50 μL/well). After incubation for 4 h, without washing, the prepared 0.5% MTT (Aladdin) in PBS solution was added (20 μL/well) and incubated at 37 ºC. After incubation for 2 h, DMSO (Leagene) was added (150 μL/well) and the absorption was analyzed at the wavelength of 490 nm. The cell viabilities of MCF-7 cells were measured with the following formula:

Cell viability (%) = (Experimental/Control) × 100

CTL Assay. Groups of BALB/c mice (n = 5) were immunized three times (days 1, 15, and 29) by subcutaneous injection of vaccine candidates into the back of the neck. Fourteen days after the third immunization, spleens were obtained from mice and processed into a single cell suspension, then employed as effector cells for CTL assay. The freshly isolated splenocytes (1×10^6 cells/well) were added and co-incubated with the MCF-7 cells (1×10^6 cells/well) in RPMI-1640 (Gibco/Thermo Fisher Scientific) for 12 h. Finally, the effector cell-mediated cytotoxicity to target cells was examined by lactate dehydrogenase (LDH) assay according to the manufacture's protocol (Beyotime Biotechnology). Each plate was centrifuged at 250 g for 4 min, then 120 μL of the cell-free supernatant was transferred to the wells of another 96-well enzymatic assay plate containing LDH assay reagents (60 μL/well). The 96-well plates were incubated at rt protected from light for 30 min. The absorptions of these plates were read at 490 nm wavelength using a microplate reader. In the meantime, the spontaneous LDH release values were determined by incubating tumor cells alone or splenocytes alone, respectively. The maximum LDH release values were determined by incubating tumor cells in RPMI-1640 containing lysis solution without FBS. The percentage of cell lysis was calculated according to the following formula:

Cytotoxicity (%) = (Experimental – Effector Spontaneous – Target Spontaneous/Target Maximum – Target Spontaneous) × 100

f. Determination of antibody binding to tumor cells by FACS analysis

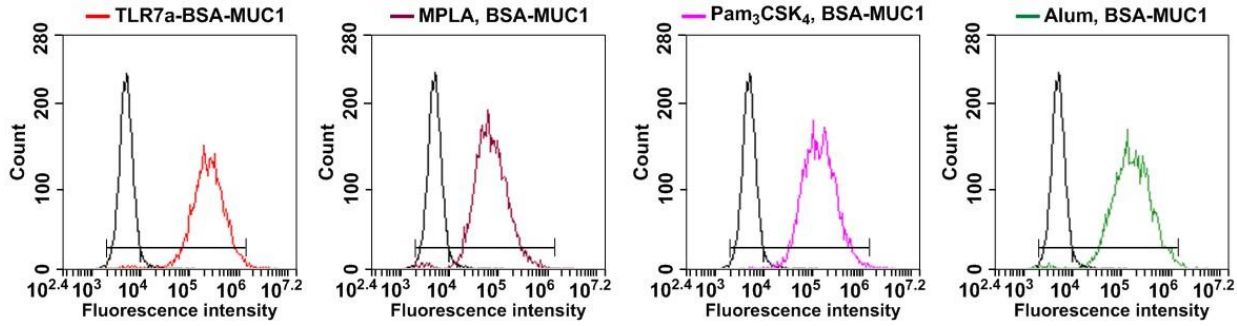

Figure S17. FACS analysis of the binding of vaccinated mouse serum samples to MCF-7 cells. Incubation with PBS group sample (black) served as a control. The images are representative of five independent experiments. Related to Figure 6.

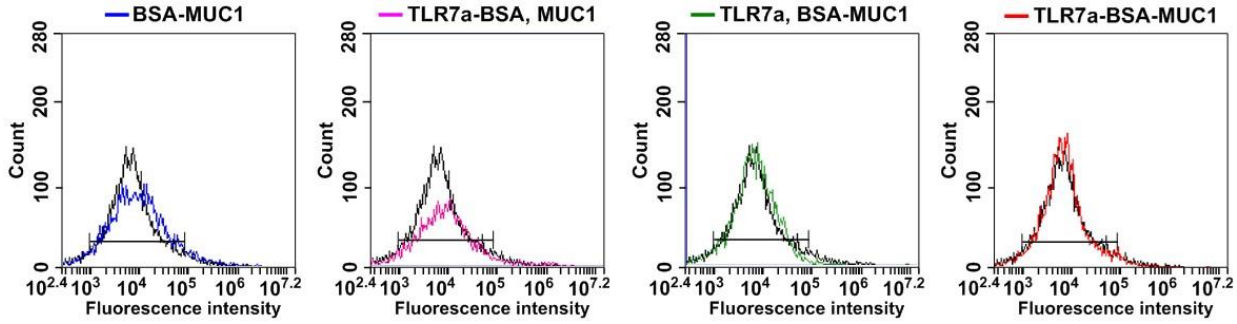

Figure S18. FACS analysis of the binding of vaccinated mouse serum samples to B16-F10 cells (Li et al., 2019). **Incubation with PBS group sample (black) served as a control.** The images are representative of five independent experiments. Related to Figure 6.

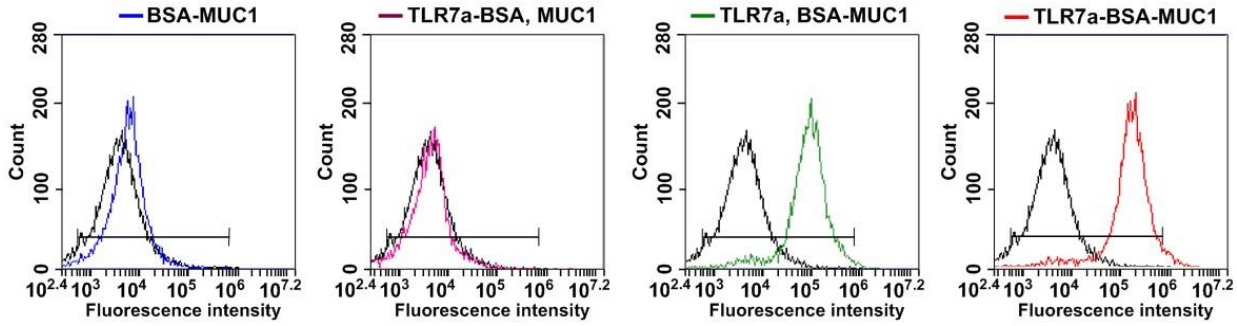

Figure S19. FACS analysis of the binding of vaccinated mouse serum samples to B16-MUC1 cells. Incubation with PBS group sample (black) served as a control. The images are representative of five independent experiments. Related to Figure 6.

g. Determination of antibody binding to tumor cells by confocal microscopy

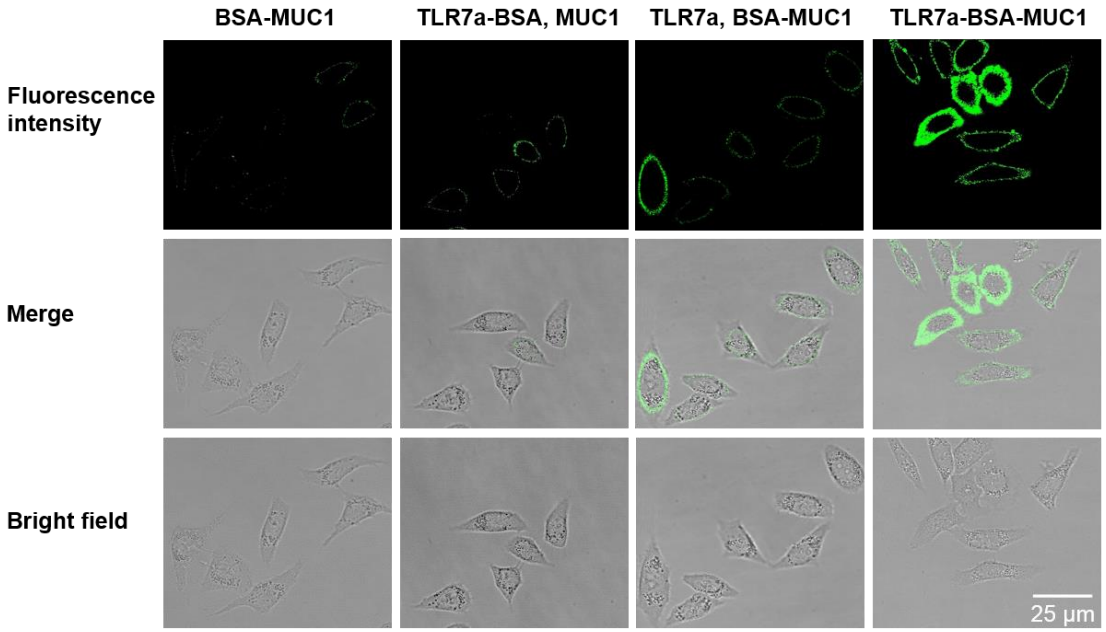

Figure S20. Confocal fluorescence microscopy images of MCF-7 cells incubated with serum samples from vaccinated mice (magnification: 63×). The images are representative of five independent experiments. Scale bar = 25 μm. Related to Figure 6.

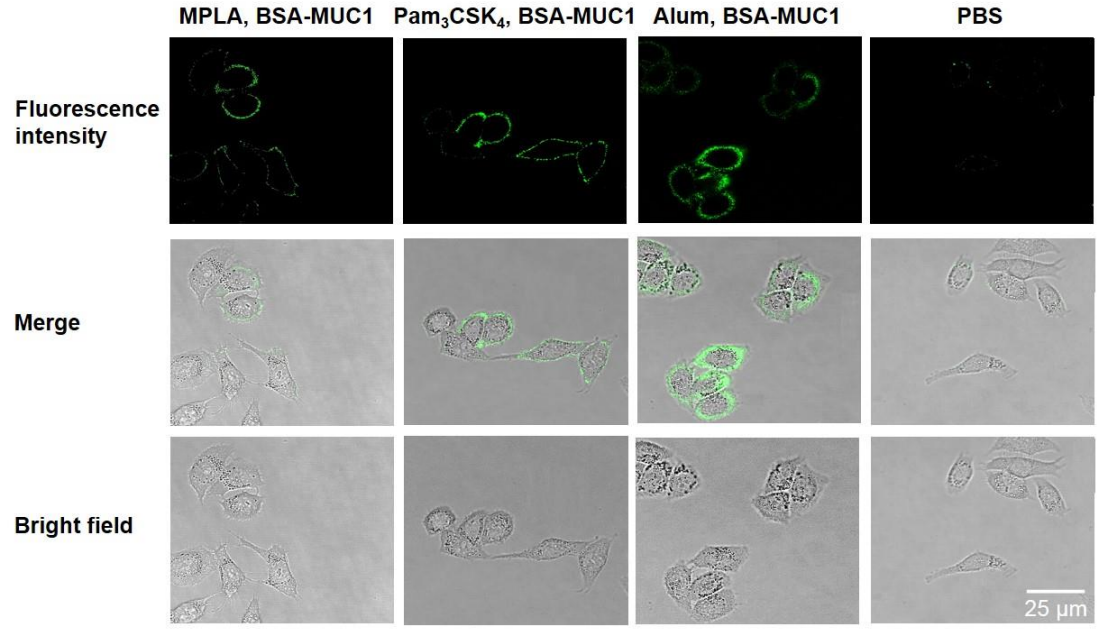

Figure S21. Confocal fluorescence microscopy images of MCF-7 cells incubated with serum samples from vaccinated mice (magnification: 63×). Incubation with PBS group sample served as a control. The images are representative of five independent experiments. Scale bar = 25 μm. Related to Figure 6.

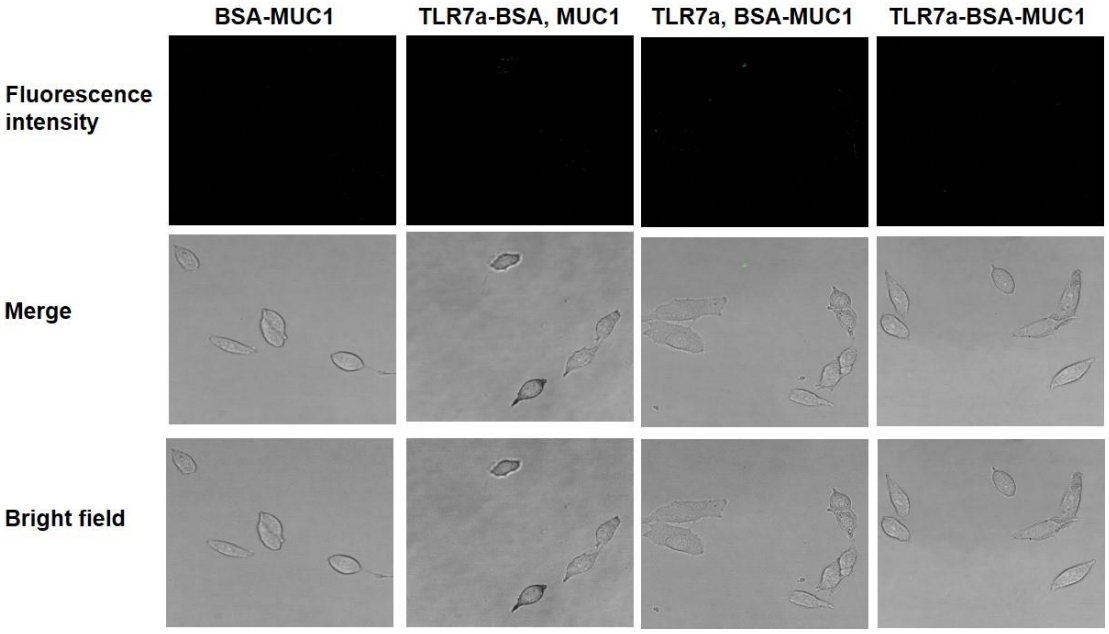

Figure S22. Confocal fluorescence microscopy images of B16-F10 cells incubated with serum samples from vaccinated mice (magnification: 63×). The images are representative of five independent experiments. Related to Figure 6.

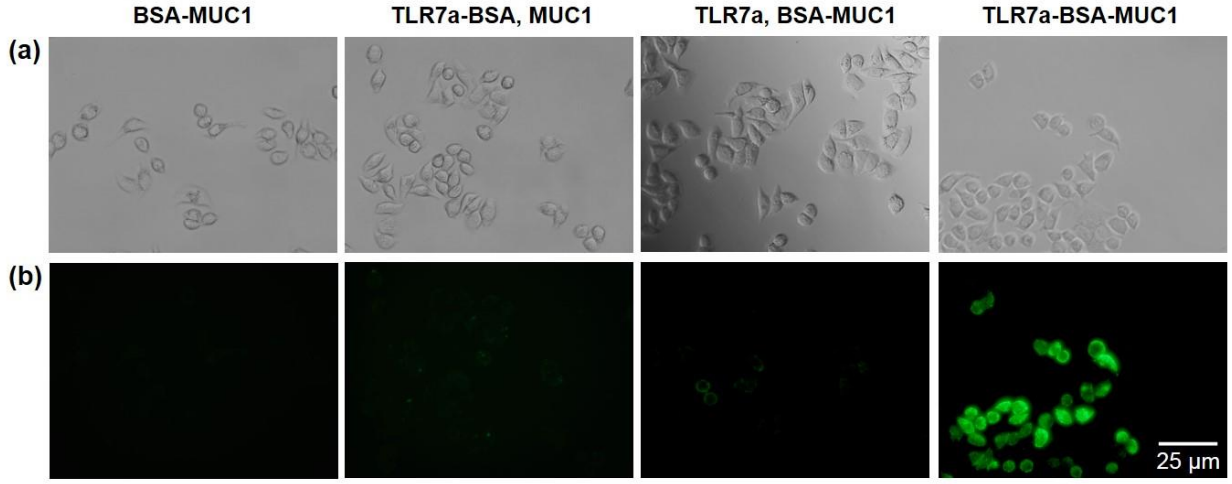

Figure S23. Fluorescence-microscopy staining of MCF-7 cells. a): bright field images. b): fluorescent images. The images are representative of five independent experiments. Scale bar = 25 μm. Related to Figure 6.

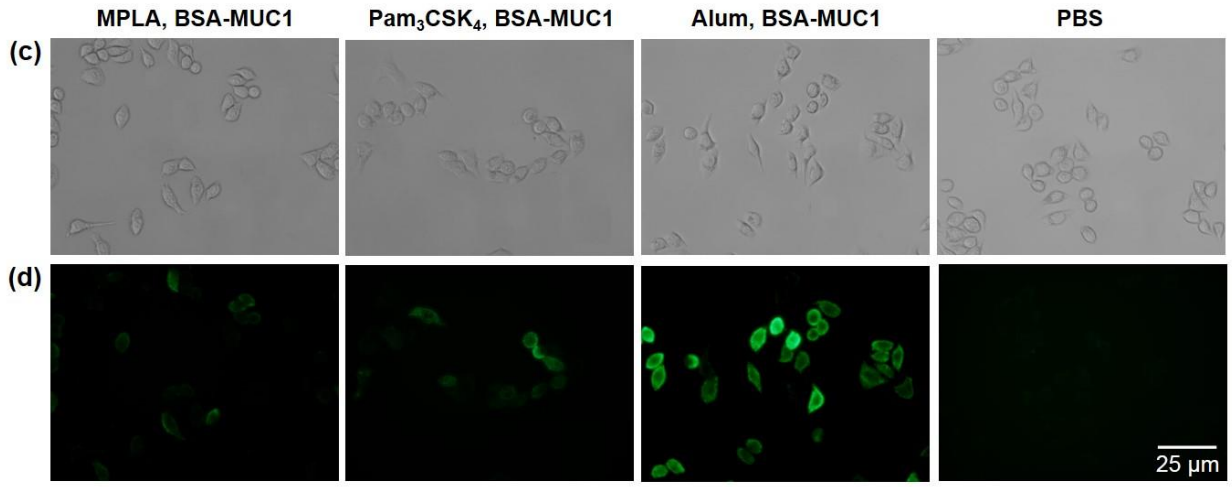

Figure S24. Fluorescence-microscopy staining of MCF-7 cells. c): bright field images. d): fluorescent images. Incubation with PBS group sample served as a control. The images are representative of five independent experiments. Scale bar = 25 μm. Related to Figure 6.

h. Preliminary evaluation of the safety of weight change

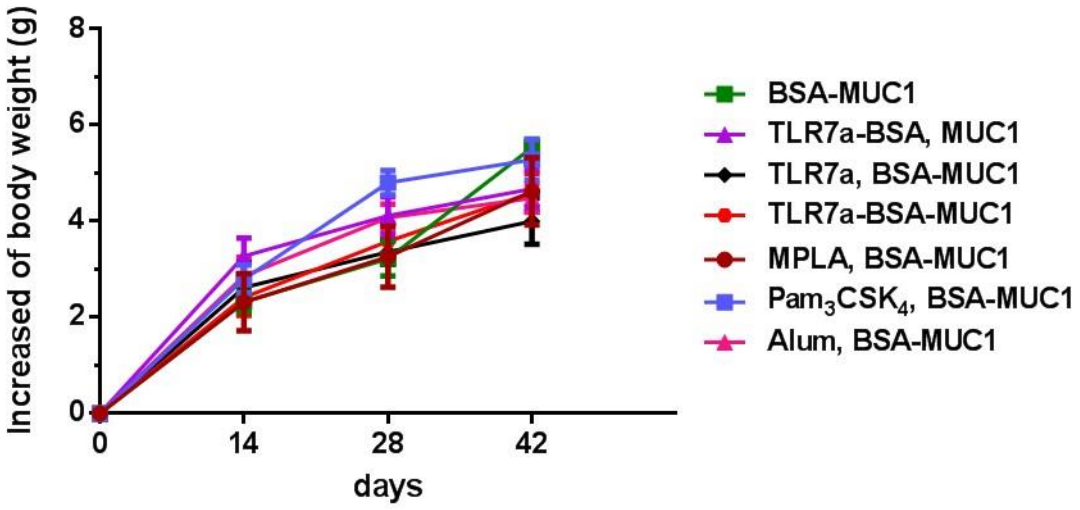

Figure S25. Assessment of the safety of MUC1-bsaed vaccines by monitoring the weight changes of immunized mice. Related to Figure 7.

4. References

Cai, H., Sun, Z.-Y., Chen, M.-S., Zhao, Y.-F., Kunz, H., and Li, Y.-M. (2014). Synthetic Multivalent Glycopeptide-Lipopeptide Antitumor Vaccines: Impact of the Cluster Effect on the Killing of Tumor Cells. Angew. Chem. Int. Ed. *53*, 1699-1703.

Chen, X.-Z., Zhang, R.-Y., Wang, X.-F., Yin, X.-G., Wang, J., Wang, Y.-C., Liu, X., Du, J.-J., Liu, Z., and Guo, J. (2019). Peptide-free Synthetic Nicotine Vaccine Candidates with α-Galactosylceramide as Adjuvant. Mol. Pharm. *16*, 1467-1476.

Du, J.-J., Gao, X.-F., Xin, L.-M., Lei, Z., Liu, Z., and Guo, J. (2016). Convergent synthesis of N-linked glycopeptides via aminolysis of ω-Asp p-nitrophenyl thioesters in solution. Org. Lett. *18*, 4828-4831.

Du, J.-J., Zou, S.-Y., Chen, X.-Z., Xu, W.-B., Wang, C.-W., Zhang, L., Tang, Y.-K., Zhou, S.-H., Wang, J., Yin, X.-G., et al. (2019). Liposomal Antitumor Vaccines Targeting Mucin 1 Elicit a Lipid-Dependent Immunodominant Response. Chem. Asian J. *14*, 2116-2121.

Gao, D., Liu, Y., Diao, Y., Gao, N., Wang, Z., Jiang, W., and Jin, G. (2015). Synthesis and Evaluation of Conjugates of Novel TLR7 Inert Ligands as Self-Adjuvanting Immunopotentiators. ACS Med. Chem. Lett. *6*, 249-253.

Li, M., Wang, Z., Yan, B., Yin, X., Zhao, Y., Yu, F., Meng, M., Liu, Y., and Zhao, W. (2019). Design of a MUC1-based tricomponent vaccine adjuvanted with FSL-1 for cancer immunotherapy. MedChemComm. *10*, 2073-2077.

5. Analytical data of compounds

a. Compound 3

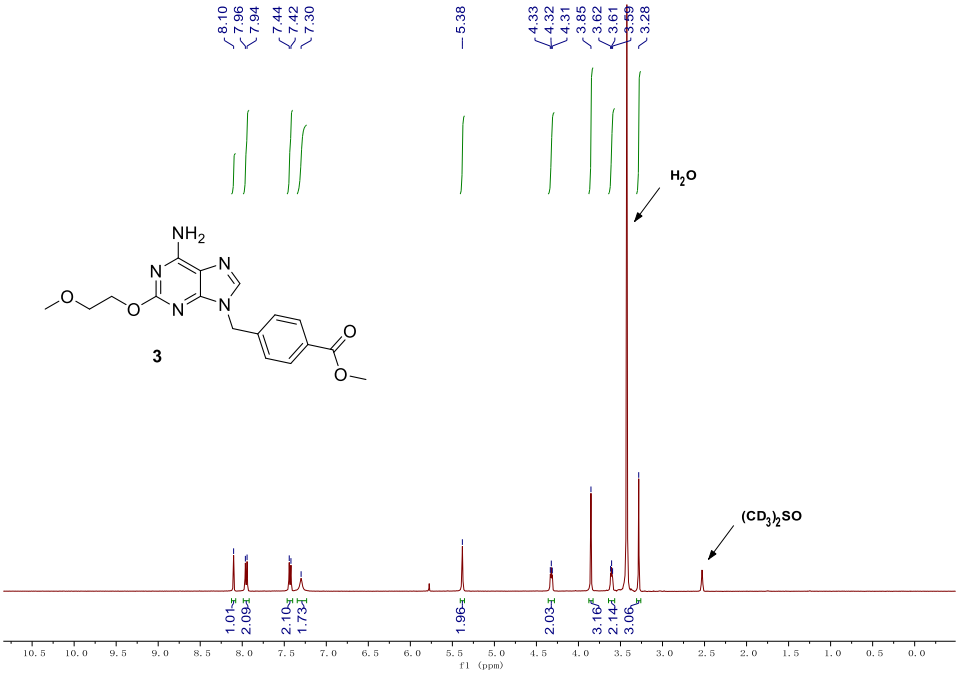

Figure S26. ^{1}H NMR spectrum for compound **3**. Related to Scheme 2.

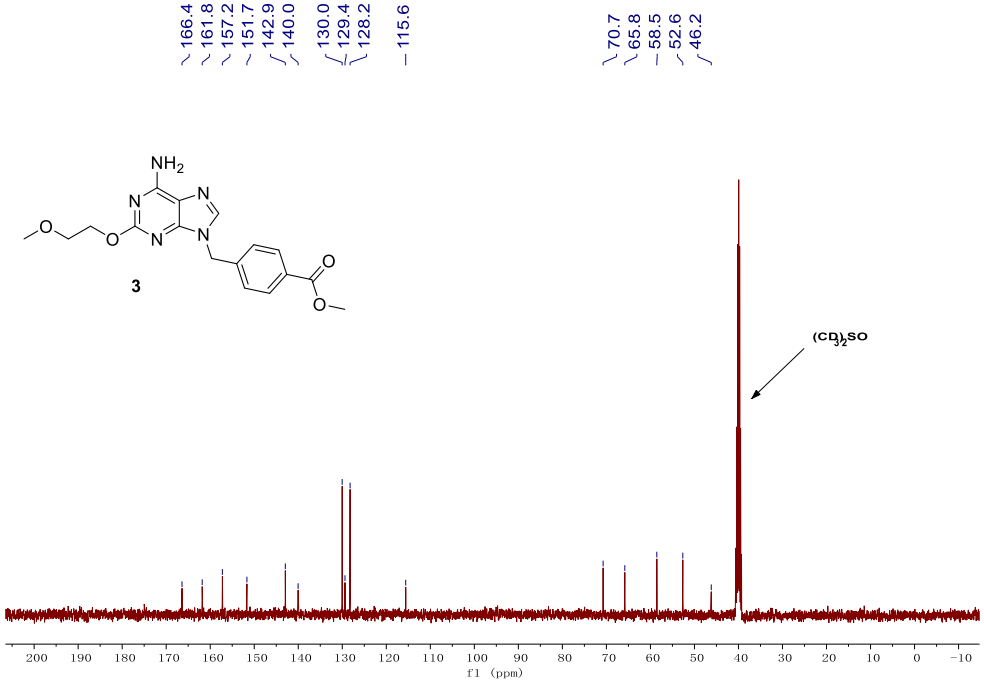

Figure S27. ^{13}C NMR spectrum for compound **3**. Related to Scheme 2.

b. Compound 4

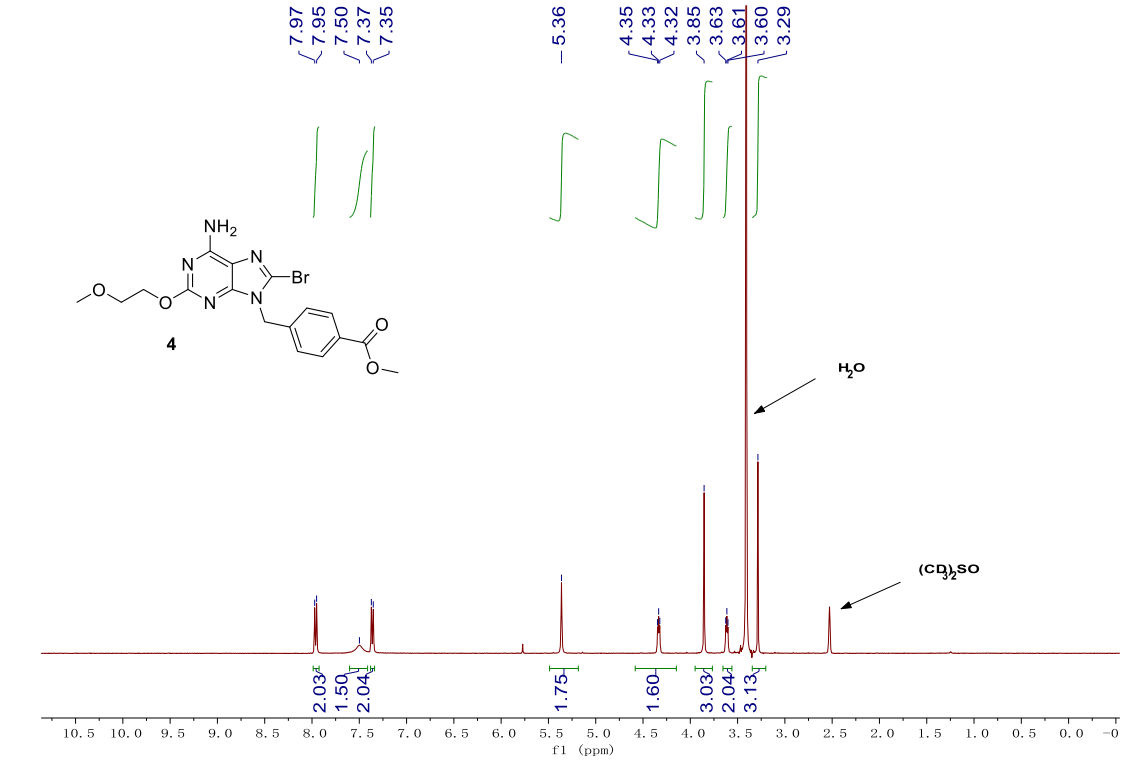

Figure S28. ^{1}H NMR spectrum for compound **4**. Related to Scheme 2.

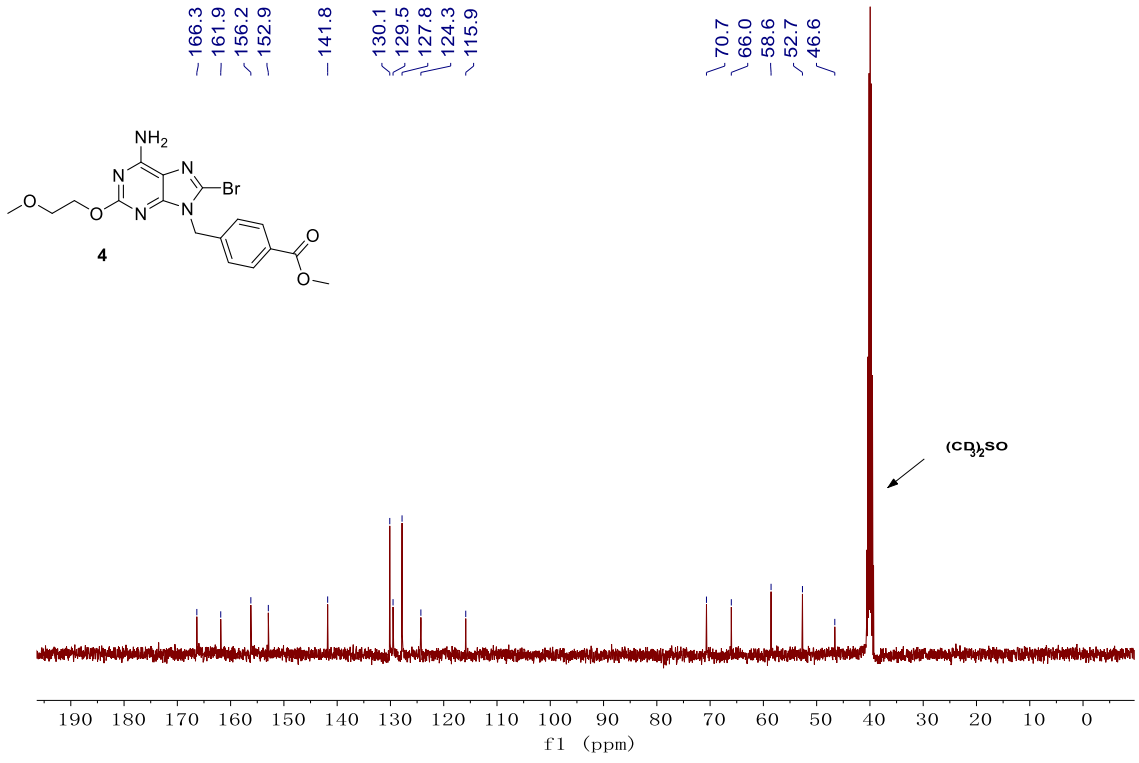

Figure S29. ^{13}C NMR spectrum for compound **4**. Related to Scheme 2.

c. Compound 5

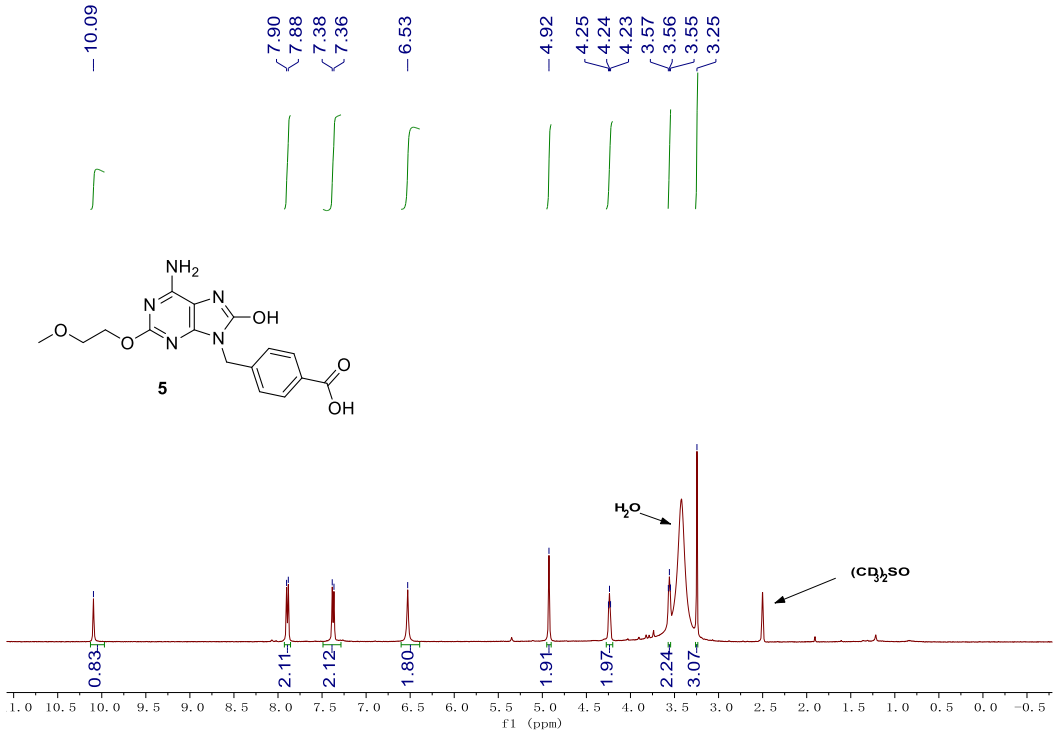

Figure S30. ^{1}H NMR spectrum for compound **5**. Related to Scheme 2.

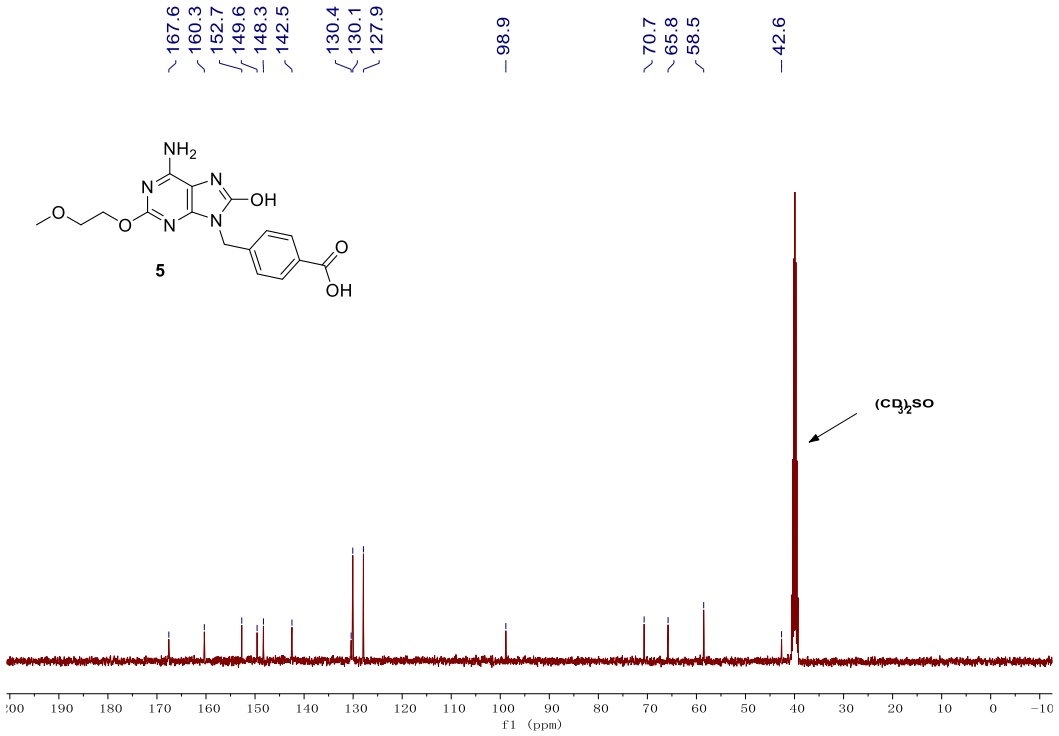

Figure S31. ^{13}C NMR spectrum for compound **5**. Related to Scheme 2.

d. MUC1 glycopeptide 8

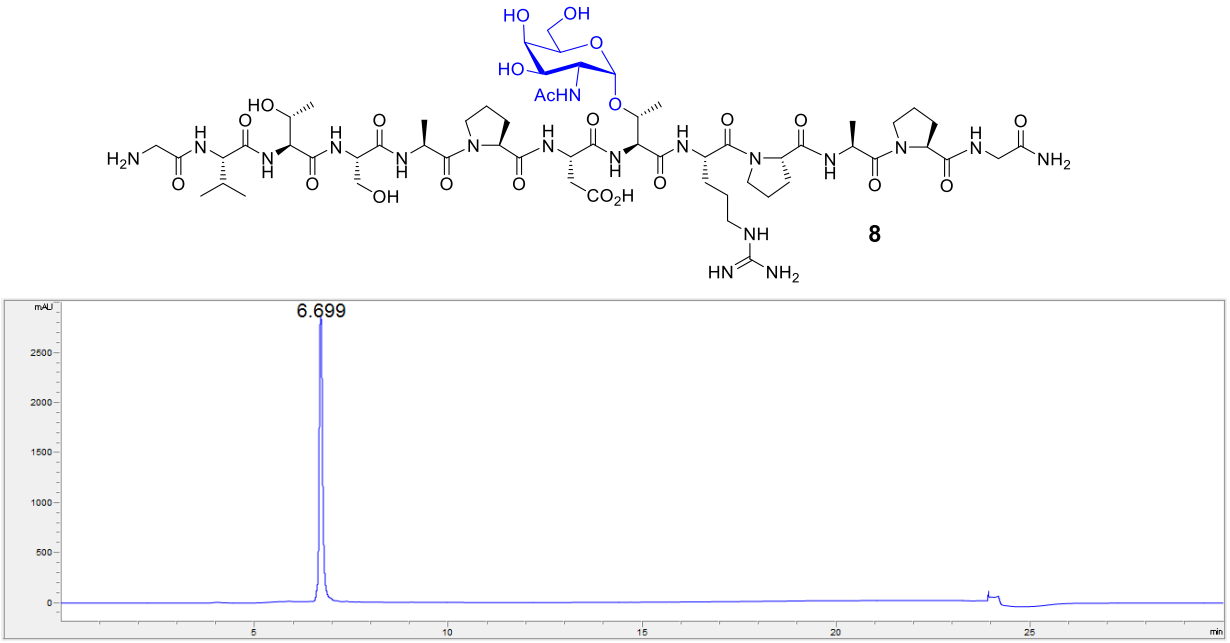

Figure S32. Analytical HPLC trace of MUC1 glycopeptide **8**. (28 mg, 42% yield). Analytic gradient is 5% to 90% of solution B (acetonitrile with 0.1% trifluoroacetic acid) in solution A (water with 0.1% trifluoroacetic acid) in 30 min on the analytic C18 column. Related to Scheme 2.

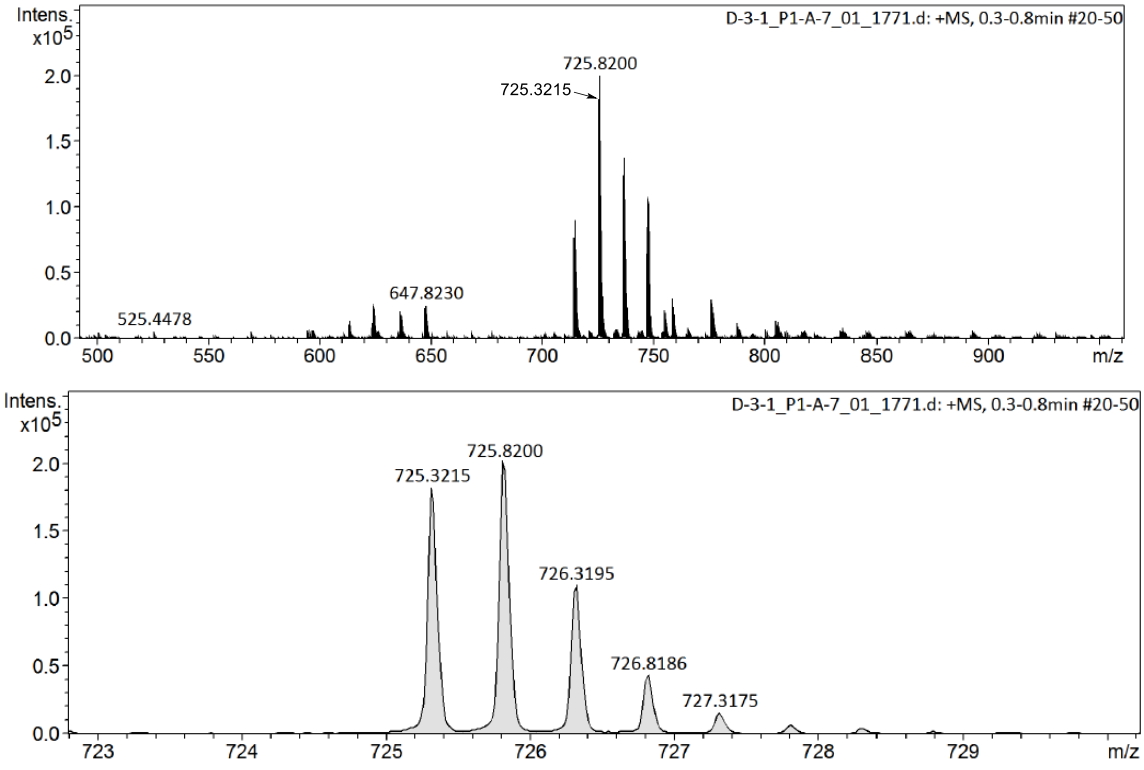

Figure S33. ESI-Q-TOF MS data of MUC1 glycopeptide **8**. Related to Scheme 2.

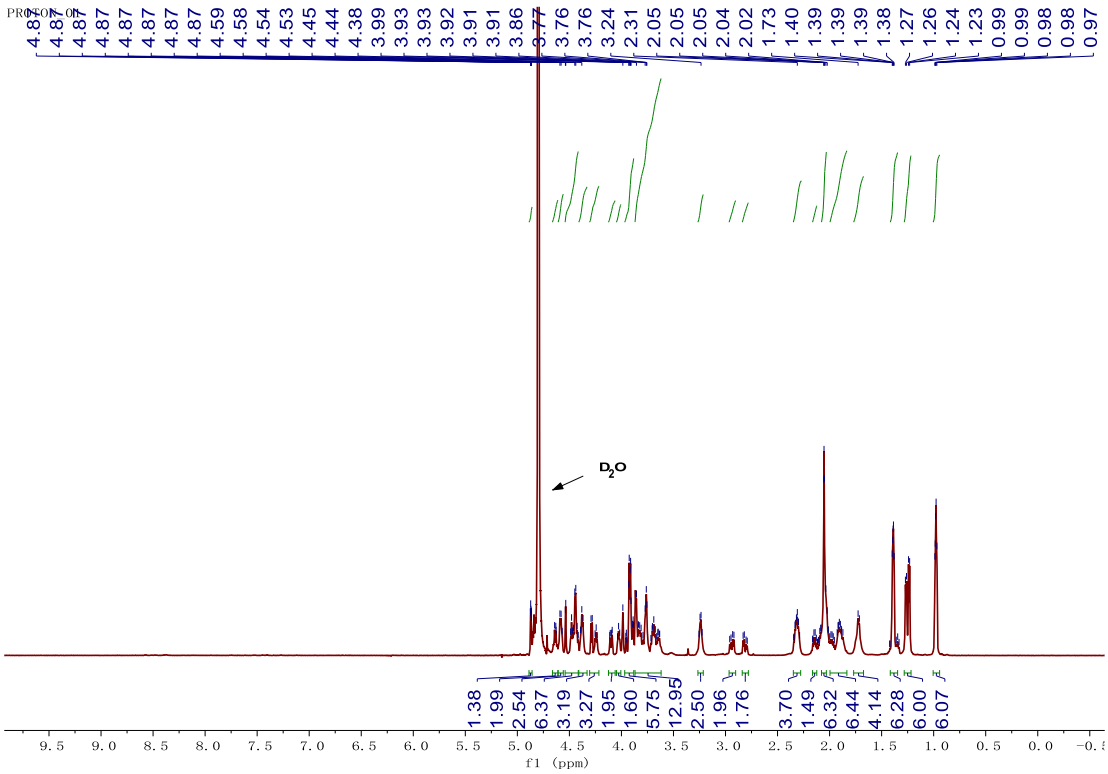

Figure S34. ^{1}H NMR spectrum for MUC1 glycopeptide **8**. Related to Scheme 2.

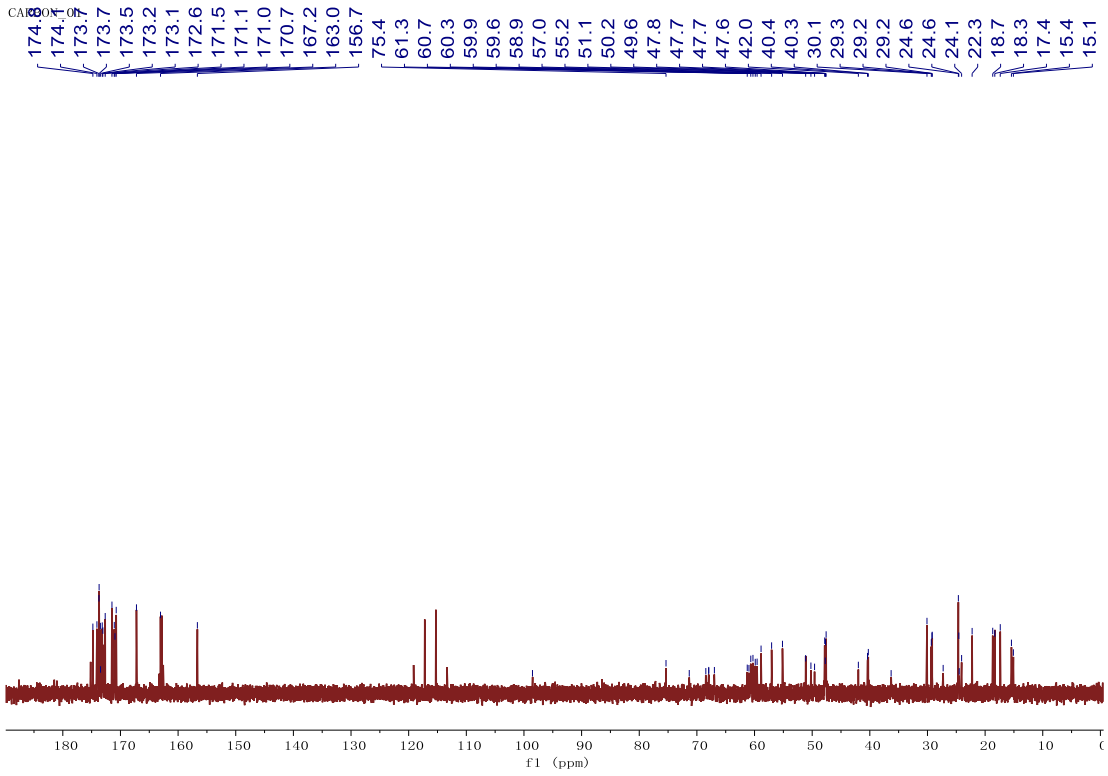

Figure S35. ^{13}C NMR spectrum for MUC1 glycopeptide **8**. Related to Scheme 2.

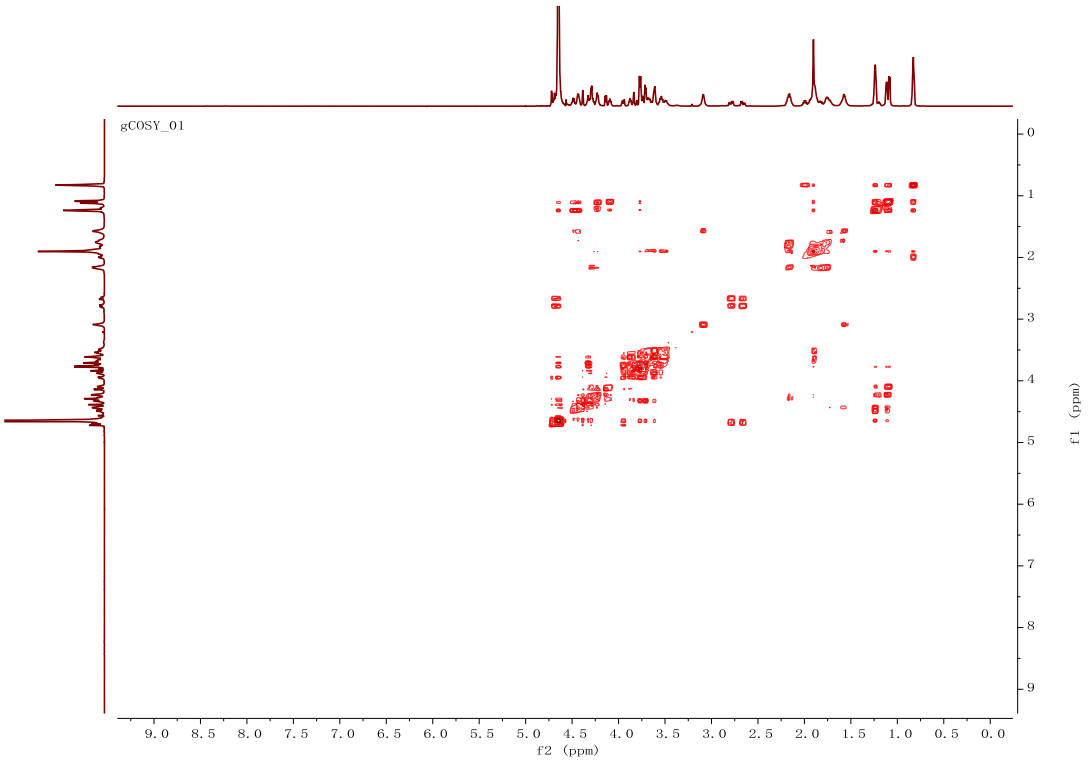

Figure S36. COSY of MUC1 glycopeptide **8**. Related to Scheme 2.

e. MUC1 glycopeptide squaric acid monoamide 10

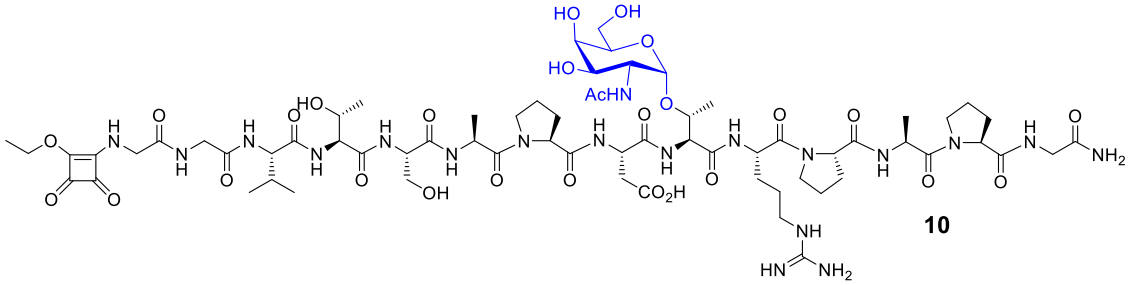

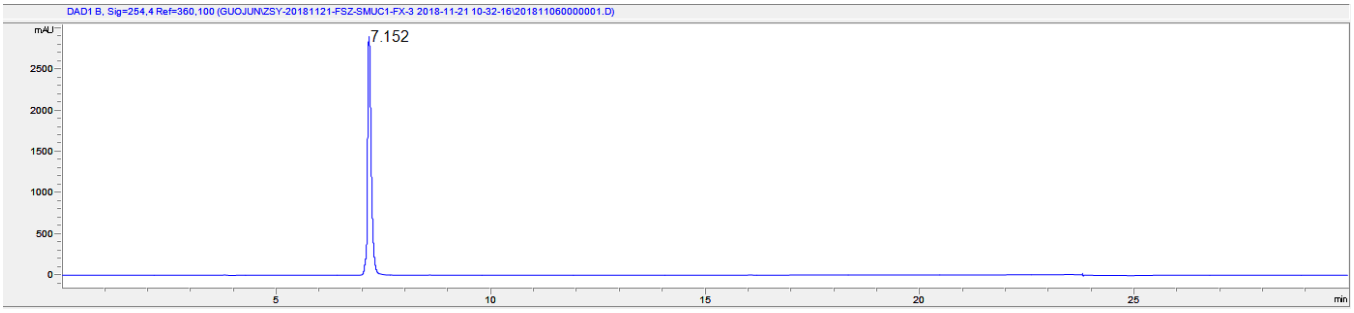

Figure S37. Analytical HPLC trace of MUC1 glycopeptide squaric acid monoamide **10**. (26 mg, 51% yield). Analytic gradient is 5% to 90% of solution B (acetonitrile with 0.1% trifluoroacetic acid) in solution A (water with 0.1% trifluoroacetic acid) in 30 min on the analytic C18 column. Related to Scheme 2.

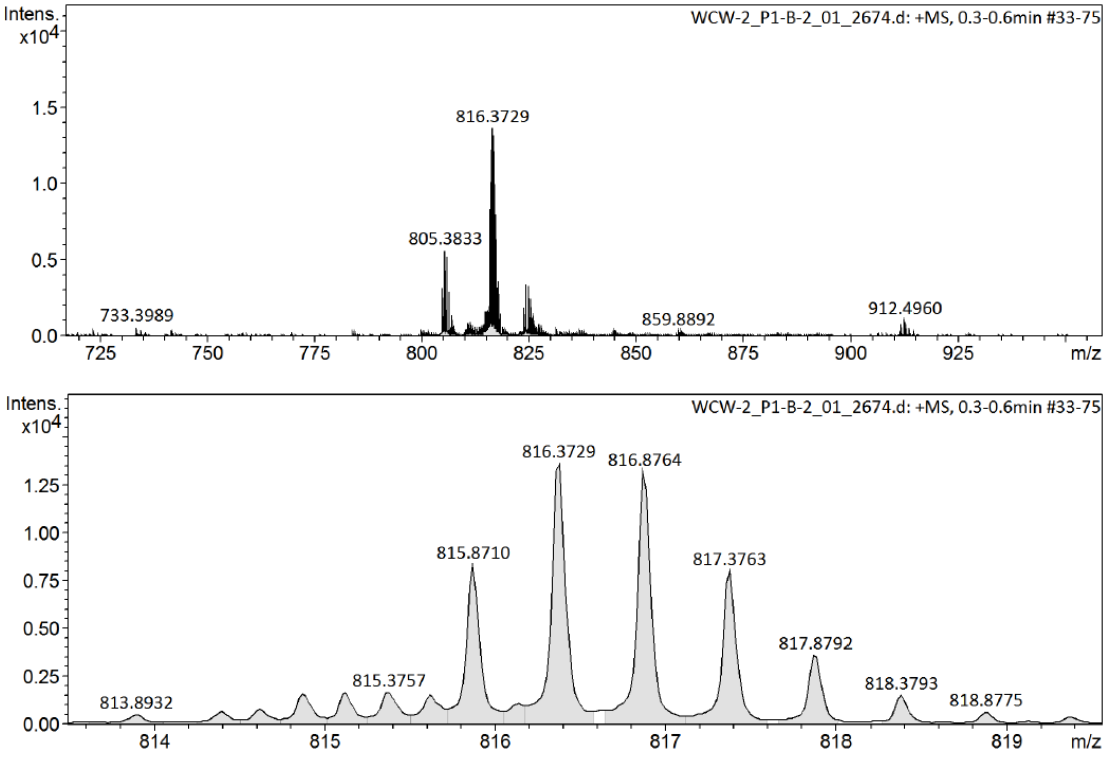

Figure S38. ESI-Q-TOF MS data of MUC1 glycopeptide squaric acid monoamide **10**. Related to Scheme 2.

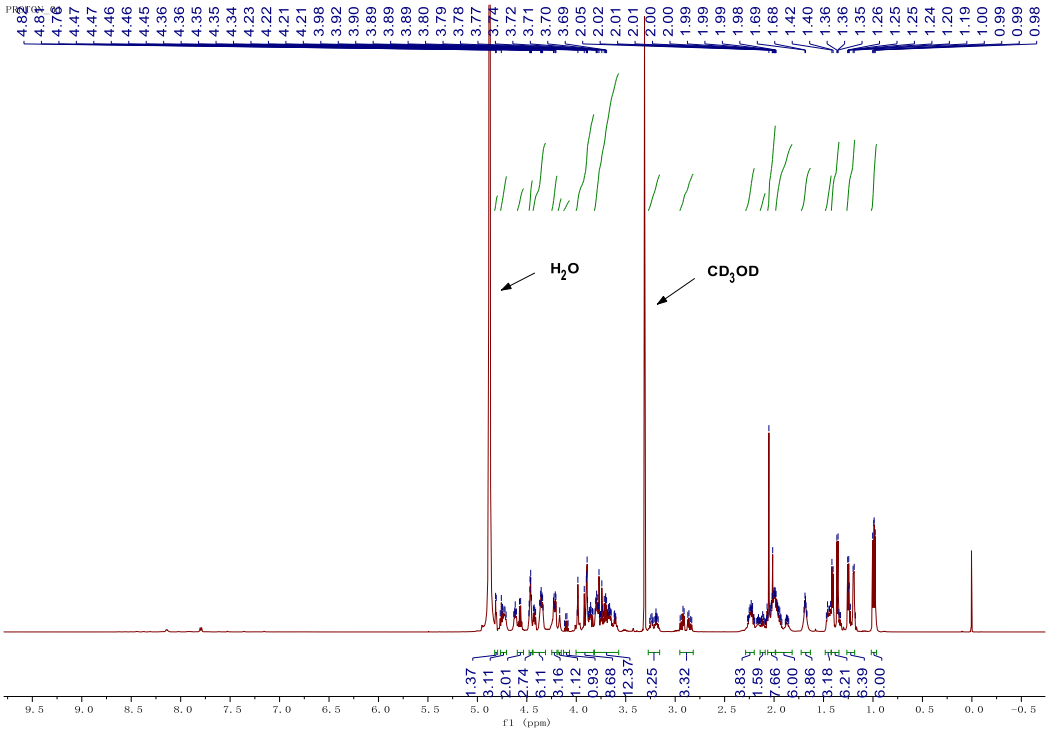

Figure S39. ^{1}H NMR spectrum for MUC1 glycopeptide squaric acid monoamide **10**. Related to Scheme 2.

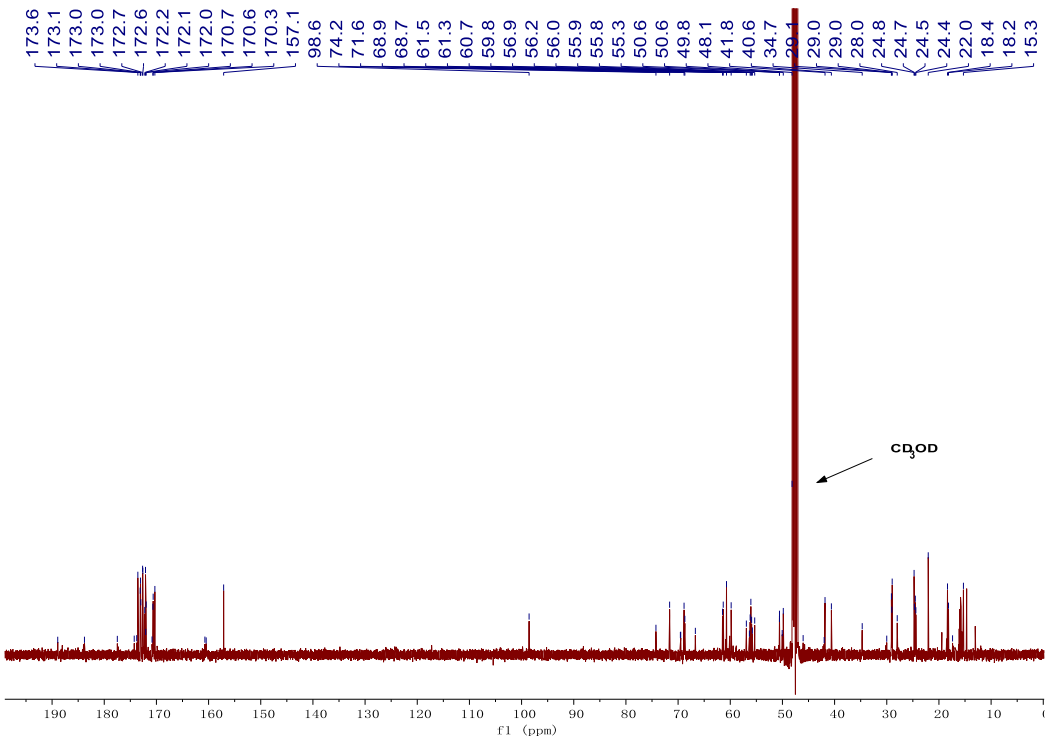

Figure S40. ^{13}C NMR spectrum for MUC1 glycopeptide squaric acid monoamide **10**. Related to Scheme 2.

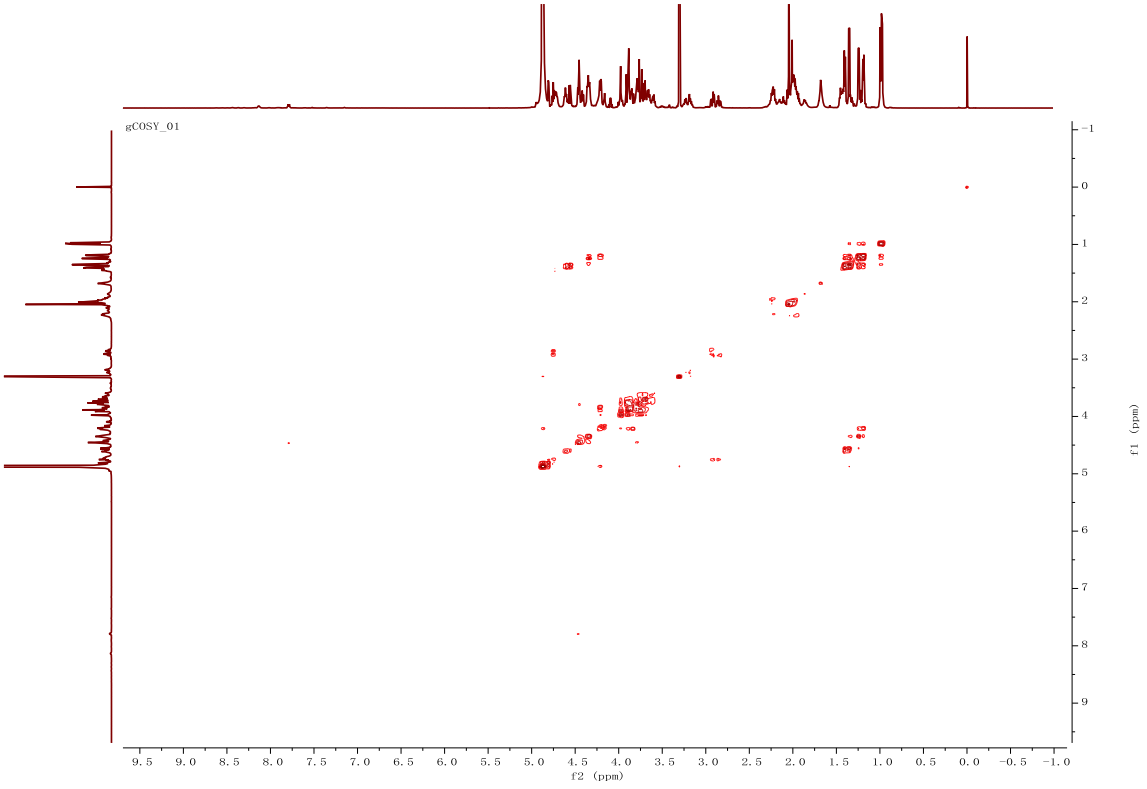

Figure S41. COSY of MUC1 glycopeptide squaric acid monoamide **10**. Related to Scheme 2.

f. Biotin-MUC1 glycopeptide 11

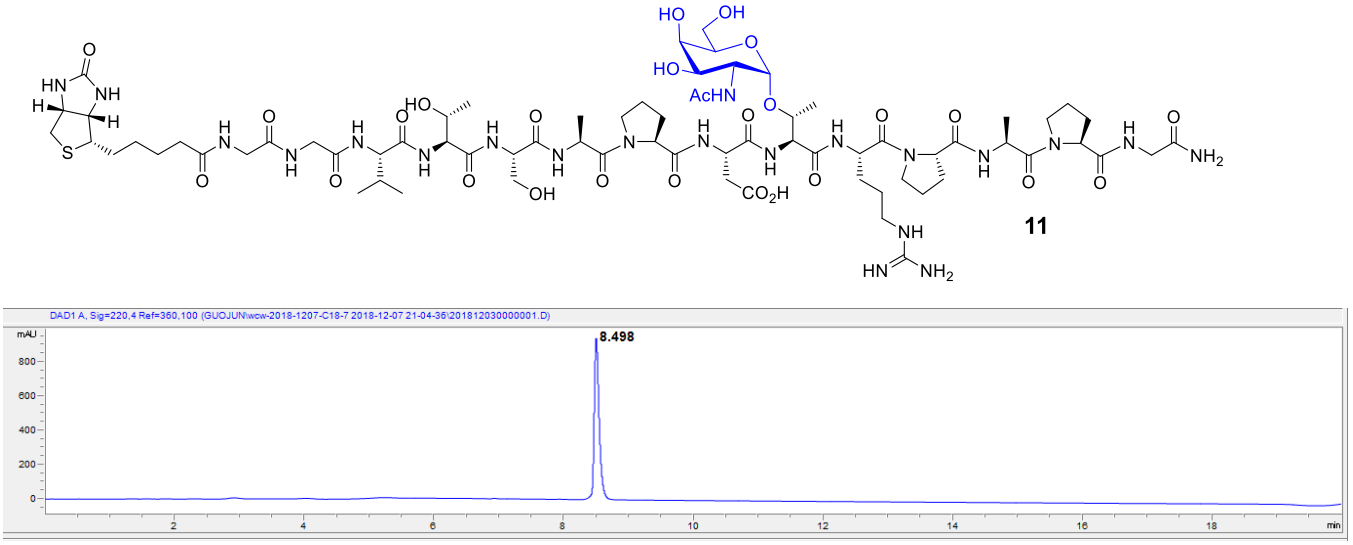

Figure S42. Analytical HPLC trace of biotin-MUC1 glycopeptide **11**. (26 mg, 46% yield). Analytic gradient is 5% to 60% of solution B (acetonitrile with 0.1% trifluoroacetic acid) in solution A (water with 0.1% trifluoroacetic acid) in 20 min on the analytic C18 column. Related to Figures 3 and 4.

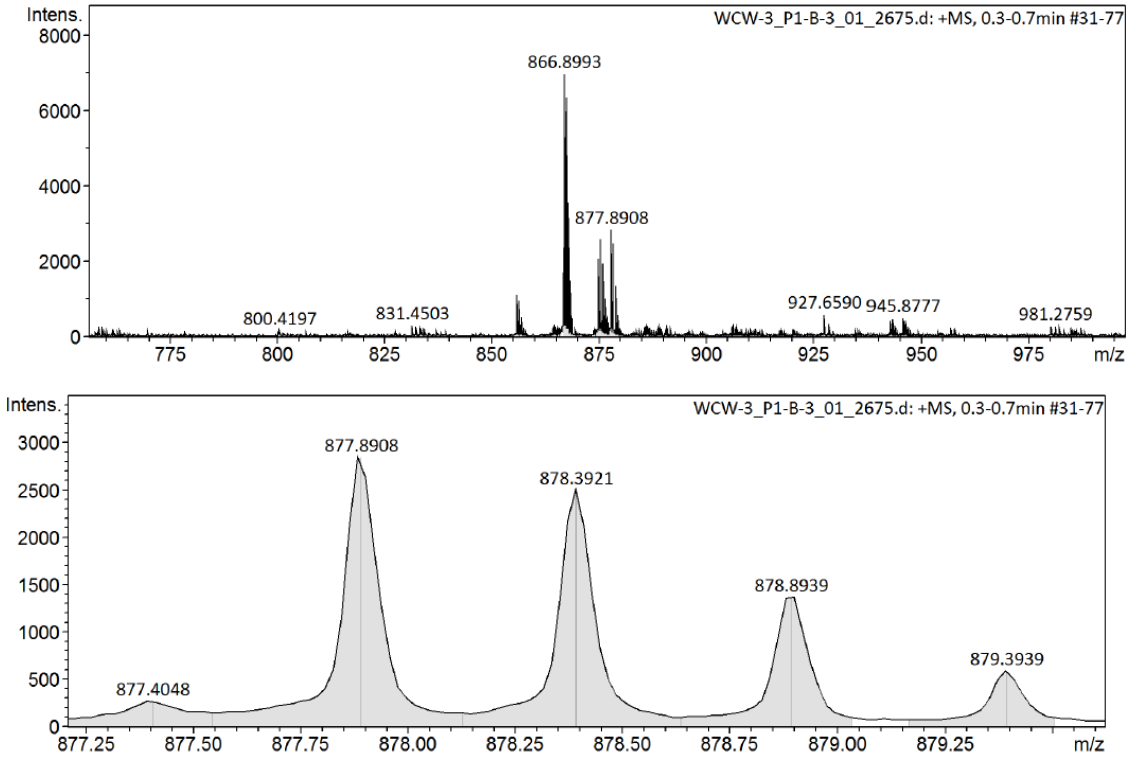

Figure S43. ESI-Q-TOF MS data of biotin-MUC1 glycopeptide **11**. Related to Figures 3 and 4.

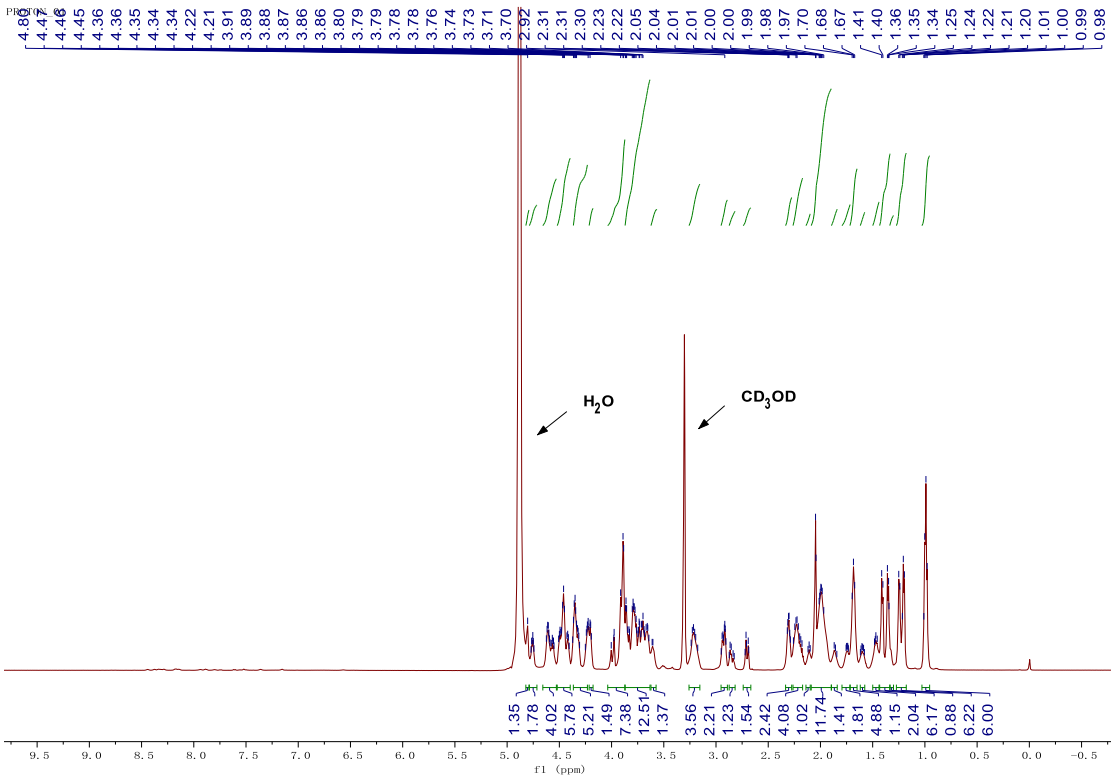

Figure S44. ^{1}H NMR spectrum for biotin-MUC1 glycopeptide **11**. Related to Figures 3 and 4.

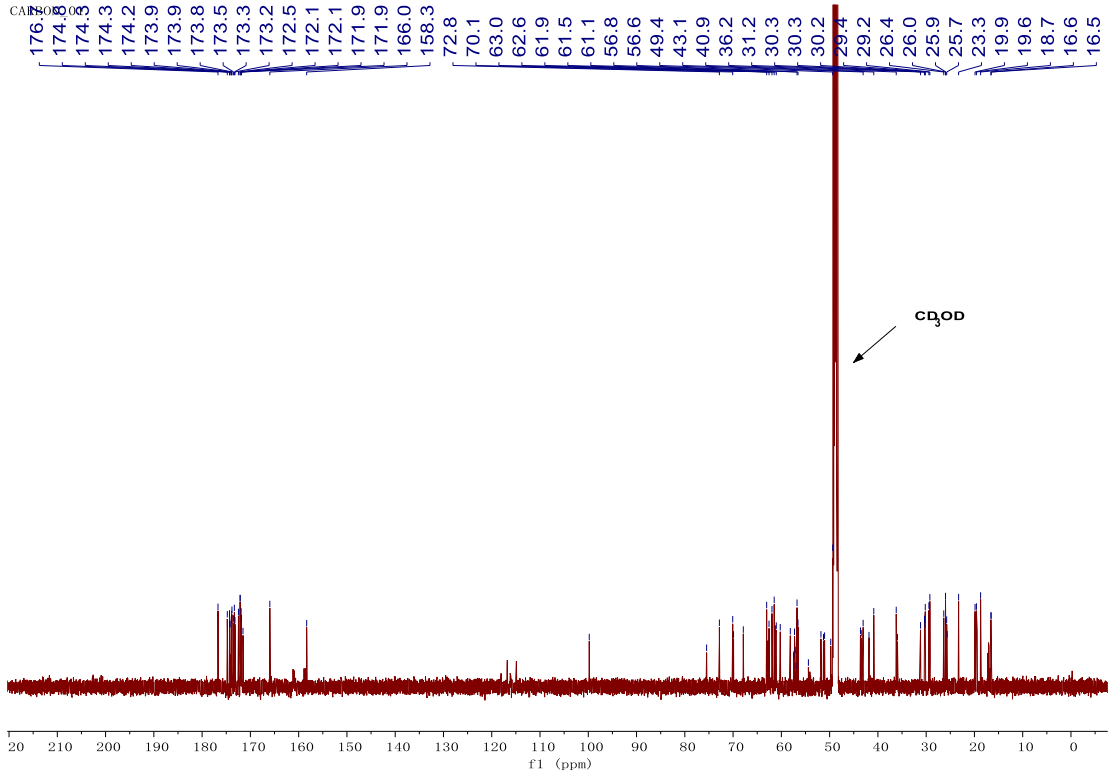

Figure S45. ^{13}C NMR spectrum for biotin-MUC1 glycopeptide **11**. Related to Figures 3 and 4.

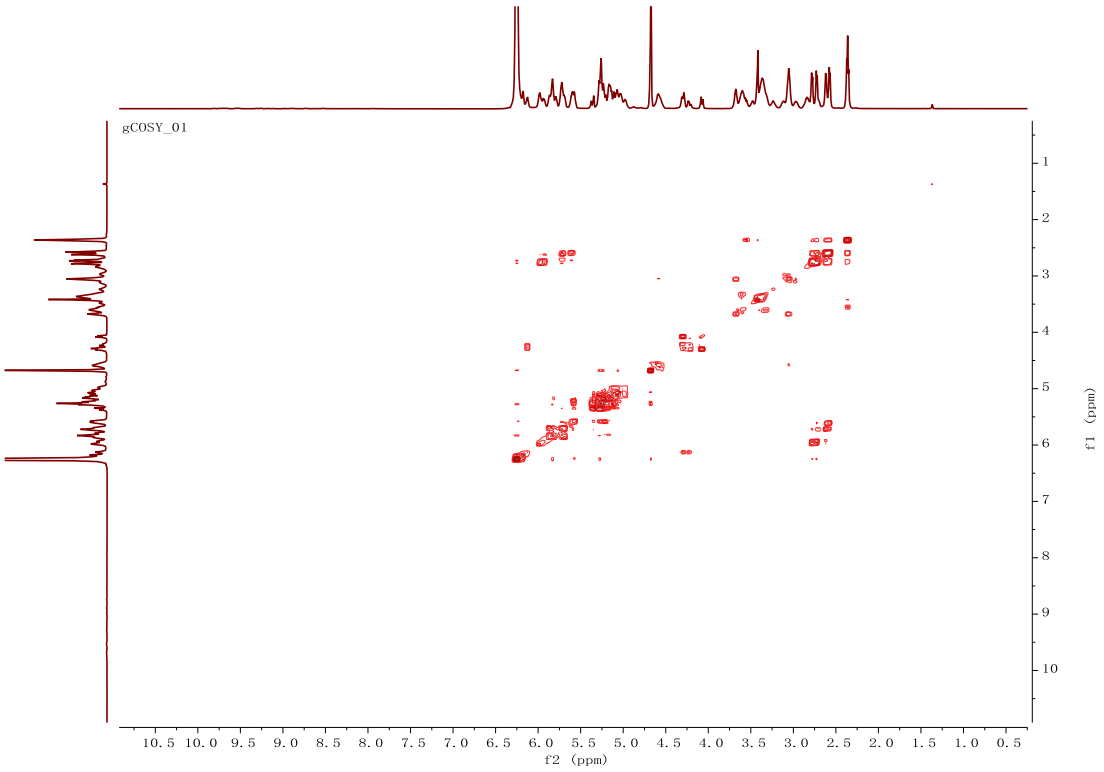

Figure S46. COSY of biotin-MUC1 glycopeptide **11**. Related to Figures 3 and 4.

g. BSA-MUC1 (12)

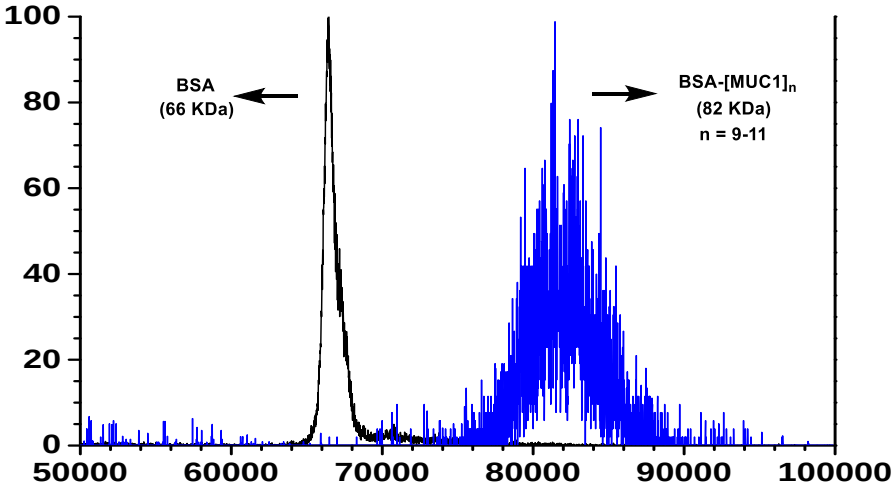

Figure S47. MALDI-TOF-MS analysis of BSA-MUC1 (**12**). Sinapic acid containing 0.1% TFA was used as the matrix. Related to Scheme 2.

h. TLR7a-BSA (14)

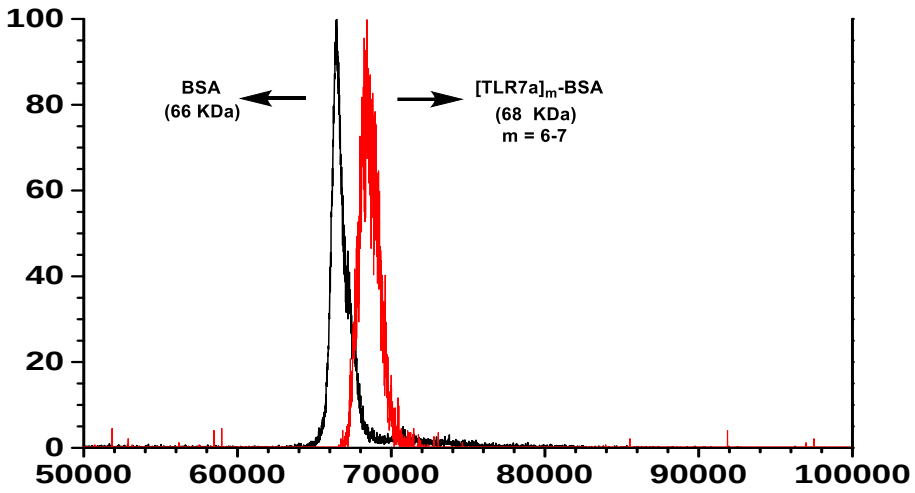

Figure S48. MALDI-TOF spectrum of BSA calibration standard and conjugated product TLR7a-BSA (**14**). Sinapic acid containing 0.1% TFA was used as the matrix. Related to Scheme 2.

i. TLR7a-BSA-MUC1 (15)

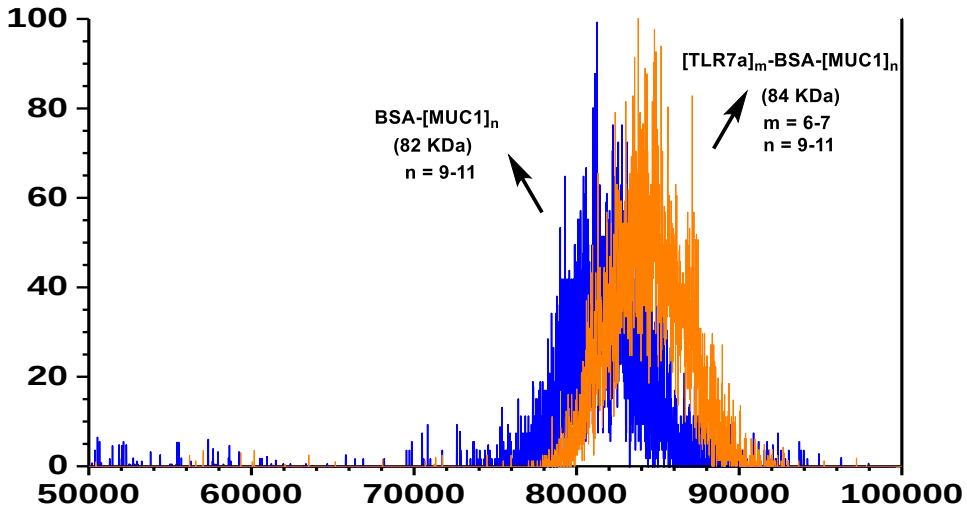

Figure S49. MALDI-TOF spectrum of BSA-MUC1 calibration standard and conjugated product TLR7a-BSA-MUC1 (**15**). Sinapic acid containing 0.1% TFA was used as the matrix. Related to Scheme 2.